# Understanding the role of heat shock protein 80 in thermotolerance and cell survival in *Neurospora crassa*

*A thesis submitted in partial fulfillment of the requirements*

*for the award of the degree of*

**DOCTOR OF PHILOSOPHY**

*By*

**Rahul Kumar Thaosen**

Registration Number: 186106012


**Department of Bosciences and Bioengineering**

**Indian Institute of Technology Guwahati**

**Kamrup-781039, Assam, India**

**July 2025**

# Understanding the role of heat shock protein 80 in thermotolerance and cell survival in *Neurospora crassa*

*A thesis submitted in partial fulfillment of the*

*requirements*

*for the award of the degree of*

**Doctor of Philosophy**

*by*

**Rahul Kumar Thaosen**

Registration Number: 186106012

*Under the supervision of*

**Prof. Ranjan Tamuli**

**Department of Biosciences & Bioengineering,**
**IIT Guwahati**


**Department of Bosciences and Bioengineering**

**Indian Institute of Technology Guwahati**

**Kamrup-781039, Assam, India**

**July 2025**

भारतीय प्रौद्योगिकी संस्थान गुवाहाटी
INDIAN INSTITUTE OF TECHNOLOGY GUWAHATI

**Department of Biosciences and Bioengineering**
**Indian Institute of Technology Guwahati**
**Kamrup-781039, Assam, India**

---

## STATEMENT

I do hereby declare that the content embodied in this thesis entitled **"Understanding the role of heat shock protein 80 in thermotolerance and cell survival in *Neurospora crassa*"** is the result of investigation carried out by me in the Department of Biosciences and Bioengineering, Indian Institute of Technology, Guwahati, India, under the guidance of **Prof. Ranjan Tamuli**. The research presented in this thesis is original and has not been submitted in part or full for any degree or diploma to any other institute or university to the best of my knowledge and belief.

Rahul Kumar Thaosen

IIT, Guwahati
March 2025

Rahul Kumar Thaosen
Enrolment No.: 186106012
Department of Biosciences and Bioengineering
Indian Institute of Technology Guwahati,
Guwahati-781039, Assam, India

भारतीय प्रौद्योगिकी संस्थान गुवाहाटी
INDIAN INSTITUTE OF TECHNOLOGY GUWAHATI

**Department of Bosciences and Bioengineering**
**Indian Institute of Technology Guwahati**
**Kamrup-781039, Assam, India**

---

## CERTIFICATE

This is to certify that the research conducted for the thesis titled **"Understanding the role of heat shock protein 80 in thermotolerance and cell survival in *Neurospora crassa*"** by **Rahul Kumar Thaosen (186106012)** was carried out at the Indian Institute of Technology Guwahati, under my direct supervision. The research presented in this thesis is entirely original and has not been submitted, either in part or in full, for the attainment of any other degree or diploma from any other academic institution or university.

Ranjan Tamuli

Guwahati
March 2025

**Dr. Ranjan Tamuli**
Professor
Department of Biosciences & Bioengineering
Indian Institute of Technology Guwahati,
Guwahati, Assam-781039, India

**Dedicated**

**to my loving parents**

**Lt. Uttam Thaosen (*Baba*)**

**and**

**Anila Thaosen (*Amai*)**

***… Rahul***

# ACKNOWLEDGEMENTS

Behind every step forward in this journey stood the quiet strength of those who supported and inspired me. Their unwavering belief gave me the courage to move forward through every challenge, and their presence made the journey meaningful.

First and foremost, I am deeply grateful to the Almighty God for His constant guidance, strength, and blessings throughout the course of this work.

I would like to express my profound gratitude and sincere thanks to **Prof. Ranjan Tamuli**, my PhD supervisor, for his unwavering support, guidance, and encouragement throughout my doctoral research. His supervision, insightful advice, and constructive criticism have been instrumental in shaping this work. I am especially grateful for the trust and freedom he gave me to explore my research independently, and for creating a supportive environment that allowed me to grow. I am equally thankful for his patience, mentorship and the invaluable lessons he imparted in scientific communication. His constant support during both the high and tough times has been a source of strength throughout this journey.

I am extremely grateful to my Doctoral Committee members **Prof. Manish Kumar**, **Prof. Pranab Goswami**, and **Prof. Subhendu Sekhar Bag** for their valuable suggestions, motivation and scientific guidance. Their insights have always helped me refine my work and navigate the challenges of my research with clarity and confidence.

I would like to express my sincere appreciation to the **Department of Biosciences and Bioengineering (BSBE)**, as well as the **HPC resource Param-Kamrupa** at IIT Guwahati, for providing the essential infrastructure and research facilities necessary to complete my work. I am also deeply thankful for the financial support extended by the **Ministry of Human Resource Development (MHRD), Government of India**, which supported my fellowship and enabled the successful execution of my research. My heartfelt thanks also go to the faculty members, administrative staff, and technical teams at IIT Guwahati for their dedication and willingness to assist in countless day-to-day tasks, which ensured that everything ran smoothly and allowed me to focus on my research. I am equally grateful to both the current and former **Directors** of the Indian Institute of Technology Guwahati (IITG) for bestowing upon me the privilege of conducting my doctoral research within the vibrant and naturally rich campus they have nurtured. Additionally, I extend my sincere appreciation to the current and past **Heads of the Department of Biosciences and Bioengineering (BSBE)**, as well as all the dedicated staff members of the

department, for their invaluable support in providing access to essential analytical instruments and laboratory facilities, which were instrumental in the successful completion of my thesis.

My heartfelt thanks also go to my seniors and lab alumni **Dr. Dibakar Gohain**, **Dr. Ajeet Kumar**, **Dr. Avishek Roy**, **Dr. Anand Tiwari**, **Dr. Christy K Marak**, **Dr. Darshana Baruah**, **Dr. Serena Ngiimei D, Shalini**, **Nayan**, **Divya**, **Mohit**, **Aravind** and **Abhilash**—for their invaluable guidance, encouragement, and support. Their experience, wisdom, and generosity helped shape my research and provided clarity during difficult times. I am equally grateful to the current members of the **RT Lab**, particularly **Surbhi**, **Sangeeta**, **Megha**, **Rebecca**, **Priyanuj**, **Ambika**, **Prince**, **Bijita** and **Seema** along with our postdoctoral researchers **Dr. Ajay** and **Dr. Himadree**. Their camaraderie, collaborative spirit and moral support made this journey enriching and enjoyable, turning everyday challenges into shared experiences.

I am deeply thankful to my friends at IIT Guwahati **Serena Di**, **Jon Da, Megha**, **Ambika, Priyanuj** and **Manas**—for their warmth, laughter, and support throughout my time on campus. They helped make my stay at IITG truly memorable, turning ordinary moments into unforgettable experiences. From shared struggles to small celebrations, their friendship provided balance during this demanding journey.

To my friends, I am deeply thankful for their unwavering support and companionship. **Suhasini** who has been a constant source of strength, understanding, and encouragement through every phase of my life and I am incredibly grateful for her belief in me. **Pulakeswar** who stood by me through all my ups and downs, offering his unwavering support in every possible way. Their presence has given my life meaning and comfort and I will forever treasure their support.

I owe my deepest gratitude to my parents **Lt. Mr. Uttam Thaosen** and **Mrs. Anila Thaosen**, and my siblings **Ringmashri**, **Ringhit** and **Sahit**. Their love, endless encouragement, and unwavering belief in me have been the foundation of my strength. From a young age, they instilled in me the values of perseverance, compassion and integrity, which have guided me throughout my life and academic journey. Their constant emotional support, sacrifices and prayers gave me the resilience needed to face both the triumphs and the challenges of this journey. I am forever grateful for their love and support, which made this achievement possible. This accomplishment is as much theirs as it is mine. Lastly, I extendmy heartfelt thanks to all those who supported me directly or indirectly , throughout this journey.

**March 2025** **- Rahul**

# Table of Contents

# Synopsis

## Abstract

Heat shock proteins (HSPs) are critical molecular chaperones that help maintain cellular protein homeostasis under stress conditions. Among these, Heat Shock Protein 80 (HSP80), a homolog of Hsp90 in *Neurospora crassa*, plays a significant role in diverse cellular stress responses, including thermotolerance, DNA repair and osmotic stress adaptation. In this study, the molecular mechanisms underlying HSP80 function were explored through both experimental and computational approaches. Using repeat-induced point mutation (RIP), four *hsp80* mutant strains (R4 A, R6 A, R9 a, and R14 a) were generated and phenotypically characterized. The mutants exhibited significantly reduced survival under elevated temperatures and various abiotic stress conditions, including oxidative, osmotic, pH and endoplasmic reticulum stress. Additional defects such as impaired aerial hyphae formation, defective cellulose utilization, reduced carotenoid biosynthesis and compromised DNA repair under UV and MMS exposure further underscored the functional importance of HSP80 in cellular stress adaptation. Transcriptional profiling revealed downregulation of key stress-responsive genes and DNA repair genes in the RIP mutants correlating with their phenotypic deficiencies. Complementary in silico analyses, including structure prediction and molecular dynamics simulations across thermal conditions (298K, 333K, 362K) showed that wild type HSP80 maintained superior conformational stability and hydrogen bond retention, while mutants especially R9 a and R14 a exhibited increased flexibility, higher RMSD/RMSF and unfavourable interaction energies under thermal stress.

**Keywords:** Heat shock proteins; *Neurospora crassa*; HSP80; stress tolerance; RIP mutants; molecular dynamics; DNA repair

**Thesis Title: Understanding the role of heat shock protein 80 in thermotolerance and cell survival in *Neurospora crassa***

**Objectives:**

1. Investigating the role of the Hsp80 gene regulation in thermotolerance in *Neurospora crassa*.
2. Cell-function of the hsp80 gene for survival under various stress conditions in *N. crassa*.
3. In-silico analysis and molecular dynamics simulations of *N. crassa* HSP80.

**Organization of the thesis**

**Synopsis**

**Chapter 1: Overview of *Neurospora crassa* and Heat Shock Proteins with a Focus on Hsp80**

**Chapter 2: Materials and Methods**

**Chapter 3: Investigating the Role of hsp80 Gene Regulation in Thermotolerance of *Neurospora crassa***

**Chapter 4: Cellular Function of the *hsp80* Gene in the Stress Response of *Neurospora crassa***

**Chapter 5: Computational Analysis and Molecular Dynamics Simulation of HSP80 in *Neurospora crassa***

**Chapter 6: Conclusion and Future Perspectives**

**Bibliography**

**Chapter 1: Overview of *Neurospora crassa* and Heat Shock Proteins with a Focus on Hsp80**

This chapter introduces *Neurospora crassa* as a genetically tractable filamentous fungus and a model system for studying eukaryotic cell biology, stress adaptation and protein homeostasis (Dunlap & Loros, 2017; Borkovich et al., 2004). It outlines the organism's life cycle, genome defense strategies and the critical role of heat shock proteins (Hsp), particularly Hsp80, in maintaining proteostasis under thermal and oxidative stress (Roy & Tamuli, 2022; Selker, 2011). *N. crassa* has been instrumental in understanding fundamental biological processes due to its

simple haploid genome, rapid growth and fully sequenced genome (Galagan et al., 2003; Colot et al., 2006). Its heterothallic life cycle and efficient homologous recombination system allow high-resolution genetic manipulation, making it suitable for functional genomics and epigenetic studies (Davis & de Serres, 1970; Perkins, 1992). The organism's genome defense mechanisms include Meiotic Silencing by Unpaired DNA (MSUD), Quelling and Repeat-Induced Point Mutation (RIP). Among these RIP is unique to fungi and introduces cytosine-to-thymine mutations in duplicated sequences, effectively silencing transposons and facilitating gene function analysis (Selker et al., 1987; Cambareri et al., 1989). This mechanism is regulated by the RID methyltransferase and contributes to genome integrity and evolution (Freitag et al., 2002; Gladyshev, 2017).

Heat shock proteins are evolutionarily conserved molecular chaperones that maintain protein homeostasis during normal growth and stress conditions (Lindquist & Craig, 1988; Hartl et al., 2011). They assist in folding nascent polypeptides, refolding misfolded proteins and preventing protein aggregation (Mayer & Bukau, 2005). Stress stimuli like heat, oxidative damage and UV exposure significantly upregulate Hsp expression, aiding in proteotoxic stress mitigation (Jakob et al., 1999; Görlach et al., 2017). Among various families, Hsp70, Hsp90 and Hsp100 play crucial roles across organisms, with Hsp80, a homolog of Hsp90 being particularly important in *N. crassa* (Roy & Tamuli, 2022). Hsp80 in *N. crassa* likely mirrors the role of Hsp90 in other fungi, regulating stress signaling, stabilizing kinases and ensuring proper activation of cellular defense mechanisms (Cowen & Lindquist, 2005; Liu et al., 2009). It contains three major domains an N-terminal ATP-binding domain, a middle domain for client interaction and a C-terminal dimerization domain with an MEEVD motif for co-chaperone binding (Li et al., 2012; Schopf et al., 2017). Hsp80 interacts with co-chaperones like HOP, p23, Aha1 and Cdc37, which fine-tune its ATPase activity and client specificity (Panaretou et al., 2002; Roe et al., 2004; McLaughlin et al., 2002). In *N. crassa*, the precise role of Hsp80 is still emerging; however, its evolutionary conservation with Hsp90 homologs in *S. cerevisiae*, *A. fumigatus* and *C. albicans* suggests shared mechanisms in thermotolerance, oxidative stress resistance and developmental regulation (Cowen et al., 2009; Taipale et al., 2010). Evidence from other systems implicates Hsp90 role in UV damage repair via ATR and p53 stabilization, ROS detoxification and regulation of signaling pathways such as MAPK and calcineurin (Richter & Buchner, 2001; Zou & Elledge, 2003; Moll et al., 2005).

**Chapter 2: Materials and Methods**

This chapter outlines the materials, media and experimental procedures employed in this study. Standard protocols for the cultivation, maintenance and genetic crosses of Neurospora crassa were followed as described by Westergaard and Mitchell (1947) and Davis and de Serres (1970). *N. crassa* strains were obtained from the Fungal Genetics Stock Center (FGSC, Manhattan, KS), while other required strains were generated in our laboratory. A plasmid used in this study was obtained from the laboratory of Dr. Maria Celia Bertolini. All chemicals and reagents were procured from certified suppliers and used following appropriate sterilization procedures. Molecular biology experiments were conducted using either standard protocols outlined in Molecular Cloning: A Laboratory Manual (Russell and Sambrook, 2001) or according to the manufacturer's instructions.

**Chapter 3: Investigating the Role of hsp80 Gene Regulation in Thermotolerance of *Neurospora crassa***

The *hsp80*$^{RIP}$ mutant strains were successfully generated through a systematic cloning and screening process. The *hsp80* ORF (3,019 bp) was cloned into the pTLS88F vector and formed the recombinant plasmid pRTHSP80 which was confirmed for correct orientation before being transformed into *N. crassa*. This process resulted in the heterokaryotic strain T9 A. Further crossing and screening of ascospores led to the isolation of four mutant strains R4 A, R6 A, R9 a and R14 a with duplicated ectophic *hsp80* copies.

Stress tolerance assays elucidated the role of Hsp80 in *N. crassa* under varying environmental conditions. In thermotolerance assays, the *hsp80*$^{RIP}$ mutants exhibited significantly reduced survival rates compared to the wild-type strain when subjected to induced thermotolerance conditions with preincubation at 44°C. Under induced thermotolerance conditions, the mutants exhibited minimal survival underscoring the essential role of *hsp80* in facilitating cellular adaptation to thermal stress. The expression levels of were assessed using quantitative RT-PCR *hsf-1*, *cna-1* and *cmd* in the *hsp80*$^{RIP}$ mutants under heat stress conditions, aiming to evaluate the impact of RIP-induced mutations on gene regulation. Notably, a significant reduction in *hsp80* expression was observed across all four mutant strains compared to the wild type. Under heat stress all *hsp80*$^{RIP}$ mutants showed lower hsp80 expression, which corresponded to impaired stress tolerance. This shows that RIP-induced mutations impacted *hsp80* transcription highlighting its importance in thermal stress adaption. The effect of pH on the growth on the mutants was also assessed, revealing significant reductions in hyphal length across acidic (pH 3.8), neutral (pH 5.8)

and alkaline (pH 7.8) conditions compared to the wild-type strain. These results suggest that *hsp80* is involved in regulating growth under fluctuating pH conditions, likely through pathways such as the PacC/PalA regulatory mechanism. The osmotic stress response further underscored the importance of Hsp80 in maintaining cellular stability. When exposed to hyperosmotic conditions induced by 0.5 M and 1 M sorbitol, the *hsp80*$^{RIP}$ mutants demonstrated significantly lower growth rates compared to the wild-type strain. Fertility assays confirmed that all the *hsp80*$^{RIP}$ mutants remained capable of sexual reproduction indicating that Hsp80 is not essential for fertility in *N. crassa*. However, their increased sensitivity to various stress conditions which suggests that Hsp80 plays a critical role in stabilizing cellular membranes and maintaining homeostasis during environmental stress.

**Chapter 4: Cellular Function of the *hsp80* Gene in the Stress Response of *Neurospora crassa.***

The ability of *N. crassa* to use cellulose as a carbon source is critical to its survival in natural conditions. Growth experiments on 2% cellulose substrate found that all the *hsp80*$^{RIP}$ mutants had much lower mycelial mass than the wild type strain, with the R9 a mutant completely unable to grow. These findings indicate that Hsp80 is critical for nutrient adaptation and efficient utilization of complex carbon sources, likely by stabilizing cellulase enzymes or modulating transcriptional pathways involved in cellulose degradation. Given the mutants inability to tolerate thermal stress from the previous chapter, their response to the endoplasmic reticulum (ER) stress was also examined. Exposure to 10 mM dithiothreitol (DTT), which induces ER stress by disrupting protein folding, revealed significantly lower survival rates in the mutants compared to the wild type. These findings suggest that Hsp80 is essential for maintaining protein homeostasis during ER stress, likely through its role in managing the unfolded protein response (UPR) showing the importance in stabilizing cellular machinery under protein-folding stress. The response of the *hsp80*$^{RIP}$ mutants to osmotic stress was evaluated by growing strains in media supplemented with 0.5 M and 1 M sorbitol. The mutants displayed significantly reduced growth rates compared to the wild type strain, indicating a critical role for Hsp80 in stabilizing membrane associated proteins and maintaining osmotic balance. Carotenoid biosynthesis, which is responsible for the orange pigmentation of *N. crassa*, was also analyzed under varying temperature conditions (8 °C, 22 °C and 30 °C). The *hsp80*$^{RIP}$ mutants exhibited significantly reduced carotenoid levels compared to the wild type strain at all temperatures indicating that Hsp80 regulates carotenoid biosynthesis during temperature stress. This regulation is likely achieved through the stabilization of enzymes involved in the biosynthetic pathway. The reduced carotenoid production in the mutants underscores Hsp80's broader role in stress induced metabolic processes.

Finally, the involvement of Hsp80 in DNA repair pathways was investigated under UV and MMS-induced DNA damage conditions, as well as through photoreactivation assays. Under UV stress, reduced *hsp80* expression in the mutants was observed, correlating with their impaired ability to manage DNA lesions such as cyclobutane pyrimidine dimers (CPDs) and (6-4) photoproducts (6-4PPs). Similarly, using a chemical agent, MMS-induced alkylation damage resulted in reduced surivival rate in the *hsp80*$^{RIP}$ mutants suggesting that *hsp80* plays a role in stabilizing repair proteins required for managing replication stress and damage bypass. In photoreactivation assays, which assess the direct repair of CPDs by photolyase, the mutants exhibited reduced efficiency compared to the wild type, indicating that *hsp80* may assist photolyase by stabilizing its activity during DNA repair. Expression analysis revealed significantly impaired induction of DNA repair genes (*upr-1, mus-26, mus-52*) in the *hsp80*$^{RIP}$ mutants following UV exposure. Compared to the wild type, the mutants exhibited attenuated transcriptional responses, indicating that Hsp80 is essential for the activation of DNA repair pathways under genotoxic stress.

**Chapter 5: Computational Analysis and Molecular Dynamics Simulation of HSP80 in *Neurospora crassa***

This chapter presents an integrative bioinformatics and molecular dynamics-based analysis of wild type HSP80 and its *hsp80*$^{RIP}$ mutant variants (R4 A, R6 A, R9 a and R14 a) to investigate the structural consequences of single amino acid substitutions. The structural model of wild HSP80 was predicted using AlphaFold and subjected to validation through Ramachandran plot assessment, energy minimization and comparison with homologous templates to ensure model reliability. Domain mapping identified three major functional regions the N-terminal ATP-binding domain, the middle co-chaperone interaction domain and the C-terminal dimerization domain along with 25 discrete structural subregions. Cavity analysis revealed 35 potential binding pockets, several of which were conserved based on ConSurf scoring, particularly within the ATP-binding and co-chaperone binding domains.

Molecular dynamics simulations were performed for the wild type and mutant variants at 298K, 333K and 362K using GROMACS on the PARAM Kamrupa supercomputing facility. RMSF analysis indicated enhanced local flexibility in the mutant proteins, notably within the substrate-binding and linker domains. R9 a and R14 a displayed the highest fluctuations across all temperatures suggesting altered dynamic behavior in regions essential for client-protein interactions.

RMSD profiles demonstrated increased global structural deviations in the mutants relative to the wild type with temperature-dependent destabilization most pronounced at 362K. The radius of gyration (Rg) analysis corroborated these findings, showing greater expansion in the mutants, particularly in R14 a, indicative of reduced structural compactness. Interaction energy analysis revealed that wild type HSP80 maintained consistently favorable internal energy profiles across temperatures, whereas the mutants, especially R9 a and R14 a, exhibited elevated energy fluctuations, indicating compromised intramolecular cohesion and reduced thermal resilience. Secondary structure analysis revealed progressive loss of helices and beta-sheets with increasing temperature, with R14 a and R9 a exhibiting the most significant structural degradation. Principal Component Analysis (PCA) further confirmed increased conformational variability in the mutants, in contrast to the compact and coordinated motion observed in the wild-type protein.

**Chapter 6: Conclusion and Future Perspectives**

This chapter investigates the functional significance of the Hsp80 molecular chaperone in *N. crassa* using RIP-induced mutant strains (R4 A, R6 A, R9 a and R14 a). Sequence and domain analysis confirmed that *N. crassa*, Hsp80 shares conserved features with eukaryotic Hsp90 family members, including an N-terminal ATP-binding domain, a middle domain for client-protein interaction and a C-terminal dimerization domain. Conserved residues such as Lys27 and Asp79 were identified as functionally critical based on structural alignment and evolutionary conservation.

Phenotypic characterisation of the *hsp80*$^{RIP}$ mutants revealed broad defects in stress adaptation. Mutants displayed pronounced sensitivity to thermal, oxidative, osmotic, pH and ER stress. Expression analysis showed downregulation of stress-related genes (*hsf-1*, *cna-1*, *cmd*) in mutants, suggesting impaired activation of stress signaling pathways. Growth assays demonstrated altered hyphal elongation and septation, though conidiation and sexual fertility remained unaffected.

To evaluate the metabolic roles of Hsp80, cellulose utilization assays were conducted. R9 a exhibited reduced biomass, extracellular glucose and protein accumulation indicating defects in cellulase secretion possibly due to impaired protein folding and ER-mediated trafficking. Sensitivity to ER stress further supported Hsp80's role in maintaining secretory homeostasis

The involvement of Hsp80 in genomic maintenance was assessed through UV and MMS induced DNA damage assays. Mutants showed reduced survival and impaired photoreactivation, accompanied by downregulation of DNA repair genes (*upr-1*, *mus-26*, *mus-52*), suggesting Hsp80's involvement in both transcriptional regulation and execution of DNA repair mechanisms.

Carotenoid biosynthesis assays revealed decreased pigment accumulation in mutants, linking Hsp80 function to photoprotective and oxidative stress-buffering metabolic pathways.

STRING based protein–protein interaction predictions indicated Hsp80's association with multiple stress-related chaperones, transcription factors and uncharacterized proteins, reinforcing its role as a central hub in proteostasis. Structural modeling and molecular dynamics simulations revealed that RIP mutations particularly R14 a compromised structural stability, increased conformational flexibility and disrupted domain coordination particularly at elevated temperatures. These findings provided a mechanistic basis for the diverse phenotypic impairments observed in the mutant strains.

Further studies on the regulation and functional significance of Hsp80 in *Neurospora crassa* will enhance our understanding of its role in stress adaptation, development, metabolism and genome stability. The future direction of this research will be:

i. Molecular Mechanisms of *hsp80* Mutations: Explore interactions with client proteins and co-chaperones to identify disrupted pathways.

ii. Expanded Computational Analysis: Extend MD simulations to assess responses to oxidative and osmotic stress. Focus on identifying additional key functional regions and regulatory mechanisms.

iii. Post-Translational Modifications: Study the impact of modifications like phosphorylation, acetylation, and ubiquitination on HSP80's activity and stability.

iv. Structural Insights for Biotechnological Advances: Use structural and functional data to design mutants with enhanced stress tolerance, which is beneficial for industrial and environmental applications.

# List of Figures

# List of Tables

# *List of Abbreviations*

| Abbreviation | Full form |
|---|---|
| ANOVA | Analysis of Variance |
| ATP | Adenosine Triphosphate |
| BOD | Biological Oxygen Demand |
| bp | Base Pair |
| CD | Circular Dichroism |
| CDD | Conserved Domain Database |
| CFW | Calcofluor White |
| cDNA | Complementary Deoxyribonucleic Acid |
| CMD | Calmodulin |
| CTAB | Cetyltrimethylammonium Bromide |
| CV | Collective Variable |
| DNA | Deoxyribonucleic Acid |
| DMSO | Dimethyl Sulfoxide |
| DNSA | 3,5-Dinitrosalicylic Acid |
| DTT | Dithiothreitol |
| EDTA | Ethylenediaminetetraacetic Acid |
| ER | Endoplasmic Reticulum |
| EtBr | Ethidium Bromide |
| FEL | Free Energy Landscape |
| MD | Molecular Dynamics |
| MEGA | Molecular Evolutionary Genetic Analysis |
| MMS | Methyl Methanesulfonate |
| NCBI | National Centre for Biotechnology Information |
| NCU | Neurospora crassa Unit |
| NER | Nucleotide Excision Repair |
| OD | Optical Density |
| ORF | Open Reading Frame |
| PCA | Principal Component Analysis |
| PCR | Polymerase Chain Reaction |
| PMF | Potential of Mean Force |
| qRT-PCR | Quantitative Real-Time Polymerase Chain Reaction |
| RID | RIP Deficient |
| RIP | Repeat-Induced Point Mutation |
| RNA | Ribonucleic Acid |
| RMSD | Root Mean Square Deviation |
| RMSF | Root Mean Square Fluctuation |
| ROS | Reactive Oxygen Species |
| SCM | Synthetic Crossing Media |

| | | | |
|---|---|---|---|
| FGSC | Fungal Genetics Stock Centre | SDS | Sodium Dodecyl Sulfate |
| FGS | Fructose, Glucose, Sorbose | SOC | Super Optimal Broth with Catabolite Repression |
| GFP | Green Fluorescent Protein | STRING | Search Tool for the Retrieval of Interacting Genes/Proteins |
| HSP | Heat Shock Protein | TAE | Tris-Acetate-EDTA |
| HSF | Heat Shock Factor | TE | Tris-EDTA |
| HSP80 | Heat Shock Protein 80 | TPR | Tetratricopeptide Repeat |
| Hsp | Heat Shock Protein | UV | Ultraviolet |
| kb | Kilobase Pair | UPS | Ubiquitin-Proteasome System |
| kDa | Kilodalton | VM | Vogel's Minimal Medium |
| MAPK | Mitogen-Activated Protein Kinase | VGN | Vogel's Glucose Medium |

# Chapter 1

## OVERVIEW OF *NEUROSPORA CRASSA* AND HEAT SHOCK PROTEINS WITH A FOCUS ON HSP80

# CHAPTER 1

# OVERVIEW OF *NEUROSPORA CRASSA* AND HEAT SHOCK PROTEINS WITH A FOCUS ON HSP80

## 1.1 Introduction to *Neurospora crassa* and its establishment as a model organism

*Neurospora crassa* is a filamentous ascomycete fungus belonging to the phylum Ascomycota, family Sordariaceae and order Sordariales. *N. crassa* is widely used as a model organism in genetics, molecular biology and biochemistry. It has simple haploid genome, rapid growth and well-characterized life cycle which make it invaluable for studying fundamental biological processes. *N. crassa* was first recognized as a model system by George Beadle and Edward Tatum in the 1940s based on their pioneering work that demonstrated the relationship between genes and enzymatic functions, leading to the "one gene–one enzyme" hypothesis (Beadle & Tatum, 1941), a breakthrough that earned them the Nobel Prize in Physiology or Medicine in 1958. Since then, *N. crassa* has contributed to understanding gene regulation, circadian rhythms, epigenetics and cellular signaling (Dunlap & Loros, 2017). *N. crassa* is commonly found on burnt vegetation, thriving on decaying organic matter (Perkins & Davis, 2000). Its rapid growth on simple media and distinct morphological features, such as clear mycelial growth and conidial formation, make it ideal for genetic studies. Its haploid life cycle allows to see phenotypic effects of mutations without complex genetic crosses. *N. crassa* also has well-characterized sexual cycle that facilitates genetic analyses and meiotic recombination studies (Davis & de Serres, 1970). The genome of *N. crassa* was fully sequenced, providing insights into fungal biology (Galagan et al., 2003). It consists of approximately 42 Mb distributed across seven chromosomes, with around 10,000 protein-coding genes. The genome is compact, with minimal non-coding regions, making it ideal for functional genomic studies. *N. crassa* also has an efficient homologous recombination system, facilitating targeted gene knockouts and precise genetic modifications. The availability of the whole genome sequence led to a high-throughput knockout project to generate gene replacement mutants for all genes (Colot et al., 2006; Collopy et al., 2010; Park et al., 2011). This has enabled the elucidation of gene functions and the identification of transcription factors regulating biochemical pathways and cellular responses (Roche et al., 2014; Seibert et al., 2016). The name Neurospora comes from the Greek words “neuron” (nerve) and “spora” (spore), referring to the beaded appearance of its spores under a microscope, resembling nerve cells (Shear & Dodge, 1927). Comparative

genomics has provided insights into fungal evolution, gene conservation and adaptation to diverse environments. Additionally, its simple cellular organization makes it an excellent system for studying intracellular trafficking, mitochondrial function and cellular differentiation (Borkovich et al., 2004).

### 1.2 Life cycle of *Neurospora crassa*

*N. crassa* is a filamentous fungus with a heterothallic life cycle needs two distinct mating types (A and a) for successful sexual reproduction (Dodge 1939; Perkins 1992). *N. crassa* reproduces both asexually and sexually that ensures efficient propagation and genetic recombination, contributing to its adaptability and evolutionary success (Davis and Perkins 2002).

Under favorable environmental conditions, *N. crassa* predominantly follows the asexual reproductive pathway by producing abundant conidia that facilitate dispersal and colonization (Springer 1993). These conidia are uninucleate mitotic spores that germinate upon encountering suitable substrates and forming a highly branched multinucleate vegetative mycelium (Davis and Perkins 2002; Borkovich et al. 2004). This hypahal mycelial network plays a crucial role in nutrient acquisition and enabling the fungus to thrive in diverse ecological niches. Asexual reproduction offers a rapid means of proliferation, ensuring the survival of the species even in the absence of compatible mating partners (Perkins and Davis 2000).

Sexual reproduction in *N. crassa* is initiated when hyphae of opposite mating types interact through specialized female reproductive structures called protoperithecia. Trichogynes, elongated receptive hyphae, facilitate chemotropic recognition and fusion with male cells, typically conidia or microconidia of the opposite mating type, leading to plasmogamy (Raju 1992; Glass and Kaneko 2003). Following plasmogamy, dikaryotic ascogenous hyphae grow within the protoperithecium, eventually giving rise to the perithecium, a flask-shaped fruiting body containing meiotic components (Raju 1994; Glass et al. 2004). Karyogamy occurs in the perithecium, causing haploid nuclei to fuse and create a diploid zygote. This diploid nucleus undergoes meiosis, followed by a post-meiotic mitotic division, generating eight haploid ascospores arranged linearly within each ascus **(Figure 1.1)** (Perkins et al. 1986; Raju 2009). The mature ascospores are characterized by their distinctive longitudinal striations and are forcibly ejected from the perithecium and dispersed by air currents that facilitating genetic exchange and adaptation to new environments (Shear and Dodge 1927; Turner et al. 2011).

When appropriate conditions are met, ascospores germinate and resume vegetative growth, bringing the *N. crassa* life cycle to an end. This dynamic reproductive strategy provides both stability through clonal propagation and genetic diversity through recombination, reinforcing its importance as a model organism for genetic and developmental research. (Davis 2000; Borkovich et al. 2004). Following the completion of meiosis and the regulation of gene expression during the life cycle, *N. crassa* employs several genome defense mechanisms to protect its genetic material from transposable elements and other disruptive sequences.

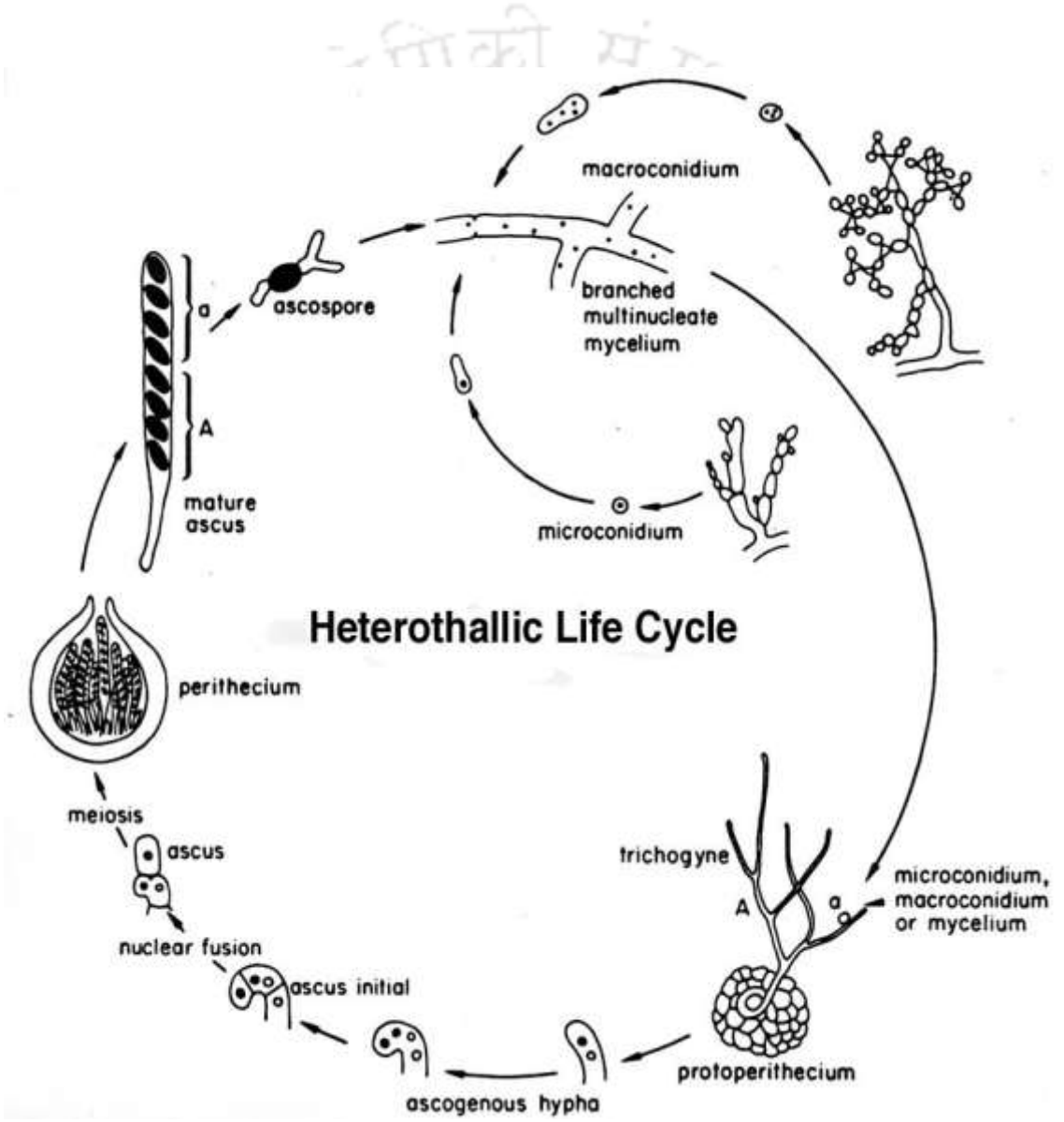


**Figure 1.1: The Life cycle of *N. crassa*.** The multinucleate, branching vegetative mycelium undergoes an asexual cycle, forming aerial hyphae that produce either multinucleate macroconidia or uninucleate microconidia. These spores disperse and germinate on suitable substrates, continuing the cycle. The sexual cycle is triggered by nitrogen starvation and low temperatures, leading to the formation of a protoperithecium in either mat A or mat a colony.

Fertilization by opposite-type conidia results in a perithecium, where mitosis and meiosis generate eight linearly arranged ascospores within an ascus. Upon heat activation, these pigmented, multinucleate ascospores germinate into new hyphae, entering either the asexual or sexual cycle. Adapted from FGSC (https://www.fgsc.net//Neurospora/sectionB2.htm).

### 1.3 Genome defense mechanisms in *N. crassa*

*N. crassa* has evolved multiple genome defense mechanisms to maintain genomic stability and regulate gene expression. These include Meiotic Silencing by Unpaired DNA (MSUD), Quelling and Repeat-Induced Point Mutation (RIP) (Galagan et al., 2003; Freitag et al., 2002; Selker, 2002). While MSUD and Quelling serve critical roles in silencing unpaired and repetitive DNA during meiosis and vegetative growth, respectively, RIP is the most extensively studied and unique mechanism in fungi, playing a dominant role in genome defense and functional genomics (Selker, 2011; Gladyshev, 2017).

MSUD is an RNAi-related defense mechanism that operates during meiosis, silencing unpaired DNA regions to prevent their expression. This system plays a critical role in genome surveillance by detecting unpaired sequences, including transposons or structural chromosomal abnormalities and silencing them at the post-transcriptional level (Shiu et al., 2001). MSUD relies on small interfering RNAs (siRNAs) and key protein components, such as SAD-1 (an RNA-dependent RNA polymerase) and SAD-2, which facilitate the targeting and degradation of aberrant RNA molecules (Hammond et al., 2013). By preventing the expression of potentially harmful genetic elements, MSUD preserves genome integrity and ensures accurate meiosis in *N. crassa*.

Quelling is a post-transcriptional gene silencing mechanism active during vegetative growth, regulating gene expression and defending against invasive DNA elements. It functions through an RNA interference (RNAi)-based pathway triggered by the presence of multiple copies of a gene, leading to the production of double-stranded RNA (dsRNA). This dsRNA is processed by Dicer enzymes into siRNAs, which associate with the RNA-induced silencing complex (RISC) to degrade complementary mRNA molecules (Romano & Macino, 1992). Quelling serves as a defense against transposable elements and viral infections, ensuring genome stability by silencing repetitive sequences and foreign DNA (Catalanotto et al., 2002; Chicas et al., 2005). Its similarities to RNAi pathways in other eukaryotes have made *N. crassa* a valuable model for studying small RNA-mediated gene regulation.

### 1.3.1 Repeat-Induced Point mutation and its role in functional genomics

Repeat-Induced Point Mutation (RIP) is a genome defense mechanism that restricts and limits the spread of transposable elements and repetitive DNA sequences in *N. crassa* (Selker et al., 1987; Cambareri et al., 1989). By introducing cytosine-to-thymine transitions in duplicated DNA regions, RIP silences transposons and preserves genomic stability (Galagan & Selker, 2004). Given the potential for transposable elements to impair genomic integrity, *N. crassa* evolved RIP to counteract their impacts, selectively by modifying repetitive sequences and controlling genome evolution (Gladyshev, 2017). Aside from its role in genome protection, RIP is an effective genetic tool for targeted gene disruption, allowing for precise functional research in *N. crassa*. This has help researchers to study gene function and regulatory pathways by generating specific mutations (Freitag et al., 2002). This approach has contributed to research on stress responses, metabolism and cellular differentiation (Lewis et al., 2009). Furthermore, RIP-induced mutations provide insights into genome architecture and stability, enabling their broader use in functional genomics (Galagan & Selker, 2004). Similar processes to RIP have been discovered in other fungal species, highlighting its evolutionary importance (Ikeda et al., 2002; Clutterbuck, 2011). According to comparative genomic research, RIP-like mechanisms help to compress the genome by removing redundant or damaging repetitive sequences (Selker, 2011). The study of RIP has greatly increased our understanding of epigenetics, gene silencing and genome evolution, making *N. crassa* an important model organism for studying these processes (Selker et al., 2003; Gladyshev, 2017). Additionally, future applications of RIP may extend to synthetic biology and biotechnology, where controlled mutagenesis could be employed to engineer stable genetic circuits or improve industrial microbial strains (Galagan & Selker, 2004).

### 1.3.2 Mechanism of Repeat-Induced Point mutation

RIP occurs in haploid nuclei before karyogamy, during early sexual reproduction in the dikaryotic ascogenous hyphae (Selker et al., 1987). It is triggered by homologous duplicated sequences exceeding 400 base pairs in length and sharing at least 80% sequence identity (Cambareri et al., 1989; Galagan & Selker, 2004). A genome surveillance system marks these sequences before the first meiotic division, initiating cytosine deamination, which results in C:G to T:A transition mutations that disrupt gene function through nonsense and missense mutations (Gladyshev, 2017). This mutational process is mediated by RIP-deficient (RID), a cytosine methyltransferase that catalyzes the formation of 5-methylcytosine (5mC), which then

undergoes spontaneous deamination, leading to irreversible sequence alterations (Freitag et al., 2002; Lewis et al., 2009). The presence of RID is essential for RIP and its loss abolishes the process, highlighting its central role in genome defense (Selker et al., 2003). Aside from mutational inactivation, RIP causes widespread DNA methylation, which strengthens transcriptional silence and promotes heterochromatin formation (Selker, 1990; Freitag et al., 2002). These epigenetic alterations give control over transposable elements and repetitive sequences, maintaining genomic stability over generations (Lewis et al., 2009; Gladyshev, 2017). The conservation of RIP-like mechanisms across fungal species emphasizes their evolutionary significance (Ikeda et al., 2002; Clutterbuck, 2011). As a genome defense mechanism and a functional genomics tool, RIP has enhanced our understanding of gene silencing, epigenetics and transposon biology. *N. crassa* remains a key model organism for studying these processes, offering a unique system for dissecting genetic regulation and genome evolution (Galagan & Selker, 2004; Selker, 2011; Gladyshev, 2017). This mechanism of genome defense is crucial in shaping the stability and evolution of essential genes, including heat shock proteins, which play fundamental roles in protein folding, stress response and cellular homeostasis.

## 1.4 Heat Shock Proteins

### 1.4.1 The significance of heat shock proteins in biological systems

Heat shock proteins (Hsp) are a highly conserved family of molecular chaperones that play a crucial role in maintaining protein homeostasis by assisting in the proper folding of nascent polypeptides, refolding misfolded proteins and preventing the aggregation of denatured proteins. They are ubiquitously expressed across all domains of life, underscoring their evolutionary significance in cellular function and stress adaptation. Under normal physiological conditions, Hsp ensure the structural integrity and functionality of proteins whereas under stress conditions such as heat shock, oxidative stress and toxin exposure their expression is significantly upregulated to prevent proteotoxic damage. This kind of stress response is essential for cell survival as Hsp stabilize partially unfolded proteins and facilitate their refolding or degradation to maintain cellular homeostasis (Lindquist & Craig, 1988; Hartl et al., 2011). Beyond their role in protein quality control, Hsp regulate key cellular processes, including signal transduction, apoptosis and immune responses. For example, Hsp90 is essential for the stability and activation of many client proteins such as steroid hormone receptors and kinases which are crucial for cell proliferation and differentiation (Pearl &

Prodromou, 2006). Another critical function of Hsp is their role in maintaining cellular stability under fluctuating temperatures. Organisms need on precise temperature management to maintain optimal enzymatic activity and immunological function and Hsp play an important role in this process. A failure to maintain body temperature can weaken cellular defenses, making organisms more susceptible to infections by fungi, bacteria and viruses. For example, opportunistic pathogens like *Candida* spp. and many pathaogens thrive in temperature-sensitive hosts, emphasizing the role of Hsp in temperature-induced immune responses (Shapiro et al., 2009).

In addition to their intracellular roles, Hsp are directly involved in modulating immune responses by acting as antigen-presenting molecules and promoting inflammation. Hsp70 and HSP60 play key roles in immune surveillance by acting as endogenous adjuvants that stimulate both innate and adaptive immune responses (Pockley, 2003). Their ability to enhance immune activation makes them highly relevant to infection control, autoimmunity and cancer immunotherapy. However, dysregulation of HSP expression has been implicated in various diseases, including cancer, neurodegenerative disorders and cardiovascular diseases. Overexpression of Hsp90 has been linked to tumor progression which leads to its exploration as a potential target for cancer therapy, whereas reduced levels of Hsp contribute to protein misfolding diseases such as Alzheimer's and Parkinson's disease (Whitesell & Lindquist, 2005). Their role in cellular adaptation and disease pathogenesis makes Hsp promising targets for therapeutic interventions. Furthermore, Hsp' ability to regulate cellular responses to environmental stresses such as temperature fluctuations highlights their importance in maintaining physiological balance which is achieve by stabilizing proteins and supporting immune function as it helps to reduce the risks associated with infections and thermal stress. The body's ability to maintain an optimal temperature range is essential for overall health and Hsp serve as one of the key factors in protecting cells from stress-induced vulnerabilities (Pratt et al., 2015). Overall, Hsp are indispensable for maintaining cellular function, responding to environmental stresses and preventing disease, making them crucial targets for further research into disease pathology and potential therapeutic applications.

### 1.4.2 Discovery and historical perspective of Hsp

Heat shock proteins (Hsp) are a conserved class of molecular chaperones that play a crucial role in cellular homeostasis, particularly under stress conditions. The discovery of Hsp originates from the pioneering work of Ferruccio Ritossa in 1962, who observed an unusual

chromosomal 'puffing' pattern in *Drosophila melanogaster* larvae exposed to elevated temperatures (Ritossa, 1962). This phenomenon indicated the activation of a specific set of genes in response to heat stress, leading to the identification of heat shock proteins. Subsequent studies in bacteria, yeast and mammalian cells later confirmed that Hsp are a universal cellular defense mechanism triggered by various stressors (Lindquist, 1986). The discovery of heat shock factors (Hsf), transcriptional regulators that control the expression of HSP genes, provided insight into how cells rapidly respond to stress at the molecular level (Wu, 1995). Further studies revealed that Hsp not only protect cells from acute stress but also play essential roles in normal cellular functions such as protein folding, trafficking and degradation. The evolutionary conservation of Hsp across species highlighted their fundamental importance in maintaining proteostasis (Craig, 1985). By the 1990s, research expanded to include the role of Hsp in disease processes, particularly in cancer, neurodegenerative disorders and infectious diseases. Their involvement in protein misfolding diseases, such as Alzheimer's and Parkinson's, underscored their significance beyond stress response mechanisms (Morimoto, 2008). In fungal biology, Hsp gained attention for their role in thermotolerance, pathogenicity and antifungal resistance, making them critical targets for studying stress adaptation in organisms like *Candida albicans* (Cowen et al., 2009). Hsp have been identified as key components of the proteostasis network in a variety of species from bacteria to humans. These proteins facilitate proper protein folding, prevent aggregation and aid in the refolding or degradation of misfolded polypeptides (Bukau et al., 2006). Their upregulation in response to stress, including heat shock, oxidative stress and exposure to toxic chemicals which highlight their critical function in maintaining cell survival under adverse conditions (Lindquist & Craig, 1988).

### 1.4.3 Role of Hsp in protein folding and stress response

Protein homeostasis, or proteostasis, is vital for cellular function and Hsp serve as key regulators in this process. Under normal physiological conditions the newly synthesized proteins must fold correctly to achieve their functional conformation. However, during various intrinsic and extrinsic stressors, such as elevated temperatures, oxidative damage, or chemical exposure, can lead to protein misfolding and aggregation, which may disrupt cellular function and contribute to diseases (Hartl et al., 2011).

Hsp mitigate such proteotoxic stress by binding to unfolded or partially folded polypeptides, preventing their aggregation and assisting in correct folding (Mayer & Bukau, 2005). Some of

the Hsp function as ATP-dependent chaperones that actively refold damaged proteins, while others act as holdases which stabilizing misfolded intermediates until the cellular environment allows proper folding (Clerico et al., 2015). Furthermore, Hsp are also involved in protein degradation pathways by interacting with the ubiquitin-proteasome system and autophagic machinery to remove irreversibly damaged proteins (Klaips et al., 2018). In addition to proteostasis, Hsp contribute to cellular signaling, immune responses and apoptosis regulation. Their involvement in stress response pathways, such as the heat shock response and also highlights their essential role in maintaining cellular integrity. In *N. crassa*, HSP have been implicated in thermotolerance, assisting in the survival of cells exposed to fluctuating temperatures (Roy and Tamuli., 2022).

### 1.4.4 Overview of Hsp families and their functions

Hsp are classified into several families based on their molecular weight and function. Each class plays a distinct role in cellular homeostasis, ensuring that proteins maintain their correct conformation and functionality under both normal and stress conditions.

i. Small Heat Shock Proteins (15–30 kDa): Small Hsp act as ATP-independent chaperones that prevent protein aggregation by binding to misfolded substrates. They are commonly involved in stress resistance and cytoskeletal stabilization (Haslbeck et al., 2019).
ii. HSP40 (40 kDa): HSP40 proteins function as co-chaperones that regulate the activity of Hsp70 by stimulating ATP hydrolysis and substrate binding. They are crucial for the proper function of Hsp70 in protein refolding and transport (Kampinga & Craig, 2010).
iii. HSP60 (60 kDa): HSP60 family members, such as GroEL in prokaryotes and mitochondrial HSP60 in eukaryotes, form large oligomeric complexes that encapsulate unfolded proteins, providing an isolated environment for proper folding (Horwich et al., 2007).
iv. Hsp70 (70 kDa): One of the most extensively studied HSP families, Hsp70 proteins are ATP-dependent chaperones that bind transiently to unfolded proteins, preventing aggregation and facilitating refolding (Mayer, 2013). They are highly conserved across species and are upregulated during heat stress.
v. Hsp90 (90 kDa): Hsp90 plays a critical role in stabilizing and activating client proteins involved in signal transduction, cell cycle regulation and stress responses

(Taipale et al., 2010). It has been widely studied in fungi, including *N. crassa*, where it contributes to thermotolerance and stress adaptation.

vi. HSP100 (100 kDa and above): HSP100 proteins, including ClpB and Hsp104, exhibit disaggregase activity, helping to resolubilize aggregated proteins under severe stress conditions (Doyle et al., 2013). Unlike other HSP families, they possess unique properties that enable them to actively recover cells from proteotoxic damage.

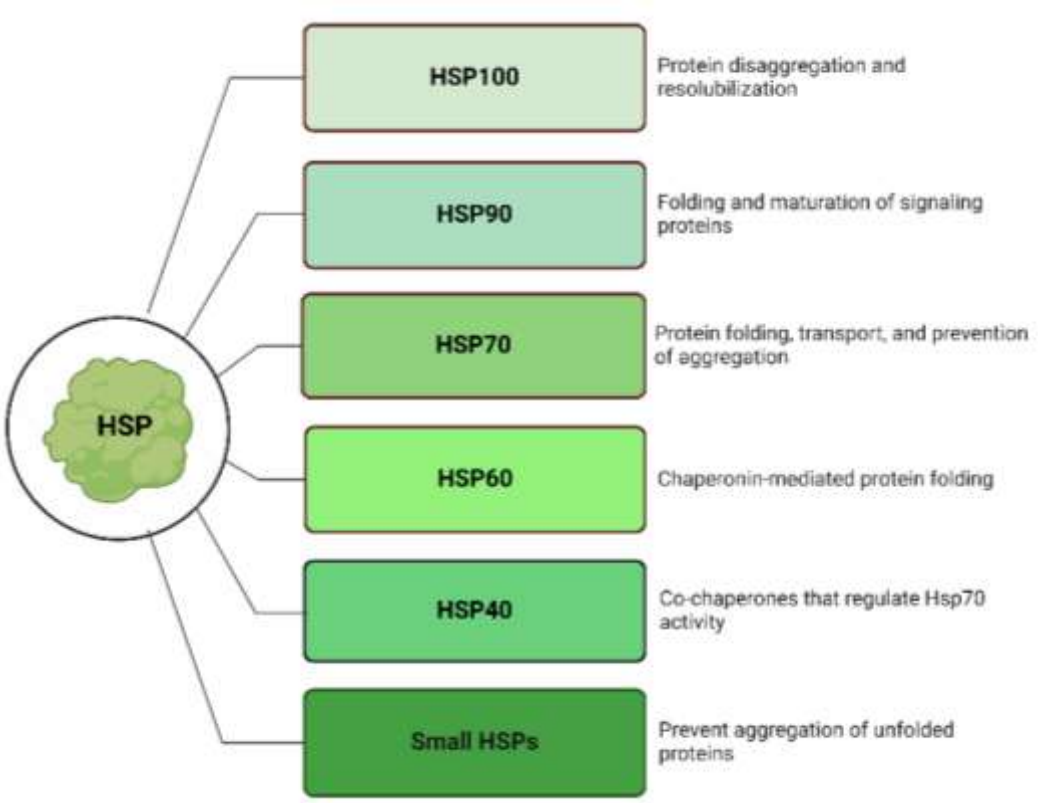


**Figure 1.2: Classification of Heat Shock Proteins.** The diagram categorizes Hsp by molecular weight, including HSP100, HSP90, HSP70, HSP60, HSP40 and small HSP These chaperones collectively maintain cellular proteostasis under stress conditions.

Together, these HSP families form an integrated network of molecular chaperones that ensure cellular homeostasis under both normal and stressful conditions **(Figure 1.2)**. In *N. crassa*, Hsp80, a member of the Hsp90 family, has been implicated in thermotolerance and calcium stress response, making it a significant target for understanding heat stress adaptation in filamentous fungi (Roy & Tamuli, 2022).

In addition to HSP-mediated protein stabilization, fungi also use a variety of different techniques to tolerate heat stress as one such strategy includes modifying membrane lipid

composition to combat the increased membrane fluidity generated by high temperatures. Fungi maintain membrane integrity and prevent cellular content leakage by adjusting the saturated fatty acid and sterol levels (Leach et al., 2012). Another key mechanism is the detoxification of reactive oxygen species (ROS), which is also build up during heat stress and causes oxidative damage to cellular components. Antioxidant enzymes such as superoxide dismutases (SODs), catalases and glutathione peroxidases play a crucial role in neutralizing ROS and protecting fungal cells from oxidative stress (Görlach et al., 2017). Protein degradation pathways also contribute to thermotolerance by removing irreversibly damaged proteins that cannot be refolded by chaperones. The ubiquitin-proteasome system (UPS) and autophagy are key mechanisms that facilitate the selective degradation of misfolded proteins and damaged organelles (Richter et al., 2010). All these pathways confiirm that cellular homeostasis is maintained even under prolonged heat stress. Furthermore, some fungi also exhibit morphological adaptations in response to high temperatures such as changes in cell wall composition or the transition between yeast and filamentous growth forms in thermally dimorphic fungi (Wang et al., 2019). Collectively, these survival strategies enable fungi to thrive in fluctuating thermal environments and maintain cellular function under heat stress conditions.

### 1.4.5 Role of Hsp and cellular adaptations in protecting against heat-induced damage

Fungi have evolved a range of mechanisms for surviving heat stress, with HSP playing a critical part in their capacity to resist extreme temperatures. These molecular chaperones contribute to maintain protein stability by preventing aggregation, facilitating proper folding and ensuring that essential regulatory proteins remain functional. Among the many HSP families, Hsp70, Hsp90 and Hsp80 are particularly crucial for fungal thermotolerance. Like, Hsp70 assists in the refolding of partially unfolded proteins and prevents aggregation by working with co-chaperones like HSP40 (Mayer, 2013). Hsp90, a highly conserved protein across eukaryotic species also stabilizes key signaling molecules and contributes to maintaining cellular homeostasis under stress (Zuehlke & Johnson, 2010). Meanwhile, Hsp80, a homolog of Hsp90 in *N. crassa* also plays a key role in thermotolerance by regulating stress response pathways and influencing the activation of heat shock factors (Hsfs) (Roy & Tamuli, 2022). Beyond Hsp, fungi rely on a broader range of cellular responses to manage heat stress. One of the primary mechanisms is the heat shock response, a highly conserved process that upregulates stress-related genes to restore cellular balance. HSR is regulated by heat shock factors (Hsfs), which

detect temperature changes and bind to heat shock elements (HSEs) in the promoters of HSP genes, rapidly increasing the production of protective chaperones (Verghese et al., 2012). These Hsp work together to prevent protein from misfolding and aggregation and allowing fungal cells to function even under extreme conditions. Fungi also modify their cellular membranes to counteract heat stress. Elevated temperatures increase membrane fluidity, which can disrupt transport processes and compromise structural integrity. To counteract this, fungi alter their lipid composition by increasing the proportion of saturated fatty acids and sterols as to enhance membrane rigidity and stability (Leach et al., 2012). This adaptation is especially important for thermotolerant and pathogenic fungi by helping them survive in high-temperature environments such as mammalian hosts.

Another challenge posed by heat stress is the accumulation of reactive oxygen species (ROS), which can cause severe oxidative damage to cellular components, including proteins, lipids and nucleic acids. In response, fungi activate antioxidant defense mechanisms by upregulating enzymes like superoxide dismutases (SODs), catalases and glutathione peroxidases so to neutralize ROS and prevent oxidative damage (Görlach et al., 2017). These responses are crucial for maintaining cellular integrity and thereby preventing apoptosis that induced oxidative stress. To further protect against heat-induced damage, fungi also rely on protein degradation and turnover mechanisms. The ubiquitin-proteasome system (UPS) identifies and eliminates misfolded proteins before they accumulate into toxic aggregates while autophagy plays a complementary role by clearing damaged proteins and organelles, recycling their components under stress conditions (Richter et al., 2010). These pathways establish the proteostasis that maintains the delicate balance between protein synthesis, folding and degradation during heat stress.

Additionally, the Hsp100 family, particularly ClpB and Hsp104 provides another layer of protection by actively disaggregating and refolding heat-damaged proteins (Doyle et al., 2013). This process is important for fungi that experience transient heat stress as it allows them to recover quickly and have a normal growth. Given the widespread role of Hsp and other adaptive mechanisms in fungal stress responses, understanding these processes has broad implications for biotechnology and antifungal drug development. Many pathogenic fungi rely on HSP-mediated mechanisms to survive within host environments by making Hsp potential targets for antifungal strategies. By disrupting fungal thermotolerance, it may be possible to weaken their ability to infect and persist in hosts. Thus, fungal thermotolerance is not governed by a single mechanism but rather by a complex interplay of molecular chaperones, stress signaling

pathways, membrane adaptations, antioxidant defenses and protein degradation systems. These mechanisms work together to maintain cellular homeostasis and protect against heat-induced damage. By further studying these adaptive responses, researchers can develop innovative approaches to enhance fungal resilience in industrial applications and combat fungal pathogens in medical settings.

### 1.4.6 Structural domains and interactions with Co-chaperones

The functional activity of Hsp90 is governed by its distinct structural domains, which enable interactions with client proteins, co-chaperones and regulatory factors. Hsp90, like other Hsp90 homologs, consists of three main domains:

i. N-terminal domain (NTD): The NTD contains an ATP-binding pocket essential for the ATPase activity of Hsp80. ATP binding and hydrolysis drive conformational changes that regulate client protein binding and release. This ATP-dependent chaperone cycle is critical for the function of Hsp90, as it enables dynamic interactions with unfolded substrates (Li et al., 2012).

ii. Middle domain (MD): The MD serves as the primary site for client protein interactions. It plays a key role in coordinating the ATPase cycle and determining substrate specificity. The MD also mediates interactions with co-chaperones that regulate Hsp80 function, including Aha1 (Activator of Hsp90 ATPase), which enhances ATP hydrolysis and p23, which stabilizes client protein complexes (Ali et al., 2006).

iii. C-terminal domain (CTD): The CTD is responsible for dimerization, a critical feature for the functional activity of Hsp90. Unlike many chaperones that function as monomers, Hsp80 exists as a constitutive homodimer, with its CTD facilitating interactions with other Hsp and co-chaperones. The CTD also contains a conserved MEEVD motif, which is recognized by tetratricopeptide repeat (TPR) domain-containing co-chaperones such as HOP (Hsp70-Hsp90 organizing protein), linking Hsp90 to the broader chaperone network (Schopf et al., 2017).


**Figure 1.3: General domain organization of Hsp90**. The schematic representation illustrates the domain architecture of Hsp90, highlighting its key functional regions. The N-terminal ATP-binding domain (blue) is responsible for ATP hydrolysis, which is essential for Hsp90's chaperone activity. Adjacent to this is the charge domain, a flexible linker that influences the conformational dynamics of Hsp90. The middle domain (green) is involved in client protein interaction and ATPase regulation. The C-terminal domain (red) is crucial for dimerization and co-chaperone binding. At the extreme C-terminus, the MEEVD motif (yellow) serves as a docking site for TPR-domain-containing co-chaperones, which regulate Hsp90 function.

The activity of Hsp90 is tightly regulated by its interactions with co-chaperones, which modulate ATPase activity, stabilize protein complexes and facilitate the transfer of substrates between different chaperone systems **(Figure 1.3)**. For example, Hsp70 acts as a "holding chaperone," delivering partially unfolded proteins to Hsp80 for final folding and activation. The co-chaperone CDC37 is particularly important for stabilizing kinases, ensuring their correct folding and functional conformation (Meyer et al., 2018). These interactions highlight the complexity of the Hsp90 chaperone cycle and its integral role in cellular protein homeostasis.

### 1.4.7 Hsp mediated regulation of stress response pathways

HSP is a central regulator of the fungal stress response, mediating protein stability, signal transduction and cellular survival under heat stress. Among the various HSP families, Hsp90 plays a crucial role in stress tolerance by interacting with key signaling proteins and modulating in stress response pathways. By ensuring proper folding and functional integrity, Hsp90 plays a pivotal role in maintaining proteostasis and facilitating cellular responses to environmental challenges. One of the primary pathways regulated by Hsp90 is the mitogen-activated protein kinase (MAPK) cascade, which governs fungal responses to diverse stressors. The MAPK pathway consists of a sequential phosphorylation cascade that transmits extracellular signals to the nucleus, activating genes essential for stress adaptation. Hsp90 stabilizes key MAPK components, preventing their degradation and ensuring efficient signal transduction. Another major pathway influenced by Hsp90 is the calcineurin signaling cascade which modulates

fungal responses to heat and osmotic stress. Calcineurin, a calcium-dependent phosphatase, orchestrates stress adaptation by regulating transcriptional programs and cell wall integrity. Hsp90 interacts with calcineurin components, promoting their stability and function. In fungal pathogens such as *Candida albicans*, inhibition of Hsp90 leads to calcineurin degradation, resulting in increased susceptibility to heat stress and antifungal agents (Cowen et al., 2009). This suggests that similar mechanisms may operate in *N. crassa*, where Hsp90-mediated stabilization of calcineurin contributes to thermotolerance and stress resilience.

Hsp90 also modulates the heat shock response by regulating the activity of heat shock factors (Hsf). Under basal conditions, Hsp90 binds to HSF, maintaining them in an inactive state. Upon heat stress, misfolded proteins compete for Hsp90 binding, leading to Hsf release and activation of *hsp* gene expression **(Figure 1.4)** (Gao et al., 2023). This feedback mechanism ensures a rapid and precise response to heat stress, allowing fungal cells to upregulate chaperone networks and restore proteostasis efficiently. Beyond its role in protein folding and stress signaling, Hsp90 influences fungal survival by modulating apoptotic and autophagic pathways. Under extreme stress conditions, fungal cells must decide whether to activate survival mechanisms or undergo programmed cell death. Hsp90 has been implicated in this decision-making process by stabilizing anti-apoptotic factors and promoting autophagy, thereby enhancing the likelihood of recovery from transient stress rather than triggering premature cell death (Richter et al., 2010). Given its multifaceted role in thermotolerance, stress adaptation and cellular homeostasis, Hsp90 serves as a crucial component of fungal survival strategies. Its involvement in regulating key signaling pathways underscores its significance in *N. crassa* and other thermotolerant fungi. Further research into Hsp90-mediated stress response mechanisms could provide valuable insights into fungal adaptation to environmental stressors and inform potential antifungal strategies targeting heat shock protein networks.

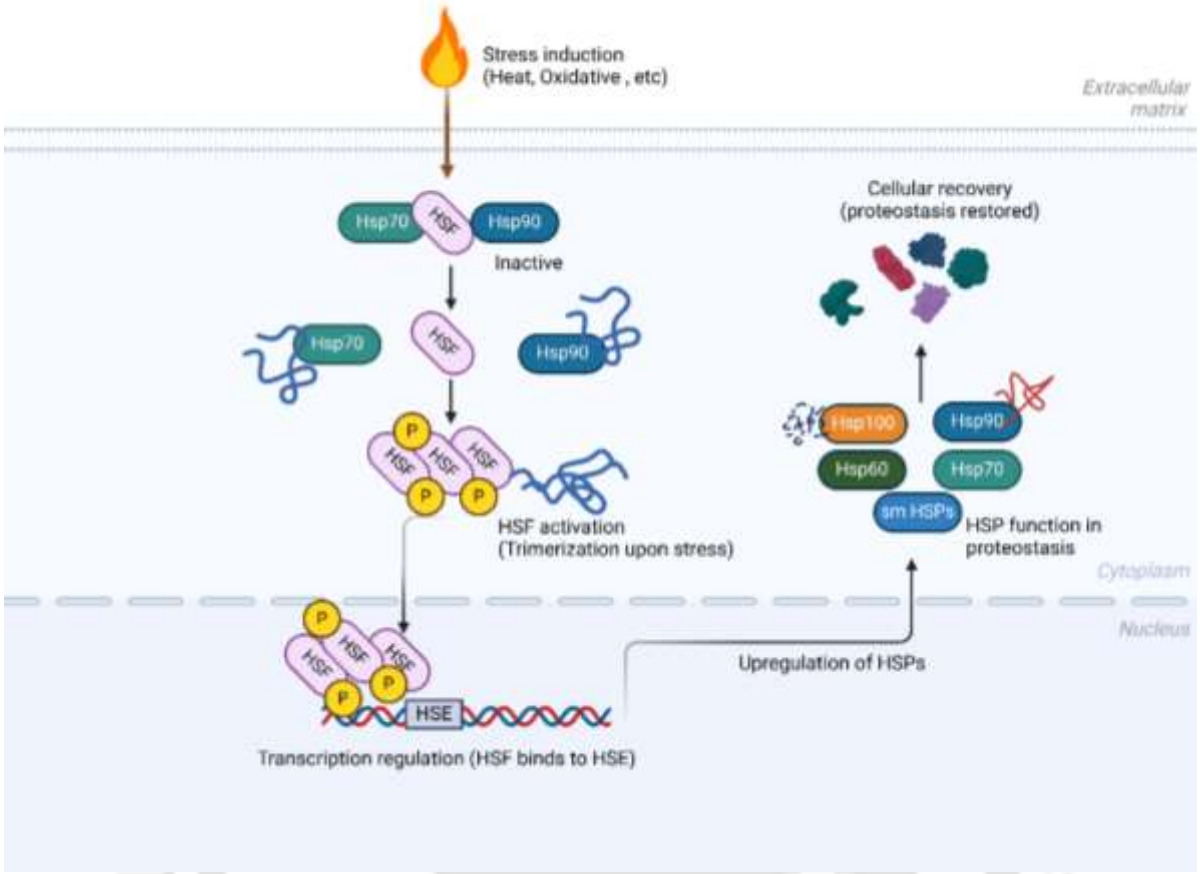


**Figure 1.4: Heat Shock Response and Hsp regulation**. This schematic illustrates the heat shock response pathway, highlighting the role of heat shock proteins (Hsp) in proteostasis. Upon stress induction (e.g., heat, oxidative stress), inactive heat shock factors (Hsf) are released from Hsp70 and Hsp90 complexes. This leads to HSF trimerization and phosphorylation, activating its binding to heat shock elements (HSE) in the nucleus. This transcriptional activation results in the upregulation of HSP genes, including Hsp100, Hsp90, Hsp70, HSP60 and small Hsp. These chaperones then restore cellular proteostasis by assisting in protein folding, disaggregation and degradation, ultimately promoting cellular recovery (adapted from Gao et al., 2023).

### 1.4.8 Heat Shock Protein networks and their crosstalk in stress response

Heat shock proteins act as an interconnected network of molecular chaperones that helps in regulating protein folding, prevent aggregation and stress recovery. Within this network Hsp80 interacts with several HSP families, forming a dynamic system that maintains cellular proteostasis in both normal and stress situations. The interaction of these Hsp is critical for maintaining protein homeostasis, especially during heat shock and other environmental challenges (Schopf et al., 2017).

Hsp90 operates in close coordination with Hsp70 and Hsp100 to facilitate protein folding, degradation and stress recovery (Zuehlke & Johnson, 2010). These interactions help proteins be refolded properly after stress exposure or ruined if irreversibly damaged. Hsp70 collaborates with Hsp90 to stabilize partially unfolded proteins, prevent aggregation and facilitate in their refolding through ATP-dependent conformational changes (Taipale et al., 2010). The co-chaperone HOP (Hsp70-Hsp90 organizing protein) bridges the two systems ensuring efficient substrate transfer and promoting effective client protein stabilization (Schopf et al., 2017). Since Hsp80 is a homolog of Hsp90, it also shares functions in signal transduction and regulatory protein stabilization, likely interacting with kinases and transcription factors involved in the fungal stress response (Roy & Tamuli, 2022).

Hsp80 does not function alone but is regulated by an array of co-chaperones that fine-tune its activity, modulate ATPase function and assist in client protein interactions. HOP (Hsp70-Hsp90 Organizing Protein) facilitates client protein transfer between Hsp70 and Hsp80 ensuring efficient substrate processing through its tetratricopeptide repeat (TPR) domains, which allow simultaneous binding to both chaperones (Wandinger et al., 2008). The co-chaperone p23 stabilizes the ATP-bound form of Hsp80, preventing premature client release and ensuring proper protein folding (McLaughlin et al., 2002; Ali et al., 2006). Aha1 (Activator of Hsp90 ATPase) enhances the ATP hydrolysis rate of Hsp80, accelerating the chaperone cycle but requiring strict regulation to prevent improper client protein folding (Panaretou et al., 2002; Meyer et al., 2018). Another important co-chaperone Cdc37, functions specifically as a kinase stabilizer, ensuring that stress-responsive kinases remain structurally intact and functional under heat stress conditions (Roe et al., 2004; Pearl & Prodromou, 2006). Hsp90 interacts with multiple co-chaperones that regulate its activity, fine-tuning the chaperone cycle and ensuring efficient protein stabilization and degradation.

Overall, Hsp90 serves as a central regulator of the fungal heat shock protein network maintaining proteostasis under extreme stress conditions. Its ability to modulate stress-responsive pathways makes it a key factor in fungal adaptation and survival. Future research into Hsp90-co-chaperone interactions and its role in fungal stress adaptation could provide deeper insights into the mechanisms of thermotolerance and identify potential targets for antifungal strategies. Understanding these molecular interactions may also have applications in industrial and biotechnological processes, where stress-resistant fungal strains are valuable for enzyme production and biofuel generation.

### 1.4.9 Role of Hsp90 in UV stress response and oxidative damage mitigation

Heat shock proteins play a crucial role in maintaining cellular homeostasis and stress response mechanisms inlcuding under ultraviolet (UV) radiation exposure, which induces DNA damage, oxidative stress and protein misfolding in organisms like *N. crassa*. Hsp90 plays a crucial role in stabilizing and regulating key proteins involved in cell survival, cell cycle control, hormone signaling and apoptosis (Hoter et al., 2018). UV exposure can lead to the formation of pyrimidine dimers, single and double-strand DNA breaks and reactive oxygen species (ROS), necessitating efficient cellular defense mechanisms. One of the critical roles of Hsp90 is its interaction with ATR (Ataxia Telangiectasia and Rad3-related protein), a key sensor of DNA damage that initiates nucleotide excision repair (NER) and homologous recombination pathways (Richter & Buchner, 2001). Hsp90 ensures the structural integrity and functionality of ATR and its associated signaling proteins, facilitating efficient DNA repair and cell survival (Pratt et al., 2008). Inhibition of Hsp90 disrupts ATR-mediated checkpoint activation, resulting in impaired DNA damage response and heightened UV sensitivity (Zou & Elledge, 2003). Furthermore, Hsp90 interacts with p53, a tumor suppressor and stress-responsive transcription factor that governs apoptosis and cell cycle arrest in response to genotoxic stress (Moll et al., 2005). By stabilizing p53 and its cofactors, Hsp90 prevents mutagenesis and ensures genomic integrity following UV-induced damage.

Beyond its role in DNA repair, Hsp90 also helps to reduce oxidative stress, which is a common side effect of UV exposure. UV radiation produces ROS, which can oxidize proteins, lipids and nucleic acids, aggravating cellular damage. Hsp90 regulates the activity of key antioxidant enzymes such as superoxide dismutase (SOD), catalase and glutathione peroxidase, preventing excessive ROS accumulation and oxidative cytotoxicity (Görlach et al., 2015). Additionally, Hsp90 facilitates the activation of heat shock transcription factors (Hsf), which upregulate stress-response genes and contribute to cellular adaptation under UV stress (Jakob et al., 1999). While Hsp90 serves as the master regulator of stress response pathways, Hsp70 and small heat shock proteins (sHsp) also contribute to UV-induced stress mitigation. Hsp70 assists in protein refolding, degradation of irreversibly damaged proteins and stabilization of NER-associated proteins, including Rad23 and XPC, which recognize and excise UV-induced DNA lesions (Chen et al., 2015). Despite Hsp90's well-established functions in heat and oxidative stress adaptation in many organism, its precise role in UV stress response within *N. crassa* is still being investigated. Given its importance in DNA repair, protein stability and oxidative stress management, Hsp90 is predicted to play a key role in the fungal response to UV radiation.

### 1.4.10 Previous studies on Hsp90 in fungal systems

Hsp90 is a highly conserved molecular chaperone essential for stress response, protein folding and signal transduction across various fungal species. In *Saccharomyces cerevisiae*, Hsp90 in has been extensively studied for its role in maintaining cellular homeostasis under stress conditions. Early studies showed that Hsp90 is essential for viability, as its deletion leads to severe growth defects and heightened sensitivity to environmental stressors (Borkovich et al., 1989). Hsp90 interacts with various client proteins, including kinases and transcription factors, to regulate pathways such as morphogenesis, stress response and antifungal resistance (Zuehlke & Johnson, 2010). Mutations affecting Hsp90 function have been linked to defects in MAPK signaling, which is crucial for heat stress adaptation (Liu et al., 1999). In *Aspergillus* sp. Hsp90 is vital in *Aspergillus* species, particularly in *Aspergillus fumigatus*, where it contributes to thermotolerance and pathogenicity. In A. fumigatus, Hsp90 is necessary for conidial germination, oxidative stress resistance and fungal virulence in mammalian hosts (Lamoth et al., 2014). Pharmacological inhibition using geldanamycin and radicicol has shown that blocking Hsp90 function impairs fungal growth and increases sensitivity to heat stress and antifungal drugs (Cowen & Lindquist, 2005). These findings ensure the role of Hsp90 beyond stress response and highlighting its importance in fungal development and survival in pathogenic settings. In *Candida albicans*, Hsp90 plays a critical role in morphogenesis by regulating the yeast-to-hyphae transition, a process crucial for virulence (Shapiro et al., 2009). Hsp90 also modulates drug resistance mechanisms, particularly in response to azole antifungals, by stabilizing essential stress-responsive kinases such as calcineurin and Hsp104 (Cowen et al., 2009). Pharmacological inhibition of Hsp90 enhances the efficacy of antifungal drugs, suggesting its potential as a therapeutic target.

Gene regulation, expression and knockout studies Hsp90 expression in fungal systems is tightly regulated by heat shock factors (Hsf) and stress-responsive transcriptional networks. In *S. cerevisiae*, the transcription factor Hsf1p activates Hsp90 expression under thermal stress, ensuring rapid cellular adaptation (Wu, 1995). In *Candida albicans*, Hsp90 expression is induced in response to antifungal treatment and environmental stressors, further reinforcing its role in fungal adaptation. Gene knockout studies have been instrumental in elucidating Hsp90 function. Conditional knockouts of Hsp90 in *S. cerevisiae* have demonstrated its essentiality for viability, with mutants exhibiting severe growth defects and impaired stress resistance (Liu et al., 1999). In *A. fumigatus*, deletion of Hsp90 results in heightened sensitivity to heat stress and antifungal drugs (Lamoth et al., 2014). Similarly, in *C. albicans*, Hsp90 knockdowns lead

to defects in hyphal formation and increased susceptibility to antifungal agents (Shapiro et al., 2009).

**Table 1: Comparative roles of Hsp90 homologs in various organisms**

| Organism | Protein | Description | References |
|---|---|---|---|
| ***Saccharomyces cerevisiae*** | Cdc37 | Essential for Hsp90-mediated maturation of protein kinases, involved in signal transduction. | Pearl & Prodromou, 2006 |
| ***Arabidopsis thaliana*** | Sgt1 | Regulates Hsp90 function in signal transduction pathways and fungal stress responses. | Hubert et al., 2009 |
| ***Aspergillus fumigatus*** | PkcA (Protein Kinase C) | Hsp90 stabilizes PkcA, ensuring proper signal transduction under stress conditions. | Silva et al., 2020 |
| ***Candida albicans*** | Sgt1 | Physically interacts with Hsp90 and Cyr1, facilitating proper signal transduction. | Bauer et al., 2012 |
| ***Neurospora crassa*** | Sti1 (Stress-Inducible Protein 1) | Acts as an adaptor linking Hsp70 and Hsp90, essential for the formation of the functional chaperone complex. | Zhang et al., 2016 |
| ***Homo sapiens*** | HOP (STIP1) | Acts as an adaptor linking Hsp70 and Hsp90, facilitating the transfer of client proteins between these chaperones. | Odunuga et al., 2004 |
| ***Homo sapiens*** | CHIP | Regulates protein degradation by directing chaperone-bound substrates toward ubiquitination and proteasomal degradation. | Connell et al., 2001 |
| ***Homo sapiens*** | Aha1 | Directly interacts with Hsp90 to promote its ATP turnover, facilitating client protein activation. | Panaretou et al., 2002 |

| | | | |
|---|---|---|---|
| ***Homo sapiens*** | p23 | Stabilizes the Hsp90-client complex by preventing premature ATP hydrolysis. | McLaughlin et al., 2002 |
| ***Homo sapiens*** | FKBP51 | Immunophilin that modulates steroid receptor-Hsp90 interactions and regulates signaling pathways. | Davies et al., 2002 |

### 1.4.11 Evolutionary conservation of Hsp90 across fungal species

While its specific function in *N. crassa* is still being explored, comparative studies across fungal species suggest that Hsp80 shares significant structural and functional similarities with Hsp90 homologs in other fungi such as *Saccharomyces cerevisiae, Aspergillus fumigatus* and *Candida albicans*. These homologs participate in thermotolerance, cellular stress regulation and the stabilization of key regulatory proteins thus making Hsp80 an essential component of fungal stress responses (Taipale et al., 2010). The primary sequence of Hsp80 in *N. crassa* shares high sequence identity with other fungal Hsp90 proteins particularly in the ATP-binding domain, middle domain and C-terminal domain. This conservation shows highlights of Hsp80's fundamental role in maintaining protein stability and cellular function in an organism. In *S. cerevisiae*, the Hsp90 homolog interacts with numerous client proteins assisting in protein folding, degradation and signaling pathways (Zuehlke & Johnson, 2010). Similarly, in *A. fumigatus*, Hsp90 is required for growth under heat stress suggesting that Hsp80 in *N. crassa* may also contribute to fungal survival under fluctuating temperatures.

Despite strong sequence conservation, functional differences exist between Hsp80 in *N. crassa* and its homologs in other fungi. In pathogenic fungi such as *C. albicans*, Hsp90 is directly involved in drug resistance and virulence, stabilizing key stress response pathways like calcineurin signaling (Cowen & Lindquist, 2005). While *N. crassa* is non-pathogenic, Hsp80 likely plays a similar role in stress signaling but without direct involvement in host-pathogen interactions. Unlike *A. fumigatus*, which must survive in host environments *N. crassa* primarily colonizes decaying organic matter and must adapt to rapid environmental shifts. This suggests a greater emphasis on Hsp80-mediated proteostasis for responding to external stresses such as heat and oxidative damage.

The conservation of Hsp80 across fungal species demonstrates its importance in cellular stress response and protein folding. Evolutionary adaptations may have enabled Hsp80 homologs in

various fungi to tailor their activities to certain ecological contexts. Studying Hsp80 in *N. crassa* can shed light on how filamentous fungus regulate stress responses at the molecular level with possible uses in fungal biotechnology and stress resistance studies.

### 1.4.12 Functional roles and importance of Hsp80 in *N. crassa*

Heat shock proteins function as a coordinated network of molecular chaperones, ensuring protein homeostasis and cellular stress adaptation. In *N. crassa*, multiple HSP families including Hsp70, Hsp90, Hsp100 and small Hsp contribute to these processes. However, Hsp80 stands out due to its critical role in thermotolerance, cellular regulation and fungal survival mechanisms making it the focus of this study. Hsp80 is a homolog of the highly conserved Hsp90 family, which serves as a central regulator of stress responses across eukaryotes. Unlike Hsp70 which primarily aids in early-stage protein folding or Hsp100 which facilitates protein disaggregation, Hsp80 plays an active role in stabilizing and refolding stress-sensitive proteins. It is particularly crucial in heat stress adaptation where it prevents protein denaturation and maintains cellular function under stress condition (Roy & Tamuli, 2022).

Beyond thermotolerance, Hsp80 is likely involved in key signal transduction pathways that regulate fungal stress responses. Similar to Hsp90 in other fungi, it is hypothesized to stabilize kinases, transcription factors and regulatory proteins necessary for environmental adaptation (Cowen & Lindquist, 2005). Its potential interaction with calcineurin a calcium-dependent phosphatase involved in osmotic and thermal stress resistance, suggests a broader role in fungal stress survival (Liu et al., 2009). Another reason for prioritizing Hsp80 is its role in fungal development and morphogenesis. Studies in other fungi show that loss-of-function mutations in Hsp90 homologs lead to defects in conidiation, mycelial growth and stress resistance (Borkovich et al., 2004) suggesting that Hsp80 may be essential for similar developmental processes in *N. crassa*. While other HSPs contribute to general protein homeostasis, Hsp80 appears to have a specialized function in fungal growth regulation. Furthermore, studying Hsp80 in *N. crassa* has broader implications for antifungal research. Many fungal pathogens, including *Candida albicans* and *Aspergillus fumigatus*, rely on Hsp90 for virulence, drug resistance and host adaptation (Cowen et al., 2009). Given the evolutionary conservation of Hsp90-family chaperones, insights from *N. crassa* may contribute to understanding stress adaptation in pathogenic fungi and aid in developing HSP-targeted antifungal therapies. By focusing on Hsp80, this study aims to uncover its regulatory mechanisms, client protein

interactions and role in fungal resilience providing valuable insights into both basic fungal biology and potential biotechnological applications.

### 1.4.13 Hsp80 and its role in cellular stress survival

Among various HSPs, the Hsp90 family of which fungal Hsp80 is a key ortholog functions at the center of protein quality control, facilitating the folding of nascent peptides, stabilizing partially folded or misfolded proteins and targeting irreversibly damaged proteins for degradation. In response to stress stimuli such as elevated temperatures, Hsp90 expression is rapidly upregulated, enhancing the cell's ability to preserve the structure and function of essential proteins. Proteomic studies have shown that temperature stress triggers a substantial reorganization of fungal protein expression, with Hsp90 and its co-chaperones among the most prominently induced molecules (Bakar, 2020). In *Candida albicans*, Hsp90 has been demonstrated to regulate not only thermal tolerance but also antifungal resistance and morphological plasticity, highlighting its multi-faceted role in fungal stress adaptation (Iyer & Cowen, 2022). These findings are supported by recent reviews that describe Hsp90 as a central stress-response regulator, especially in pathogens that frequently encounter host-induced stresses. Beyond heat shock, Hsp90 is also critically involved in mediating survival under oxidative, chemical, and nutrient stress. It contributes to redox balance by stabilizing antioxidant proteins and buffering oxidative damage during conditions of elevated reactive oxygen species (Neves-da-Rocha et al., 2023). Moreover, across eukaryotic systems including plants and fungi, Hsp90 family proteins are implicated in cold, osmotic and salinity stress tolerance, underscoring their conserved and broad-spectrum role in abiotic stress responses (Sadura & Janicka, 2024). Hsp80 is also involved in long-term stress adaptation by supporting memory-like responses through interactions with signaling pathways, transcriptional regulators and co-chaperones. A recent study demonstrated that environmental $CO_2$ levels can potentiate antifungal drug efficacy by interfering with Hsp90 function, further emphasizing its relevance in stress driven cellular outcomes (Rosiana et al., 2024). At a systems level, Hsp90-family proteins are recognized not only for their client-specific functions but also for their network-level influence on evolvability, signal buffering and long-term proteome stability (Somogyvári et al., 2022). Together, these findings position Hsp80 as a fundamental component of the cellular defense system orchestrating both immediate and adaptive responses to a wide array of environmental challenges.

## 1.5 Objectives of the Study

This study aims to investigate the molecular regulation, functional role and computational modeling of Hsp80 in *Neurospora crassa*, focusing on its involvement in thermotolerance, stress adaptation and structural dynamics. The key objectives of this study are:

**(i)** Investigating the role of the *hsp80* gene regulation in thermotolerance in *Neurospora crassa*.

**(ii)** Cell-function of the *hsp80* gene for survival under various stress conditions in *N. crassa*.

**(iii)** In-silico analysis and molecular dynamics simulations of *N. crassa* HSP80.

# Chapter 2

# MATERIALS AND METHODS

# CHAPTER 2

# MATERIALS AND METHODS

## 2.1 Materials

### 2.1.1.1 Chemicals and reagents

The chemicals and reagents utilized in this study are listed in **Table 2.1**. Glassware and plasticware were sourced from Borosil (Mumbai, India) and Jain Scientific Glassworks (Ambala, India). Plasticware materials were procured from Genaxy (New Delhi, India) and Tarsons (Kolkata, India).

**Table 2.1: Chemicals and reagents used in this study**

| SI. No. | Chemical | Chemical Formula | Make | Cat. No. |
|---|---|---|---|---|
| 1 | L-Arginine | C6H14N4O2 | HIMEDIA | PCT0302-25G |
| 2 | Luria Bertani Broth | - | HIMEDIA | M1245-500G |
| 3 | Luria Bertani Agar | - | HIMEDIA | M1151-500G |
| 4 | SOC Growth Medium | - | HIMEDIA | G015-500G |
| 5 | Agar Powder | - | HIMEDIA | GRM026-500G |
| 6 | Peptone | - | HIMEDIA | RM001-500G |
| 7 | Yeast Extract | - | SRL | 34266 |
| 8 | Skim Milk Powder | - | HIMEDIA | M530-500G |
| 9 | Silica Gel | - | SIGMAALDRICH | 214426-1KG |
| 10 | D-Glucose | C6H12O6 | SRL | 42738 |
| 11 | Sodium chloride | NaCl | HIMEDIA | GRM853-500G |
| 12 | Potassium chloride | KCl | TITAN | 386 |
| 13 | Citric Acid Monohydrate | C6H8O7.H2O | SRL | 0348216 |

| | | | | |
|---|---|---|---|---|
| 14 | Zinc Sulphate Heptahydrate | ZnSO4.7H2O | SRL | 264745 |
| 15 | Copper Sulphate | CuSO4.5H2O | SRL | 0347102 |
| 16 | Manganous Sulphate | MnSO4.H2O | Qualigens | 25255 |
| 17 | Boric Acid | H3BO3 | SRL | 0244112 |
| 18 | Sodium Molybdate | Na2MoO4.2H2O | SRL | 1947166 |
| 19 | Sodium Citrate | Na3C6H5O7.2H2O | HIMEDIA | GRM255-500G |
| 20 | Ammonium Nitrate | NH4.NO3 | Fisher Scientific | 21445 |
| 21 | Magnesium Sulphate | MgSO4.7H2O | Fisher Scientific | 18955 |
| 22 | Calcium Chloride | CaCl2.2H2O | SRL | 0349152 |
| 23 | D-Biotin | C10H16N2O3S | SRL | 0248120 |
| 24 | Potassium Nitrate | KNO3 | TITAN | 761 |
| 25 | di-Potassium Hydrogen Phosphate | K2HPO4 | HIMEDIA | GRM1045-500G |
| 26 | Potassium Dihydrogen Orthophosphate | KH2PO4 | HIMEDIA | GRM249-500G |
| 27 | Calcium D-panthonate | C9H16O5N.1/2Ca | HIMEDIA | CMS178-100G |
| 28 | Ethidium Bromide | C21H20N3Br | SRL | 054817 |
| 29 | EDTA | C10H16N2O8 | SRL | 18240 |
| 30 | Formaldehyde | CH2O | SRL | AS017-500ML |
| 31 | Ethanol | C2H5OH | Merck | 1.00983.0511 |
| 32 | Chloroform | CHCl3 | HIMEDIA | AS040-500ML |
| 33 | Acetone | C3H6O | SRL | 11340 |
| 34 | DEPC | C6H10O5 | SRL | 46791 |
| 35 | Lithium Chloride | LiCl | SRL | 76359 |
| 36 | Sorbitol | C6H14O6 | SRL | 14281 |
| 37 | APS | N2H8S2O8 | SRL | 0148134 |

| | | | | |
|---|---|---|---|---|
| 38 | Bathocuproinedisulfonic acid disodium salt (BCS) | C26H18N2Na2O6S2 | SIGMA | B1125-1G |
| 39 | Dimethyl pimelimidate dihydrochloride (DMP) | [CH3OC(NH)CH2CH2]2 CH2•2HCl | SIGMA | D8388-250MG |
| 40 | Sodium Lauryl Sulphate (SDS/SLS) | C12H25SO4Na | SRL | 194821 |
| 41 | Bromophenol Blue | C19HBrO5S | SRL | 0240168 |
| 42 | Sodium Hydroxide Pellets | NaOH | TITAN | 439 |
| 43 | Tris Buffer | C4H11NO3 | RANKEM | T0350 |
| 44 | EGTA | C14H24N2O10 | HIMEDIA | MB130-10G |
| 45 | MOPS Buffer | C7H15NO4S | SRL | 69824 |
| 46 | PIPES buffer | C8H18N2O6S2 | HIMEDIA | RM659-25G |
| 48 | DTT | C4H10O2S2 | SRL | 17315 |
| 49 | Sodium Bicarbonate | NaHCO3 | SRL | 89399 |
| 50 | Hydrogen Peroxide | H2O2 | MERCK | 61765305001730 |
| 51 | Glycine | C2H5NO2 | SRL | 69422 |
| 52 | Sorbose | C6H12O6 | LOBA Chemie | 0607700025 |
| 53 | PMSF | C7H7FO2S | SRL | 329-98-6 |
| 54 | Cetyltrimethylamonium Bromide (CTAB) | C19H42NBr | aMResco | 0833-500G |
| 55 | Diethyl ether | C4H10O | SRL | 60-29-7 |
| 56 | Triethanolamine | C6H16NO3 | HIMEDIA | AS117-500ML |
| 57 | Isopropanol | C3H8O | SRL | 62986 |
| 58 | Acrylamide | C3H5NO | SRL | 89314 |
| 59 | N, N'-Methylene Bisacrylamide | C7H10N2O2 | SRL | 38516 |

| | | | | |
|---|---|---|---|---|
| 60 | BHT (Butylated Hydroxytoluene) | C15H24O | SRL | 82010 |
| 61 | n-Hexane | C6H14 | SRL | 12534 |
| 62 | Petroleum ether 40-60 °C | - | SRL | 26440 |
| 63 | N-Phenyl-1-napthylamine | C10H7NHC6H5 | SIGMAALDRICH | 104043 |
| 64 | Methanol | CH3OH | MERCK | 1.95416.2521 |
| 65 | Hydrochloric Acid | HCl | HIMEDIA | AS003-500ML |
| 66 | Dimethyl Sulfoxide (DMSO) | C2H6OS | MERCK | 67-68-5 |
| 67 | PIPES | C8H18O6S2 | HIMEDIA | RM659-25G |
| 68 | Phenol:Chloroform:Isoamyl Alcohol (25:24:1) | - | SRL | 69031 |
| 69 | Amersham Hybond-LFP | - | GE Healthcare | RPN303LFP |
| 70 | Calcofluor White Stain | - | SIGMAALDRICH | 18909-100ML-F |
| 71 | FPIC | - | SIGMA | P8215-1ML |
| 72 | TRIzol Reagent | - | Life Technology | 15596018 |
| 73 | NPN-40 | - | HIMEDIA | MB143-100ML |
| 74 | Tween 20 | - | HIMEDIA | PCT1310-500ML |
| 75 | Tween 80 | - | MERCK | 61771205001730 |
| 78 | Ampicillin | C16H18N3NaO4S | HIMEDIA | 000266713 |
| 79 | L-Histidine | C6H9N3O2 | HIMEDIA | GRM050 |
| 80 | Tryptophan | C11H12N2O2 | HIMEDIA | GRM067 |

### 2.1.2 Organisms and strains

#### 2.1.2.1 Neurospora crassa strains

The *N. crassa* strains used in this study were either obtained from the Fungal Genetics Stock Center (FGSC, University of Missouri, Kansas City, MO 64110; McCluskey 2003; McCluskey et al. 2010) or generated in our laboratory (**Table 2.2**).

**Table 2.2: *N. crassa* strains used in this study**

| Sl. No. | Strain Name | Strain Type or NCU no. | Genotype | Source |
|---|---|---|---|---|
| 1 | 74-OR23-IVA | Wild Type | Wild type; *mat A* | FGSC 2489 |
| 2 | ORS-SL6a | Wild type | Wild type; *mat a* | FGSC 4200 |
| 3 | *his-3* | Histidine auxotroph | *his-3; mat A* | FGSC 6032 |
| 4 | N83 Y2198 | Tryptophan auxotroph | *tol trp-4; mat a* | FGSC 2337 |
| 5 | T-9 A | Heterokaryon | *Pccg-1::hsp80:: mcherry::6X his; mat A* | Our laboratory (This study) |
| 6 | T-42 A | Homokaryon | *Pccg-1::hsp80:: mcherry::6X his; mat A* | Our laboratory (This study) |
| 7 | T-11 a | Homokaryon | *Pccg-1::hsp80:: mcherry::6X his; mat* | Our laboratory (This study) |
| 8 | R4 A | Homokaryon, RIP strain | *Pccg-1::hsp80RIP:: mcherry::6X his; mat A* | Our laboratory (This study) |
| 9 | R6 A | Homokaryon RIP strain | *Pccg-1::hsp80RIP:: mcherry::6X his; mat A* | Our laboratory (This study) |
| 10 | R9 a | Homokaryon RIP strain | *Pccg-1::hsp80RIP:: mcherry::6X his; mat a* | Our laboratory (This study) |
| 11 | R14 a | Homokaryon RIP strain | *Pccg-1::hsp80RIP:: mcherry::6X his; mat a* | Our laboratory (This study) |

#### 2.1.2.2 Bacterial strains

The *Escherichia coli* DH5α strain (SupE44 ΔlacU169 (φ80lacZ ΔM15) hsdR17 recA1 endA1 gyrA96 thi-1 relA1) was used for bacterial cloning, plasmid transformation, growth and isolation, following standard methods (Sambrook & Russell, 2001).

### 2.1.2.3 **Plasmid** vector (pTLS88F)

The plasmid vector pTLS88F (8,887 bp) was obtained from the laboratory of Maria Celia Bertolini, Department of Biochemistry and Organic Chemistry, São Paulo State University, Brazil. It is designed for molecular cloning and gene expression studies in *Neurospora crassa*. The plasmid carries the mCherry-Nc gene (5013–5717 bp), encoding the mCherry fluorescent protein, along with a 6x His-tag for protein purification **(Figure 2.1)**. The mCherry stop codon is located at 5742–5744 bp, ensuring proper translation termination. A key regulatory element in pTLS88F is the ccg-1 promoter (4060–4979 bp), which is inducible under stress or glucose deprivation conditions, allowing controlled gene expression. For bacterial selection, the plasmid contains a β-lactamase gene (468–1327 bp), conferring ampicillin resistance, while 5′ and 3′ his-3 flanking sequences (6947–8887 bp and 2374–4005 bp, respectively) enable homologous recombination at the his-3 locus, facilitating targeted genomic integration. The mCherry reporter system in pTLS88F is based on improved fluorescent protein designs, enhancing brightness and stability for imaging applications. The vector also provides multiple restriction sites, including PacI, XbaI and NotI, allowing efficient cloning and genetic modifications.

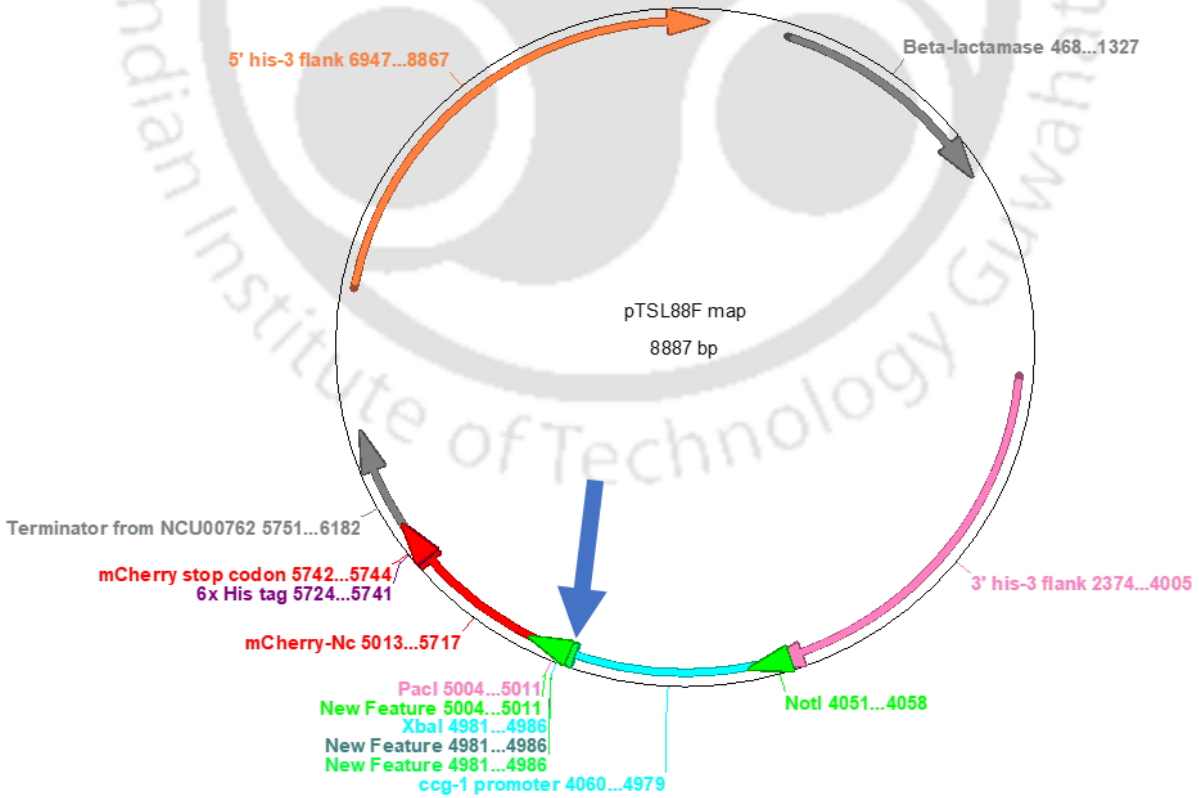


**Figure 2.1: Schematic representation of pTSL88F vector.** The pTSL88Fvector is 8.8 kb in size, it consists of unique restriction sites at the MCS region.

### 2.1.3 Media for Bacterial growth, antibiotics and commonly used reagents

1. **Bacterial Media:** Various bacterial growth media, including Luria Bertani (LB) broth, LB Agar, Terrific broth, SOB and SOC media, were procured from Himedia (Mumbai, India). These media were prepared by dissolving in water as per the manufacturer's instructions and sterilized through autoclaving.
2. **Ampicillin:** A 100 mg/ml stock solution was prepared by dissolving 200 mg of ampicillin in 2 ml autoclaved water and stored at -20 °C in 200 µl aliquots.
3. **Hygromycin B:** A 50 mg/ml ready-to-use solution of hygromycin was obtained from Himedia (Mumbai, India).
4. **1 M Sorbitol:** 18.21g sorbitol was dissolved in distilled water, the volume was adjusted to 100 ml, sterilized by autoclaving and stored at 4 °C.
5. **1 M Glycine:** 7.5g of glycine was dissolved in 70 ml distilled water, volume adjusted to 100 ml and stored at room temperature.
6. **8 M Lithium Chloride (LiCl):** A 100 ml solution was prepared by dissolving 33.9g LiCl in DEPC-treated sterile distilled water, sterilized via autoclaving and stored.
7. **3 M Sodium Acetate (pH 5.2)**: 24.61g sodium acetate was dissolved in 70 ml distilled water, pH adjusted to 5.2 with glacial acetic acid and the final volume set to 100 ml.
8. **5 M Calcium Chloride ($CaCl_2.2H_2O$)**: 36.7g $CaCl_2$ was dissolved in 50 ml distilled water, sterilized by autoclaving and stored.
9. **2 M Potassium Chloride (KCl)**: A 100 ml solution was prepared by dissolving 14.9g KCl in 80 ml distilled water, adjusted to final volume and stored at room temperature.
10. **10 N Sodium Hydroxide (NaOH):** 40g NaOH pellets were slowly dissolved in 80 ml distilled water while placed on ice. The final volume was adjusted to 100 ml and the solution was stored at room temperature.
11. **Ethidium Bromide (EtBr):** A 10 mg/ml stock was prepared by dissolving 10mg EtBr in 1 ml distilled water, stored at 4 °C.

12. **6X Gel Loading Buffer (Type III):** A solution containing 0.25% (w/v) bromophenol blue, 30% glycerol and 0.25% (w/v) xylene cyanol was dissolved in sterile water and stored at 4 °C.

13. **1X TE Buffer:** Prepared by combining 10 mM Tris-HCl (pH 8.0) and 1 mM EDTA (pH 8.0), stored at 4 °C.

14. **50X TAE Buffer:** 242 g Tris base was dissolved in 600 ml distilled water, followed by 57.1 ml glacial acetic acid and 100 ml 0.5 M EDTA (pH 8.0). The final volume was set to 1 L, stored at 4 °C.

15. **10X MOPS electrophoresis buffer:** To prepare 10X MOPS stock solution, 4.18g of MOPS was dissolved in 40 ml of DEPC-treated water, the pH was adjusted to 7.0 with 2 N NaOH, then 2 ml of 1 M sodium acetate solution (20 mM) and 2 ml of 0.5 M EDTA pH 8.0 (10 mM) were added. The final volume was then adjusted to 100 ml with DEPC-treated water. The solution was filter sterilized using a 0.45 µm syringe filter (HIMEDIA, SF182E) and stored in the dark at room temperature.

16. **0.5 M PIPES buffer (pH 6.7):** To prepare 0.5 M PIPES buffer (pH 6.7), 1.5 g PIPES was dissolved in 5 ml sterile distilled water, pH was adjusted to 6.7 by adding 10 N NaOH solution, the final volume was adjusted to 10 ml. The solution was sterilized using 0.45 µm syringe filter (HIMEDIA, SF182E) and stored at −20 °C.

17. **10% Sodium Dodecyl Sulfate (SDS):** 10 g SDS was dissolved in 70 ml sterile distilled water, stirred at 60 °C for 30-40 minutes, then adjusted to 100 ml total volume and stored at room temperature.

18. **1 M Magnesium Chloride ($MgCl_2$):** 20.33g $MgCl_2.6H_2O$ was dissolved in 80 ml distilled water, volume adjusted to 100 ml, sterilized and stored at room temperature.

19. **1 M Tris-HCl (pH 7.5 & 8.0):** 12.11g Tris base was dissolved in 70 ml distilled water, pH adjusted to 7.5 or 8.0 using HCl, volume adjusted to 100 ml, autoclaved and stored at 4 °C.

20. **1.5 M Tris-HCl (pH 8.8):** 18.17g Tris base was dissolved in 70 ml distilled water, pH adjusted to 8.8 and volume set to 100 ml before autoclaving and storage at 4 °C.

21. **0.5 M EDTA (pH 8.0):** 18.61g EDTA was dissolved in 70 ml distilled water, pH adjusted to 8.0 with NaOH, final volume set to 100 ml, sterilized and stored at 4 °C.

22. **Lysis Buffer for *N. crassa* DNA Isolation**: Contains 10 mM Tris-HCl (pH 7.5), 0.5 M NaCl, 10 mM EDTA, 1% SDS and 1% CTAB.

23. **Lysis Buffer for DNA Isolation:** This buffer was composed of **10 mM Tris-HCl (pH 7.5), 0.5 M NaCl, 10 mM EDTA, 1% SDS and 1% CTAB**, providing optimal conditions for genomic DNA extraction.
24. **RNA Isolation Lysis Buffer for *N. crassa*:** This buffer consisted of **100 mM Tris-HCl (pH 8.0), 0.6 M NaCl, 10 mM EDTA (pH 8.0), 4.5% SDS and 2% β-mercaptoethanol**, which aided in RNA extraction by lysing cells and inhibiting RNase activity.
25. **0.5 M Tris-HCl (pH 6.8): 6.06g Tris base** was dissolved in **80 ml distilled water**, the pH was adjusted to **6.8** using **HCl** and the final volume was set to **100 ml**. The solution was sterilized by autoclaving and stored at **4 °C**.
26. **0.5 M EGTA (pH 8.0): 19.017g EGTA** was dissolved in **60 ml sterile water** and the pH was adjusted to **8.0** by adding **NaOH pellets**. The final volume was set to **100 ml**, followed by autoclaving and storage at **4 °C**.
27. **10X MOPS Buffer: 4.18g MOPS** was dissolved in **70 ml DEPC-treated water**, followed by the addition of **2 ml 1 M Na-acetate solution (20 mM) and 2 ml 0.5 M EDTA (10 mM)**. The pH was adjusted to **7.0** using **10 N NaOH** and the final volume was set to **100 ml**. The solution was sterilized using a **0.45 µm syringe filter** and stored in an **amber reagent bottle** to protect from light.
28. **0.5 M PIPES Buffer (pH 6.7): 1.5g PIPES** was dissolved in **6 ml distilled water** and the pH was adjusted to **6.7** by adding **10 N NaOH**. The final volume was set to **10 ml**, filtered through a **0.45 µm syringe filter** and stored at **-20 °C**.
29. **1 M HEPES Buffer (pH 7.5): 2.38g HEPES** was dissolved in **6 ml distilled water** and the pH was adjusted to **7.5** using **10 N NaOH**. The final volume was set to **10 ml**, sterilized by filtration and stored at **-20 °C**.

30. **10X TBE Buffer (pH 8.0): 10.8g Tris base** and **5.5 g boric acid** were dissolved in **50 ml distilled water**, followed by the addition of **4 ml 0.5 M EDTA (pH 8.0)**. The final volume was adjusted to **100 ml** and stored at **room temperature**.
31. **100 mM DTT: 0.30g DTT** was dissolved in **2 ml of 100 mM HEPES buffer (pH 7.5)**. The solution was stored at **-20°C** in the dark to prevent oxidation.
32. **0.5 M $NaHCO_3$: 0.21g $NaHCO_3$** was dissolved in **8 ml distilled water** and the final volume was set to **10 ml**. The solution was stored at **room temperature**.
33. **10% Sodium Deoxycholate: 1g sodium deoxycholate** was dissolved in **8 ml distilled water**, volume adjusted to **10 ml** and stored at **room temperature**.
34. **Alkaline Lysis Solution I:** This solution consisted of **50 mM glucose, 25 mM Tris-Cl (pH 8.0) and 10 mM EDTA (pH 8.0)**, was autoclaved and stored at **4 °C**.
35. **Alkaline Lysis Solution II:** This freshly prepared solution contained **0.2 N NaOH and 1% SDS** and was prepared just before use to maintain effectiveness.
36. **Alkaline Lysis Solution III:** Prepared by mixing **60 ml of 5 M potassium acetate, 11.5 ml glacial acetic acid and 23.5 ml distilled water**, with the final volume adjusted to **100 ml**. The solution was autoclaved and stored at **4 °C**.
37. **Lysis Buffer for RNA Extraction from *N. crassa*:** This buffer contained **100 mM Tris-HCl (pH 8.0), 0.6 M NaCl, 10 mM EDTA (pH 8.0), 4.5% SDS and 2% β-mercaptoethanol**, ensuring effective RNA isolation**.**
38. **L-Histidine:** From a stock of 50 mg/ml, 2 ml per 100 ml medium is added. The stock solution of L-Histidine was autoclaved and stored at 4 °C.

### 2.1.4 Solutions for growth, maintenance and crossing of *N. crassa* strains

#### (i) Biotin solution

A 5 mg stock solution of biotin was prepared by dissolving it in 100 ml of 50% (v/v) ethanol. The solution was stored at 4°C for long-term use.

#### (ii) Trace element solution

The trace element solution was prepared by sequentially dissolving the required components in 90 ml of distilled water while stirring continuously. The final volume was adjusted to 100 ml and 1 ml of chloroform was added as a preservative. The solution was stored at 4°C.

| Component | Amount |
|---|---|
| $C_6H_8O_7 \cdot H_2O$ | 5.00 g |
| $ZnSO_4 \cdot 7H_2O$ | 5.00 g |
| $Fe(NH_4)_2(SO_4)_2 \cdot 6H_2O$ | 1.00 g |
| $CuSO_4 \cdot 5H_2O$ | 0.25 g |
| $MnSO_4 \cdot H_2O$ | 0.05 g |
| $H_3BO_3$ | 0.05 g |
| $Na_2MoO_4 \cdot 2H_2O$ | 0.05 g |

**(iii) Vogel's Medium N (VGN)**

A 50× stock solution of Vogel's Medium N was prepared by sequentially adding all required components into 75 ml of distilled water with constant stirring. The final volume was adjusted to 100 ml and chloroform was added as a preservative.

| Component | Amount |
|---|---|
| $Na_3C_6H_5O_7 \cdot 2H_2O$ | 12.5 g |
| $KH_2PO_4$ | 25 g |
| $NH_4NO_3$ | 10 g |
| $MgSO_4 \cdot 7H_2O$ | 1 g |
| $CaCl_2 \cdot 2H_2O$ (pre-dissolved in 5 ml $H_2O$) | 0.5 g |
| Biotin Solution | 500 µl |
| Trace Element Solution | 500 µl |

**(vi) 4X Synthetic Crossing Medium (SCM)**

A 4X stock solution of Synthetic Crossing Medium was prepared by sequentially dissolving the required components in 80 ml of distilled water with constant stirring. The final volume was adjusted to 100 ml and the solution was sterilized by autoclaving.

| Component | Amount / Concentration |
|---|---|
| $KNO_3$ | 0.4 g |
| $K_2HPO_4$ | 0.28 g |
| $KH_2PO_4$ | 0.2 g |

| | |
|---|---|
| $MgSO_4 \cdot 7H_2O$ | 0.2 g |
| $CaCl_2 \cdot 2H_2O$ | 40 mg |
| NaCl | 40 mg |
| Biotin Solution | 20 µl |

**(v) SCM agar**

SCM Agar was prepared by combining a 1× concentration of SCM with 1.5% (w/v) glucose and 1.5% (w/v) agar.

| Component | Amount / Concentration |
|---|---|
| SCM | 1X |
| Glucose | 1.5% (w/v) |
| Agar | 1.5% (w/v) |

**(vi) 10× FGS (Fructose, Glucose, Sorbose) stock**

A 10× stock solution containing fructose, glucose and sorbose was prepared by dissolving the components in 80 ml of distilled water. The final volume was adjusted to 100 ml and the solution was sterilized by autoclaving.

| Component | Amount / Concentration |
|---|---|
| Fructose | 5% (w/v) |
| Glucose | 5% (w/v) |
| Sorbose | 20% (w/v) |

**(vii) FGS agar**

FGS Agar was prepared by mixing a 1× concentration of FGS with 1× Vogel's Medium N and 1.5% (w/v) agar.

| Component | Amount / Concentration |
|---|---|
| FGS | 1X |
| Vogel's Medium N | 1X |
| Agar | 1.5% (w/v) |

**(viii) Top agar**

Top Agar was prepared using a 1× concentration of FGS and 1× Vogel's Medium N, with agar at a final concentration of 2.8% (w/v).

| Component | Amount / Concentration |
|---|---|
| FGS | 1X |
| Vogel's Medium N | 1X |
| Agar | 2.8% (w/v) |

### 2.1.5 Primers used in this study

Custom oligonucleotide primers that are used in this study were purchased from Bioserve Biotechnologies (India) Pvt. Ltd. (Hyderabad, India) as well as from Integrated DNA Technologies (Iowa, USA). List of primers used in this study are enlisted in **Table 2.3**.

**Table 2.3: List of primers used in this study**

| Sl.No | Primer | Sequence 5'→3' |
|---|---|---|
| 1 | hsp80 Fw (XbaI) | GCTCTAGAATGGCGACCGCCGAGACTT |
| 2 | hsp80 Rv (PacI) | CCTTAATTAAGTCAACCTCCTCCATGGCG |
| 3 | mCherry Fw | ATGGTGAGCAAGGGCGAGG |
| 4 | mCherry Rw | CTTGTACAGCTCGTCCATGC |
| 5 | pccg-1 Fw | CCATCATCAGCCAACAAAGC |
| 6 | Hsp80endo Fw | AACCATCGTGCACATATAAAGT |
| 7 | Hsp80endo Rv | TAACAAAATGCCCGTCAGTAAA |
| 8 | Mcherry mid Rv | TTGAAGCGCATGAACTCCTTG |
| 9 | Hsp80 Int Fw | TTCACCATCAGACCTGACAC |

| | | |
|---|---|---|
| 10 | Hsp80 Int Rw | AGATGTTCTTCTGGTGCTCG |
| 11 | RT Upr-1Fw | CTGTATGTCGAGTATGACGG |
| 12 | RT Upr-1 Rw | CAGCGAAATCCGTGCTACAT |
| 13 | RT mus-52 Fw | CCTCAGATCTTCAAGGGACT |
| 14 | RT mus-52 Rw | CTTTGGTGGTATAGACGAGC |
| 15 | RT mus-26 Fw | GATGTACTTTTACCGTGGCC |
| 16 | RT mus-26 Rw | GTCTTGACACCTCCAACATC |
| 17 | RT hsf-1 Fw | CGACAACATTGAGCGCCTC |
| 18 | RT Hsf-1 Rw | CTTATCAGACCAGCGGATGA |
| 19 | RTNCU04054F | TTGAGGACCAGATGCGCAAC |
| 20 | RTNCU04054R | TTGAAGAGCTCCTGGATGGC |
| 21 | RTNCU03804F | CTATGGATCATCAGGGAGGG |
| 22 | RTNCU03804R | CTTAATTAACGATCGCTTGCG |
| 23 | RTNCU04120F | GTGAGGCCTTCAAGGTGTTC |
| 24 | RTNCU04120R | CGTCATCAGTGAGCTTCTCG |

## 2.2 Methods

### 2.2.1 Growth conditions of *N. crassa*

The *N. crassa* strains were cultivated and maintained following standard protocols. Vegetative growth was carried out using Vogel's media, including both liquid and solid (agar) forms. For sexual reproduction and crossing experiments, Synthetic Crossing Medium (SCM) was used. Germination of ascospores was performed on FGS media. Additionally, for screening *N. crassa*

knockout mutants containing the hph cassette, FGS agar was supplemented with 220 µg/ml hygromycin.

### 2.2.2 Setting up crosses and harvesting ascospores

For crossing experiments, *N. crassa* strains of opposite mating types were placed approximately 2 cm apart on SCM agar plates and incubated at 22 °C for 18–21 days. After 14 days, the plates were inverted to facilitate ascospore shooting onto the lid. Between 16–18 days, the ascospores were collected by rinsing the lid with 1 ml sterile distilled water. The harvested ascospores were then plated onto FGS agar and germinated by heat activation at 55–65 °C for 30–60 minutes, followed by incubation at 30 °C for vegetative growth. Individual germinated ascospores were selected using a dissecting microscope and transferred to Vogel's agar slants, where they were incubated at 30 °C.

### 2.2.3 Maintenance of stocks

To ensure long-term preservation, both silica and glycerol stocks were prepared for *N. crassa* strains. For silica stocks, cultures were first grown in Vogel's agar slants at 30 °C for three days in darkness, followed by an additional four days at room temperature under continuous light. Silica gel beads were sterilized by autoclaving and dried at 60 °C before use. Cryotubes (4.5 ml) were filled with the pre-sterilized silica gel and pre-cooled on ice for 30 minutes. A 5% autoclaved skimmed milk solution was added to each culture tube, followed by vigorous vortexing to prepare a spore suspension. The suspension was transferred into the silica-filled cryotubes and vortexed for five minutes to disperse any clumps. These tubes were vortexed regularly over 8 to10 days and stored at -20 °C for future use.

For glycerol stock preparation, conidia were suspended in 1 ml sterile water and transferred to microcentrifuge tubes. An equal volume of 40% sterile glycerol was added, mixed thoroughly and stored at -80 °C for long-term preservation.

Similarly, glycerol stocks of *S. cerevisiae* were prepared by growing cells in YPD medium at 30 °C with shaking at 180 rpm overnight. After reaching the exponential phase, 600 µl of the culture was transferred to a microcentrifuge tube and 400 µl of sterile 87% glycerol was added. The mixture was then stored at -80 °C. When needed, cells were revived by streaking onto YPD agar plates.

### 2.2.4 Colony morphology and growth rate analysis

To assess colony morphology, *N. crassa* strains were cultured in 50 ml Vogel's medium in 250 ml flasks. The cultures were incubated at 30 °C for three days, followed by four days under light at room temperature.

For radial growth measurement, a mycelial plug was placed at the center of a 90-mm Petri dish and incubated at 30 °C. The colony diameter was recorded at three-hour intervals between 12 to 18 hours to calculate the radial growth rate.

Apical growth was determined using the race tube method, where 13 ml of media was poured into race tubes and a mycelial plug was inoculated at one end. The cultures were incubated at 30 °C and the hyphal growth front was recorded every 12 hours for three days. The distance traveled by the growth front was measured and growth rates were expressed as cm/hour (radial growth) and cm/day (apical growth).

### 2.2.5 Aerial hyphae development analysis

To analyze aerial hyphae height, test tubes containing Vogel's medium were inoculated with a conidial suspension at $1\times10^6$ conidia/ml and incubated at 30 °C in complete darkness for three days, followed by four days under light at room temperature. The height of aerial hyphae was measured.

### 2.2.6 Hyphal morphology analysis

For microscopic examination of hyphal morphology, *N. crassa* strains were grown at 30°C for 12–16 hours on a thin layer of Vogel's agar medium spread on glass slides. The hyphal structures were observed under a Leica S9i Stereo Microscope (Leica Microsystems, Wetzlar, Germany).

### 2.2.7 Conidial cell count

To quantify conidia production, mycelial plugs were inoculated onto 55-mm Petri dishes containing Vogel's agar medium and incubated in darkness at 30 °C for three days, followed by four days under light at 22 °C. The conidia were scraped from the agar surface using 1 ml of sterile distilled water, collected into microcentrifuge tubes and gently mixed to ensure proper resuspension. The conidial suspension was appropriately diluted and conidia were counted using a hemocytometer under a Nikon ECLIPSE E200 trinocular microscope (Nikon, Japan).

### 2.2.8 Carotenoid accumulation estimation

To estimate carotenoid accumulation, conidia (~$1\times10^6$ conidia/ml) were inoculated into 90-mm sterile Petri dishes containing Vogel's medium supplemented with 0.2% Tween 80. The cultures were initially incubated at 30 °C for 48 hours in the dark, followed by an additional 24 hours at 8 °C, 22 °C and 30 °C under white light.

Mycelial samples were harvested, lyophilized and ground into a fine powder using a mortar and pestle. Carotenoid was extracted from 50 mg of dry mycelial powder using acetone and hexane. The extraction process involved mixing 50 mg of powdered mycelia with 1 ml of acetone, followed by five hours of continuous mixing on a rotating mixer. The suspension was centrifuged at 12,000 × g for 10 minutes at room temperature and the supernatant was transferred to a fresh microcentrifuge tube. The extract was stored at -80 °C for two hours, then left at room temperature overnight with the tube lids open. The following day, 1 ml of hexane was added and the carotenoid was extracted.

The total carotenoid content was determined by measuring absorbance at 470 nm, using the following equation:

$$\text{Total carotenoid content}(\mu g/g) = \frac{\text{Total absorbance} \times \text{Total volume of extract (1 ml)} \times 10^4}{\text{Absorption coefficient (2500)} \times \text{Sample weight (g)}}$$

This calculation method follows the protocol described by Rodriguez-Amaya and Kimura (2004).

### 2.2.9 Fertility assay

The fertility assay was conducted to evaluate the male and female fertility of *N. crassa* mutant strains. Mating-type strains of opposite types were used, with one strain designated as the female parent and the other as the male parent. Crosses were set up in 55-mm Petri dishes containing SCM agar, where an agar plug of the female parent was first inoculated and incubated at 22°C for seven days. After this period, a conidial suspension of the opposite mating type (male parent) was introduced and incubated at 22°C for another seven days. After seven days post-fertilization, the development of perithecia was examined using a Leica S9i Stereo Microscope (Leica Microsystems, Wetzlar, Germany) and documented through photography.

### 2.2.10 Visualization of Internal septation

To observe internal septation, *N. crassa* strains were cultured on a thin layer of Vogel's agar medium on glass slides and incubated at 30°C for 12–16 hours. The growing hyphae were stained using calcofluor white (CFW; 0.1% in 0.05 M PBS) in darkness for 10–15 minutes. The stained samples were then analyzed using DAPI filters with an exposure time of 300–400 ms under a trinocular inverted fluorescence microscope (Olympus CKX53, Japan).

### 2.2.11 Submerged culture conidiation assay

To assess conidiation in submerged conditions, conidial suspensions ($10^6$ conidia/ml) were inoculated in Vogel's liquid medium, either supplemented with 2% (w/v) peptone or without it. The cultures were incubated at 30 °C in 250 ml flasks with shaking at 180 rpm for 16 hours. To examine conidiophore development, aliquots from these cultures were observed under a Nikon Eclipse Ti-S inverted microscope (model DS-Fi2-U3, Japan) at 20X magnification.

### 2.2.12 Thermotolerance assay

To assess thermotolerance, conidial suspensions ($1 \times 10^6$ conidia/mL) were inoculated into Vogel's glucose medium and incubated with shaking at 180 rpm for 2 hours at 30 °C in the dark to allow germination. The 2-hour germlings were then subjected to one of three heat treatments: (i) a control condition where samples were maintained at 30 °C throughout, (ii) an uninduced condition where samples were maintained at 30 °C for 30 minutes followed by a lethal heat shock at 52 °C for 20 minutes and (iii) an induced thermotolerance condition where samples were pre-treated at 44 °C for 30 minutes (prelethal heat shock) prior to the same lethal heat shock at 52 °C for 20 minutes. Following treatment, all samples were plated on Vogel's sorbose agar medium supplemented with pantothenate and incubated at 30 °C for 14–16 hours (Yang and Borkovich, 1999). Thermotolerance was determined by calculating percent survival, defined as the number of colonies recovered after heat treatment (induced or uninduced) divided by the number of colonies in the untreated control (30 °C) and multiplied by 100.

### 2.2.13 Endoplasmic Reticulum (ER) stress assay

The effect of ER stress on *N. crassa* strains was evaluated using dithiothreitol (DTT) as a stress-inducing agent. A conidial suspension ($10^6$ conidia/ml) was inoculated into sterile test tubes containing Vogel's liquid medium, supplemented with varying concentrations of DTT (0.5 mM, 1 mM and 2 mM). The cultures were incubated at 30°C in complete darkness for three

days, followed by an additional two days under light. Aerial hyphal height was measured to assess the impact of ER stress on fungal growth.

### 2.2.14 Cellulose degradation assay

To study cellulose degradation under different zinc concentrations, a $10^6$ conidia/ml suspension was inoculated into 50 ml of 1X Vogel's Medium supplemented with 2% microcrystalline cellulose (VC). Cultures were incubated at 30 °C with shaking at 180 rpm for seven days in darkness and fungal growth was observed and photographed. The efficiency of cellulose degradation was assessed by analyzing fungal growth on microcrystalline cellulose.

### 2.2.15 Glucose concentration estimation using DNSA

Glucose released in the VC medium under varying zinc concentrations was quantified using 3,5-Dinitrosalicylic acid (DNSA) reagent, following previously established protocols. A D-glucose standard curve was prepared by using glucose solutions of known concentrations. 3 ml of each test sample and standard were transferred into separate test tubes, followed by the addition of 3 ml of DNSA reagent. The test tubes were placed in a boiling water bath (99–100 °C) for five minutes, then allowed to cool to room temperature. Absorbance was recorded at 575 nm and a standard curve of absorbance vs. glucose concentration was used to determine the glucose content in the samples.

### 2.2.16 Estimation of protein concentration using Bradford method

Protein concentration in the VC medium under different zinc conditions was determined using the Bradford assay. Bovine Serum Albumin (BSA) was used as the standard protein. BSA solutions of varying concentrations were prepared to generate a standard curve. In separate test tubes, 20 µl of each unknown sample and BSA standard were mixed with 180 µl of Bradford reagent. The reaction mixtures were incubated for 5–10 minutes in complete darkness and absorbance was measured at 595 nm. A standard curve of absorbance vs. BSA concentration was plotted to determine the protein concentration in the samples.

### 2.2.17 Osmotic stress assay

For osmotic stress analysis, mycelial agar plugs (~1 cm diameter) were taken from fresh *N. crassa* cultures and inoculated at the center of 90-mm Petri dishes containing Vogel's agar medium supplemented with varying concentrations of NaCl, KCl and sorbitol (0 M (control),

0.5 M, 1 M and 1.5 M). The plates were incubated at 30 °C in complete darkness and colony diameter was measured at three-hour intervals from 12 to 24 hours. Growth rates were calculated, with the control condition (0 M) set as 100% and relative growth rates at different osmotic stress levels were expressed as percentages of the control.

### 2.2.18 pH Stress assay

To examine pH tolerance, freshly harvested conidial suspensions ($10^6$ conidia/ml) from five-day-old cultures were inoculated into sterile test tubes containing Vogel's liquid medium with pH values of 3.8, 5.8 and 7.8. The cultures were incubated at 30 °C in darkness for three days, followed by four days in light at room temperature. Aerial hyphal height was measured and photographed. Growth at pH 5.8 was taken as the 100% control and relative growth rates at pH 3.8 and 7.8 were expressed as a percentage of the control.

### 2.2.19 Preparation of Ultracompetent *E. coli* cells

Ultracompetent *E. coli* cells were prepared following established protocols. A single colony of *E. coli* DH5α was picked from a freshly streaked LB agar plate, inoculated into 10 ml LB broth and incubated overnight at 37 °C with shaking at 180 rpm. The next day, 1% of the overnight culture was transferred to 50 ml of fresh LB broth and incubated under the same conditions until the culture reached the log phase. Optical density (OD600) was monitored and once it reached 0.450–0.600, the culture was rapidly chilled on ice.

Cells were collected by centrifugation at 3000 × g for 10 minutes at 4 °C and the pellet was resuspended in 16 ml of ice-cold Inoue transformation buffer (10 mM PIPES pH 6.7, 15 mM $CaCl_2$, 250 mM KCl, 55 mM $MnCl_2$). After chilling on ice for 10 minutes, the cells were centrifuged again and the pellet was resuspended in 4 ml of Inoue transformation buffer containing 7% DMSO. The suspension was divided into 100 µl aliquots, flash-frozen in liquid nitrogen and stored at -80 °C for future use.

### 2.2.20 Small-scale isolation of Plasmid DNA from bacterial culture

Plasmid DNA was isolated from bacterial cultures using the alkaline lysis method. An overnight bacterial culture (~5 ml) was collected in a 1.5 ml microcentrifuge tube and centrifuged at 12,000 × g for 60 seconds at 4 °C. The supernatant was discarded and the pellet was resuspended in 100 µl of Alkaline Lysis Solution I by vigorous vortexing.

Next, 200 µl of freshly prepared Alkaline Lysis Solution II was added, mixed immediately by inverting the tube, followed by the addition of 150 µl of Alkaline Lysis Solution III. The sample was gently mixed and incubated on ice for five minutes. The lysate was centrifuged at 12,000 × g for 10 minutes at 4 °C and the clear supernatant was transferred to a fresh tube.

An equal volume of phenol:chloroform:isoamyl alcohol (25:24:1) was added and the mixture was centrifuged at 12,000 × g for 10 minutes at 4 °C. The aqueous phase was transferred to a new microcentrifuge tube and plasmid DNA was precipitated by adding 1 ml of absolute ethanol. The solution was gently inverted multiple times and centrifuged at 12,000 × g for 10 minutes at 4 °C to pellet the plasmid DNA. The pellet was washed with 70% ethanol, centrifuged at 12,000 × g for 5 minutes, air-dried at room temperature and resuspended in 20 µl of 1X TE buffer (pH 8.0) for storage at 4 °C.

### 2.2.21 Digestion of Plasmid DNA with Restriction endonuclease

Plasmid DNA was digested using restriction endonucleases according to the manufacturer's guidelines. The digestion reaction was set up in a 50 µl reaction volume, containing 1 µg of plasmid DNA, 1 µl (10 units) of restriction enzyme and the recommended buffer. The reaction was incubated under conditions specified by the manufacturer. The resulting DNA fragments were analyzed via agarose gel electrophoresis.

### 2.2.22 Ligation of digested vectors and inserts

Ligation of digested vectors and inserts was performed using the Quick Ligation™ Kit. A 20 µl ligation reaction mixture was prepared, consisting of 50 ng of linearized vector DNA, a 3-fold molar excess of insert DNA, 10 µl of 2X ligation buffer, 1 µl of Quick T4 DNA ligase and nuclease-free water to make up the final volume. The reaction was incubated in a circulating water bath at 25 °C for 15–30 minutes.

### 2.2.23 Transformation of Ultracompetent *E. coli* cells by heat shock

Competent *E. coli* cells were either freshly prepared or retrieved from -80°C and thawed on ice. Approximately 100 ng of ligated DNA was added to 100 µl of competent cells, gently mixed and incubated on ice for 20–30 minutes. The cells were then subjected to heat shock at 42°C for 90 seconds in a water bath, followed by immediate transfer to ice for 10–20 seconds.

To allow cell recovery, 600 µl of pre-warmed SOC medium was added and the mixture was incubated at 37 °C with shaking at 180 rpm for one hour. Following recovery, 150–200 µl of the transformed culture was plated onto 90-mm LB agar plates supplemented with 100 µg/ml ampicillin. The plates were incubated overnight at 37°C and colony formation was observed the next day.

### 2.2.24 Transformation of *N. crassa* strain by electroporation

Transformation of *N. crassa* conidia through electroporation was carried out using a previously established protocol. The recipient strain was cultured in Vogel's agar medium at 30 °C for seven days in 250 ml conical flasks. Conidia were collected using sterile water and filtered through autoclaved cheesecloth attached to a 250 ml conical flask to separate them from the mycelial mass. The suspension was transferred to Falcon tubes and centrifuged at 1500 rpm for 5 minutes at 4 °C. The pellet was washed twice with 25 ml of sterile water, resuspended in ice-cold 1 M sorbitol at a concentration of $3\times10^9$ spores/ml and mixed with the plasmid construct. The mixture was then transferred to a pre-chilled 2 mm sterile electroporation cuvette and electroporation was performed using a BioRad Gene Pulsar apparatus under the following conditions: 1.5 kV voltage gradient, 25 µF capacitance and 600 Ω resistance, with a time constant ranging from 13–15 milliseconds. Immediately after the electric pulse, 1 ml of chilled 1 M sorbitol was added and the cuvette was incubated on ice for 3–5 minutes. The transformant conidial suspension was mixed with top agar, plated onto FGS agar plates and incubated at 30 °C. Transformant colonies typically appeared after 2–3 days, yielding around 5–10 transformants per plate. To confirm that no contamination occurred, a control transformation was performed without the plasmid construct.

### 2.2.25 Isolation of genomic DNA from *N. crassa*

Genomic DNA was extracted from *N. crassa* strains cultivated in Vogel's liquid medium at 30 °C with shaking at 180 rpm for three days. The harvested mycelial mass was finely chopped, lyophilized and ground into a fine powder. Approximately 150 mg of mycelial powder was transferred to a 2 ml microcentrifuge tube and 1 ml of DNA lysis buffer (10 mM Tris-HCl pH 7.5, 0.5 M NaCl, 10 mM EDTA, 1% SDS, 1% CTAB) was added. The mixture was incubated at 65°C for 45 minutes, followed by centrifugation at 12,000 rpm for 10 minutes. The supernatant was transferred to a new tube and 600 µl of phenol:chloroform:isoamyl alcohol (25:24:1) was added and mixed thoroughly before incubation on a rotating mixer for 15–20

minutes. The mixture was centrifuged at 12,000 × g for 10 minutes and the upper aqueous phase was extracted and subjected to another round of chloroform purification. DNA was precipitated by adding 1 ml of pre-chilled absolute ethanol, gently mixed and incubated at room temperature for 30 minutes. The sample was then centrifuged at 12,000 × g for 10 minutes, washed with 70% ethanol and air-dried for 20–30 minutes before dissolving in 30 µl of 1X TE buffer (pH 8.0) for storage at 4 °C.

### 2.2.26 Isolation of RNA from *N. crassa*

Total RNA was isolated from *N. crassa* conidia cultured in Vogel's liquid medium at 30 °C with shaking at 180 rpm for 12–16 hours. The harvested mycelia were finely cut, frozen immediately in liquid nitrogen and ground into a fine powder using a sterilized glass rod. To extract RNA, 400 µl of TRIzol reagent was added, followed by 750 µl of lysis buffer (0.6 M NaCl, 10 mM EDTA, 100 mM Tris-HCl pH 8.0, 4% SDS) and 750 µl of phenol:chloroform:isoamyl alcohol (25:24:1). The mixture was incubated on a rotating mixer for 20 minutes, followed by centrifugation at 10,000 × g for 10 minutes. The aqueous phase was extracted and the purification step was repeated with phenol:chloroform:isoamyl alcohol. RNA was precipitated by adding 750 µl of 8 M LiCl and incubated at 4 °C for 20–24 hours. The next day, the RNA was pelleted by centrifugation at 10,000 × g for 10 minutes, washed with 70% ethanol, air-dried at room temperature and dissolved in 20–30 µl of DEPC-treated water before storage at -80 °C.

### 2.2.27 Quantification of nucleic acids

The concentration of nucleic acids was determined by measuring absorbance at 260 nm using a NanoPhotometer® (IMPLEN, Germany). The standard conversions used were: an OD260 of 1 corresponds to ~50 µg/ml for double-stranded DNA, 40 µg/ml for single-stranded DNA and RNA and ~20 µg/ml for single-stranded oligonucleotides. The OD260/OD280 ratio was calculated to assess sample purity, with values of 1.8 for pure DNA and 2.0 for pure RNA.

### 2.2.28 Polymerase Chain Reaction (PCR)

PCR was carried out using Taq DNA Polymerase for routine amplifications, Dynazyme II DNA Polymerase for high-fidelity reactions and Phusion® High-Fidelity DNA Polymerase for cloning applications requiring low error rates. PCR conditions were optimized based on primer

annealing temperatures and product size and reactions were performed using a Thermal Cycler (Arktik Thermal Cycler, Thermo Fisher Scientific, USA).

### 2.2.29 Reverse Transcription PCR (RT-PCR) for cDNA synthesis

RT-PCR was conducted for gene expression analysis using Verso cDNA Synthesis Kit (Thermo Fisher Scientific, USA). A total of 2 µg of RNA was used in a 20 µl reaction, with the following reaction conditions: 42 °C for 30 minutes, followed by 95°C for 2 minutes. The resulting cDNA was used for quantitative real-time PCR (qRT-PCR).

### 2.2.30 Quantitative Real-Time PCR (qRT-PCR)

qRT-PCR was performed using ABI 7500 Fast (Applied Biosystems, USA) and AriaMx Real-Time PCR System (Agilent, India). The reaction mixture contained 4.5 µl of cDNA (~100 ng), 0.25 µl of forward primer, 0.25 µl of reverse primer and 5 µl of SYBR® Select Master Mix. For negative controls, sterile DEPC-treated water was used instead of cDNA. The thermal cycling conditions included 95 °C for 10 minutes, followed by 40 cycles of 95 °C for 15 seconds and 60 °C for 1 minute. Gene expression analysis was performed using the $2^{-}\Delta\Delta CT$ method, with β-tubulin as a reference gene and the wild-type strain as the calibrator.

### 2.2.31 Agarose gel electrophoresis

To analyze DNA samples, 1 µl of 6X DNA loading dye (composed of 0.25% bromophenol blue, 0.25% xylene cyanol and 30% glycerol) was added to each sample before loading. Depending on the DNA fragment size, 0.7% to 1.5% agarose gels were prepared using 1X TAE buffer and supplemented with 0.5 µg/ml ethidium bromide (EtBr). Electrophoresis was carried out at 80–100 V in 1X TAE buffer and DNA fragment sizes were estimated by comparing them to a 1 kb DNA ladder (NEB #B7025, NEB, Ipswich, MA, USA). Visualization of EtBr-stained DNA was performed using a gel documentation system (Image 4.1, Bio-Rad, USA; or Mega Bio Print, Vilbert Lourmat, France). Similarly, RNA samples were resolved on a 1.5% agarose gel prepared with 2.2 M formaldehyde, 1X MOPS buffer and 0.5 µg/ml EtBr to ensure optimal separation and visualization.

### 2.2.32 UV sensitivity assay

To evaluate UV sensitivity, strains were grown on FGS agar plates, where $10^3$ conidia were evenly spread using a sterile glass spreader. The conidia were suspended in sterile water to

ensure uniform distribution before plating. Plates were exposed to ultraviolet (UV-C, 254 nm) radiation at intensities of 0, 100, 200 and 300 J/m² using a UVP Crosslinker (CL-1000) with lids removed. After exposure, plates were incubated in complete darkness at 30 °C for two days to allow for recovery. Following incubation, the surviving conidia were counted based on their ability to germinate, providing a direct measure of UV exposure impact on conidial viability.

### 2.2.33 Photoreactivation assay

The strains of were grown on FGS agar plates, where $10^3$ conidia were evenly spread. The conidia were suspended in sterile water to ensure uniform distribution before plating. The plates were exposed to ultraviolet (UV-C, 254 nm) radiation at intensities of 0, 100, 200 and 300 J/m². After UV exposure, the strains were illuminated with visible light (400-700 nm) for 30 minutes to induce photoreactivation. Following the light exposure, the plates were incubated in complete darkness at 30°C for two days to allow for recovery. After the incubation period, the surviving conidia were counted based on their ability to germinate, providing a direct measure of photoreactivation and UV exposure impact on conidial viability.

### 2.2.34 MMS treatment assay

The strains were grown on FGS agar plates, where $10^3$ conidia were evenly spread using a sterile glass spreader. The conidia were suspended in sterile water to ensure uniform distribution before plating. The plates were prepared with FGS media containing 0.03% methyl methanesulfonate (MMS) and incubated at 30°C for 24 hrs**.** After MMS treatment, the plates were incubated in complete darkness at 30°C overnight to allow for recovery. Following the overnight incubation, the surviving conidia were counted based on their ability to germinate, providing a direct measure of MMS-induced damage and recovery.

### 2.2.35 Statistical analysis

All quantitative experiments in this study were conducted at least three times (n = 3) to ensure reproducibility. Statistical analysis was carried out using one-way or two-way analysis of variance (ANOVA) with multiple comparisons, followed by Tukey's post hoc test for pairwise comparisons. The statistical analyses were performed using GraphPad Prism 8.2.4. Data variability is represented by error bars indicating mean ± standard deviation (SD). Statistical significance is denoted using asterisks, where one asterisk (*) represents $p < 0.05$ (significant),

two asterisks (**) indicate $p < 0.01$ (very significant) and three asterisks (***) indicate $p < 0.001$ (extremely significant).

### 2.3 Databases and software programs used in this study

i. Basic Local Alignment Search Tool (BLAST): The BLAST program (Altschul et al. 1990, 1997) was used for sequence comparison against reference databases. Available at: http://blast.ncbi.nlm.nih.gov/Blast.cgi.

ii. Clustal X: The Clustal X software (Thompson et al. 1997) was used for multiple sequence alignment of DNA and proteins. Available at: http://www.clustal.org/clustal2/.

iii. Conserved Domain Database (CDD): The CDD online program (Yang et al. 2020) was used to identify conserved protein domains. Available at: https://www.ncbi.nlm.nih.gov/cdd/.

iv. Dali Webserver: The Dali protein structure comparison server (Holm 2022) facilitates 3D protein structure comparison. Available at: http://ekhidna2.biocenter.helsinki.fi/dali/.

v. ExPasy Translate Tool: The ExPasy Translate tool was used for DNA/RNA-to-protein sequence translation. Available at: https://web.expasy.org/translate/.

vi. GalaxyWEB (GalaxyRefine): The GalaxyWEB tool (Ko et al. 2012) was used for protein structure refinement. Available at: https://galaxy.seoklab.org/cgi-bin/submit.cgi?type=REFINE.

vii. GeneDoc: The GeneDoc software (Nicholas et al. 1997) was used for editing and annotating multiple sequence alignments. Available at: http://nrbsc.org/gfx/genedoc.

viii. ImageJ/Fiji: The ImageJ/Fiji (Schindelin et al. 2012) software was used for biological image analysis. Available at: https://imagej.net/software/fiji/.

ix. AlphaFold: AlphaFold is an artificial intelligence system for predicting protein structures with high accuracy. Available at: https://www.alphafold.ebi.ac.uk/.

x. Genome Databases: Genome resources for *Neurospora crassa* are available at: http://fungidb.org and the Fungal Genetics Stock Center at: http://www.fgsc.net/.

xi. NCBI/EMBL: The NCBI and EMBL servers were used to retrieve protein and nucleic acid sequences. Available at: http://www.ncbi.nlm.nih.gov/ and http://embl.org/.

xii. STRING: The STRING database (Szklarczyk et al. 2019) was used for predicting protein-protein interactions. Available at: https://string-db.org/.

xiii. Reverse-Complement Tool: The sequence manipulation suite (SMS) was used to generate reverse-complement DNA sequences. Available at: http://www.bioinformatics.org/sms/index.html.

xiv. DeepTMHMM: DeepTMHMM (Hallgren et al. 2022) was used for predicting transmembrane protein topology. Available at: https://dtu.biolib.com/DeepTMHMM.

xv. UCSF ChimeraX: UCSF ChimeraX (Pettersen et al. 2004) was used for interactive molecular structure visualization. Available at: https://www.cgl.ucsf.edu/chimera/.

xvi. UniProt: The UniProt server was used to retrieve protein sequences. Available at: https://www.uniprot.org.

xvii. GROMACS (version 2023.3) was chosen for the simulations due to its efficiency, scalability and extensive support for biomolecular systems.

xviii. Python (Matplotlib): Matplotlib is a widely used Python library for creating high-quality plots of molecular dynamics data such as RMSD, RMSF and radius of gyration.

xix. Computational Resources. All MD simulations were performed using the supercomputing facility (Param-Kamrupa) at IIT Guwahati, which provides high-performance computational resources essential for large-scale molecular simulations.

### 2.4 Molecular Dynamics simulation workflow for Hsp80 Wild Type and mutants

To visualize the structural dynamics and stability of HSp80 and its RIP mutants, molecular dynamics simulation were performed as illustrated in **Figure 2.2**

#### 2.4.1 Structure preparation

The wild type HSP80 structure was obtained from the Protein Data Bank and refined using AlphaFold to enhance its structural accuracy. Mutant HSP80 proteins were first sequenced-

designed and their PDB structures were generated using AlphaFold. The resulting structures were validated for accuracy and converted into GROMACS-compatible formats for molecular dynamics simulations.

### 2.4.2 System setup

A dodecahedral simulation box with a 1.0 nm buffer was defined around the protein to ensure sufficient solvent coverage. The system was solvated using the SPC216 water model, followed by ion neutralization using $Na^+$ and $Cl^-$ ions to maintain electrostatic balance.

### 2.4.3 Energy minimization

To remove steric clashes and optimize the molecular geometry, energy minimization was performed using the steepest descent algorithm. The minimization was terminated when the maximum force acting on any atom was reduced below 1000 kJ/mol/nm, with a step size of 0.01 nm and a maximum of 50,000 steps. Electrostatic interactions were calculated using the Particle Mesh Ewald (PME) method, with a 1.0 nm cutoff for both electrostatics and van der Waals interactions. After energy minimization, the system underwent additional steepest descent minimization following ion addition to ensure stability.

### 2.4.4 Equilibration

Equilibration was conducted in two phases: NVT equilibration (constant Number, Volume and Temperature) and NPT equilibration (constant Number, Pressure and Temperature), both without position restraints.

During NVT equilibration, the system was stabilized at three different temperatures (298K, 333K and 368K) using the V-rescale thermostat, with separate coupling for Protein and Non-Protein molecules. The simulation ran for 100 ps (50,000 steps) with a 2 fs timestep and initial velocities were assigned using a Maxwell-Boltzmann distribution at the respective temperatures. Neighbor lists were updated every 20 fs and PME electrostatics with a 1.0 nm cutoff was applied. Following NVT, the NPT equilibration phase stabilized pressure and system density, using the Parrinello-Rahman barostat for isotropic pressure coupling at 1.0 bar with a compressibility of 4.5e-5 $bar^{-1}$. The simulation ran for another 100 ps, with identical settings to NVT, except that velocity generation was disabled.

### 2.4.5 Production MD simulation

The production MD run was conducted for 10 ns (5,000,000 steps, 2 fs timestep) at each of the three temperatures to analyze the dynamic behavior of the wild-type and mutant Hsp80 proteins. The Parrinello-Rahman barostat maintained a constant 1.0 bar pressure, while the V-rescale thermostat controlled the temperature. PME electrostatics with a 1.0 nm cutoff was applied and hydrogen bonds were constrained using the LINCS algorithm. To optimize data storage, trajectory data were saved every 2 ps for later analysis. MD simulations were performed at 298K (normal), 333K (mild heat stress) and 368K (extreme heat stress) to assess protein stability and conformational changes under increasing thermal stress.

### 2.4.6 Parameter analysed

To assess protein dynamics and structural behavior across different temperatures, several parameters were analyzed. Root Mean Square Deviation (RMSD) and Root Mean Square Fluctuation (RMSF) were used to evaluate overall structural stability and local flexibility, respectively. Secondary Structure Analysis (DSSP) tracked conformational transitions, while Radius of Gyration (Rg) provided insights into protein compactness. Hydrogen bond analysis assessed intramolecular and solvent interactions and interaction energy calculations quantified system stability. Clustering analysis identified dominant conformations and Principal Component Analysis (PCA) captured the major collective motions within the simulation trajectory.

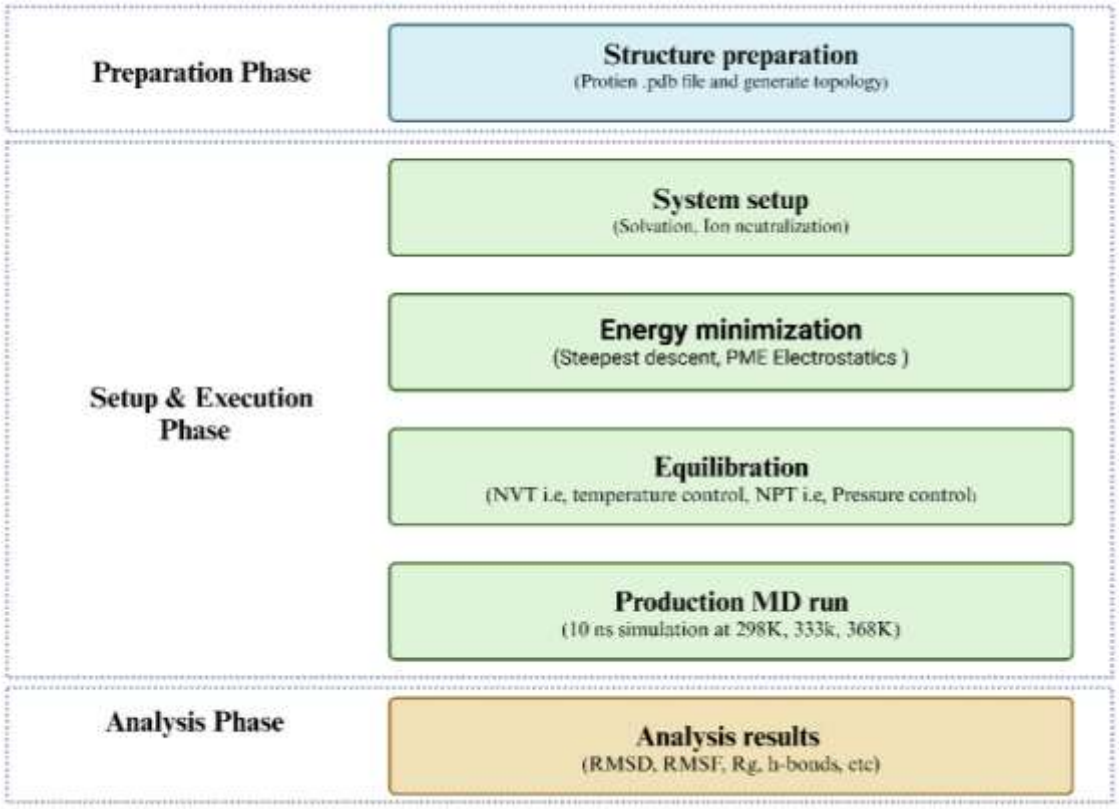


**Figure 2.2: Molecular Dynamics simulation workflow**

# Chapter 3

# INVESTIGATING THE ROLE OF *hsp80* GENE REGULATION IN THERMOTOLERANCE OF *NEUROPSORA CRASSA*

# CHAPTER 3

# INVESTIGATING THE ROLE OF *HSP80* GENE REGULATION IN THERMOTOLERANCE OF *NEUROSPORA CRASSA*

## 3.1 Introduction

The genome sequence of *N. crassa* reveals the presence of multiple heat shock proteins that play an essential role in protein folding, stabilization and stress adaptation. Among them, Hsp90 is a highly conserved ATP-dependent molecular chaperone that plays a crucial role in maintaining protein homeostasis by facilitating protein folding, stabilization and degradation (Krishna & Gloor, 2001; Taipale et al., 2010). It ensures the proper folding of newly synthesized proteins and prevents misfolded protein aggregation under normal and stress conditions (Mayer & Bukau, 2005). Environmental stresses such as heat shock, oxidative stress and osmotic stress can lead to the accumulation of unfolded proteins, triggering the heat shock response and upregulating Hsp90 expression (Lindquist & Craig, 1988; Morano et al., 1999). This dynamic regulation of Hsp90 enables the stabilization of key regulatory proteins involved in cellular signaling, growth and stress resistance, allowing cells to adapt to fluctuating environmental conditions (Johnson & Brown, 2009; Schopf et al., 2017).

In *Neurospora crassa*, the *hsp80* gene (NCU04142) encodes HSP80, a protein highly homologous to other eukaryotic Hsp90 family members which is located on the right arm of linkage group IV and shares 85% sequence identity with yeast Hsp82. Hsp80 plays a crucial role in the organism's response to various stress conditions, including heat shock, osmotic stress and oxidative stress. Under such conditions, the transcription factor SEB-1 translocates to the nucleus and binds to the Stress Response Element (STRE) in the promoters of stress-responsive genes, regulating their expression to help *N. crassa* adapt to environmental challenges.

Hsps, including Hsp90, are essential for maintaining cellular proteostasis, ensuring that misfolded or denatured proteins are either refolded or degraded via proteasomal pathways (Taipale et al., 2010). Different abiotic factors, such as high temperature, oxidative stress and nutrient starvation, induce Hsp90 expression in eukaryotic systems (Morano et al., 1999; Mayer & Bukau, 2005). A failure in the Hsp90-regulated chaperone system leads to the accumulation of misfolded proteins, triggering intrinsic stress and leading to cellular dysfunction and death

(Neckers & Workman, 2012). Therefore, *N. crassa* maintains a harmonized protein quality control system, Hsp and co-chaperones that regulate ATP-dependent protein folding and stabilization (Borkovich et al., 2004). Hsp90 functions as part of a multi-chaperone complex, interacting with Hsp70, co-chaperones and regulatory factors, which modulate its ATPase cycle and substrate specificity (Johnson & Brown, 2009; Schopf et al., 2017). It plays a key role in activating the heat shock response pathway, which is regulated by heat shock factors to restore cellular homeostasis under stress conditions (Richter et al., 2010). Additionally, Hsp90 is implicated in regulating fungal growth, conidiation and sexual reproduction, particularly under thermal and nutrient stress conditions (Leach et al., 2012; Lamoth et al., 2014; Cowen & Lindquist, 2005). The *hsp80* gene in *N. crassa* is an essential gene, making it difficult to generate *hsp80* mutants using conventional knocknout approaches. Therefore, to study the functional significance of specific amino acid residues, I generated *hsp80* mutants using repeat-induced point (RIP) mutation, a genome defense mechanism in *N. crassa* that introduces G:C to A:T transition mutations in duplicated DNA sequences during the sexual cycle (Cambareri et al., 1989; Kumar et al., 2020). *N. crassa* possesses three different gene silencing mechanisms: quelling, RIP and meiotic silencing, which operate at different stages of the life cycle to regulate genome integrity and suppress transposable elements (Selker et al., 1993; Galagan et al., 2003). RIP effectively introduces G:C to A:T mutations and methylation of duplicated sequences, ensuring genome defense by preventing the persistence of redundant or foreign DNA sequences (Galagan & Selker, 2004).

In this study, I generated four RIP mutants of *hsp80* and identified key amino acid residues critical for its chaperone activity. Using these RIP mutants, I examined how Hsp80 regulates fungal growth, conidiation and sexual development under heat stress and nutrient-limited conditions. I also evaluated the stress tolerance capabilities of *hsp80*$^{RIP}$ mutants under various abiotic stress conditions, including oxidative stress, high salt and extreme temperatures. In summary, this study identified key amino acid residues necessary for Hsp80 function in *N. crassa*, highlighting its role in cellular stress response and proteostasis.

## 3.2 Results

### 3.2.1 Cloning of hsp80 into pTLS88F *(Pccg-1::hsp80::mcherry::6X His)*

The strain was generated by cloning the *hsp80* ORF (3019 bp). The *hsp80* ORF was PCR-amplified from wild type using primers hsp80 Fw (XbaI) and hsp80 Rv (PacI). The PCR product was gel purified and used in subsequent steps of cloning. The vector pTLS88F (*Pccg-1::mcherry::6X His*) was linearized by using the restriction enzymes PacI and XbaI (New England Biolabs, Ipswich, MA). The reaction mixture comprised 100 ng of a linearized DNA vector, a 3-fold molar excess of insert, 10 µl of 2× ligation buffer and 1 µl of quick DNA ligase enzyme. The reaction was incubated at 25 °C overnight in a circulating water bath. The ligated product was transformed into *Escherichia coli* DH5α ultra-competent cells **(Figure 3.2)**. The recombinant plasmid pRTHSP80 was isolated and PCR to confirm the correct orientation of the construct. This plasmid, which contains the construct *Pccg-1::hsp80::mcherry::6X His*, was then transformed into the *N. crassa* his-negative strain 6032 A **(Figure 3.1)**. The initial transformants were screened on VG agar medium without histidine supplement and a heterokaryotic transformant strain (T-9A) was isolated.

**Table 3.1: Primers used for cloning and sequencing of *hsp80***

| Sl.No | Primer | Sequence 5'→3' |
|---|---|---|
| 1 | hsp80 Fw (XbaI) | GCTCTAGAATGGCGACCGCCGAGACTT |
| 2 | hsp80 Rv (PacI) | CCTTAATTAAGTCAACCTCCTCCATGGCG |
| 3 | mCherry Fw | ATGGTGAGCAAGGGCGAGG |
| 4 | mCherry Rw | CTTGTACAGCTCGTCCATGC |
| 5 | pccg-1 Fw | CCATCATCAGCCAACAAAGC |
| 6 | Hsp80endo Fw | AACCATCGTGCACATATAAAGT |
| 7 | Hsp80endo Rv | TAACAAAATGCCCGTCAGTAAA |
| 8 | Mcherry mid Rv | TTGAAGCGCATGAACTCCTTG |

| | | |
|---|---|---|
| 9 | Hsp80 Int Fw | TTCACCATCAGACCTGACAC |
| 10 | Hsp80 Int Rw | AGATGTTCTTCTGGTGCTCG |

### 3.2.2 Generation of the *hsp80*$^{RIP}$ strains

The T-9 A heterokaryotic strain, which became prototrophic after transformation, was crossed with the auxotrophic *tol trp-4* a strain (tryptophan-negative) to generate a homokaryon opposite mating type progeny. The ascospores were germinated on FGS agar medium without histidine supplement, given the auxotrophic nature of T-9 A. Germinated ascospores were grown on VG agar slants and crossed with wild-type strains (4200 a and 2489 A) to determine mating types. Two homokaryon progenies, T-42 A and T-11 a were isolated after PCR screening using specific sets of primers. Since both the progenies contained duplicated copies of the *hsp80* gene, they were crossed to generate *hsp80*$^{RIP}$ mutant strains **(Figure 3.3)**. Ascospores were harvested twice, first on day 18 to remove early ascospores and again on day 30, given the increased frequency of RIP over time. Ascospores harvested on the 30$^{th}$ day were germinated on an FGS medium and transferred to VG agar slants for further studies. In the initial screening of several hundred progenies for growth phenotype to identify potential RIP mutants, four progenies (R4 A, R6 A, R9 a and R14 a) was selected. These progenies were PCR amplified and confirm.

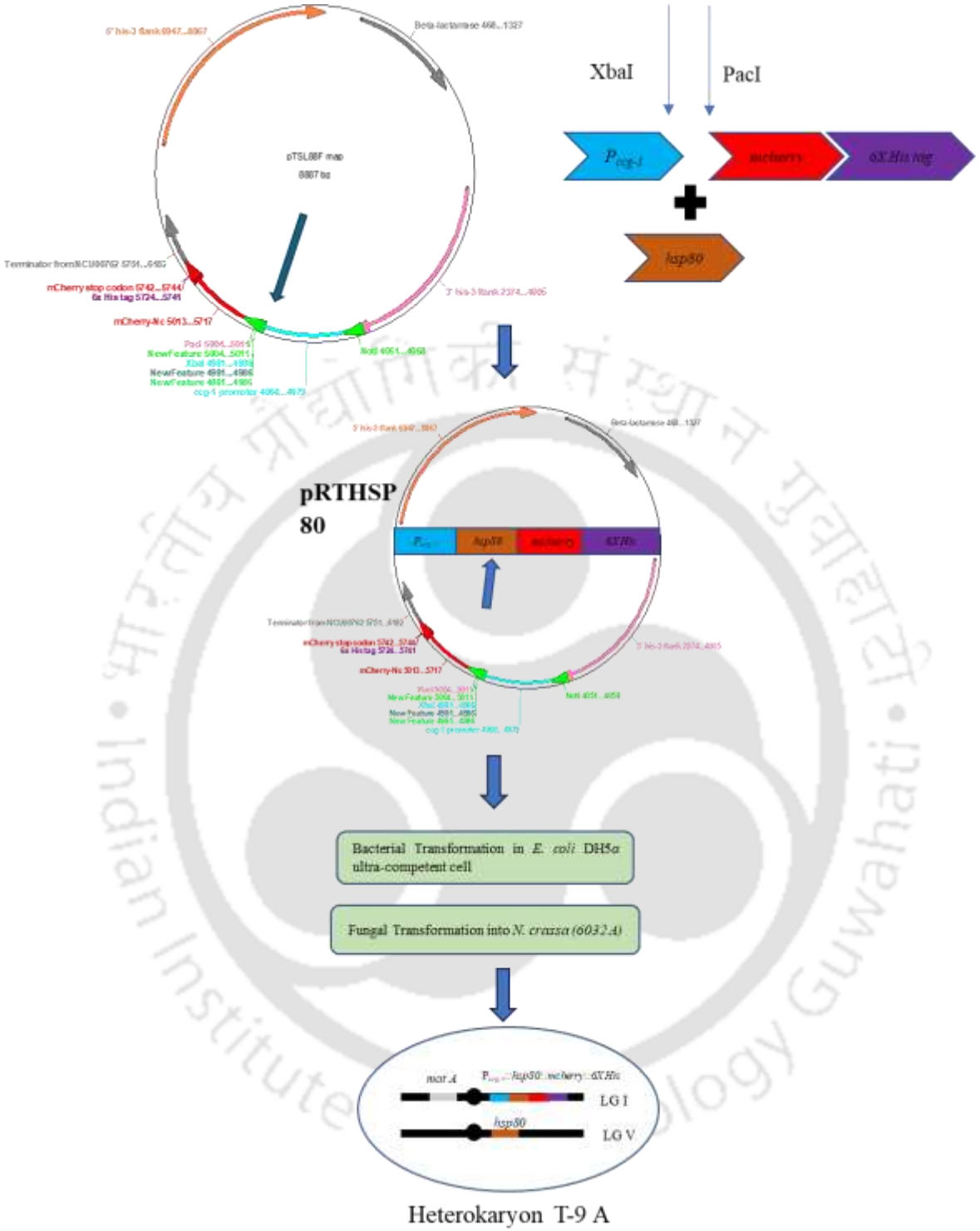


**Figure 3.1: Schematic showing the construction of the pRTHSP plasmid and transformation into *N. crassa* (6032 A).** The hsp80 gene was cloned into the PacI and XbaI site of the plasmid pTLS88F, alongside an *mcherry::6X histag* construct, under the control of the *Pccg-1* promoter. The resulting recombinant plasmid, pRTHSP, was transformed into E. coli DH5α ultra-competent cells for amplification. After plasmid extraction, the construct was transformed into *N. crassa* strain his negative 6032 A, integrating into Linkage Group I, while the endogenous hsp80 gene remained on LG V.

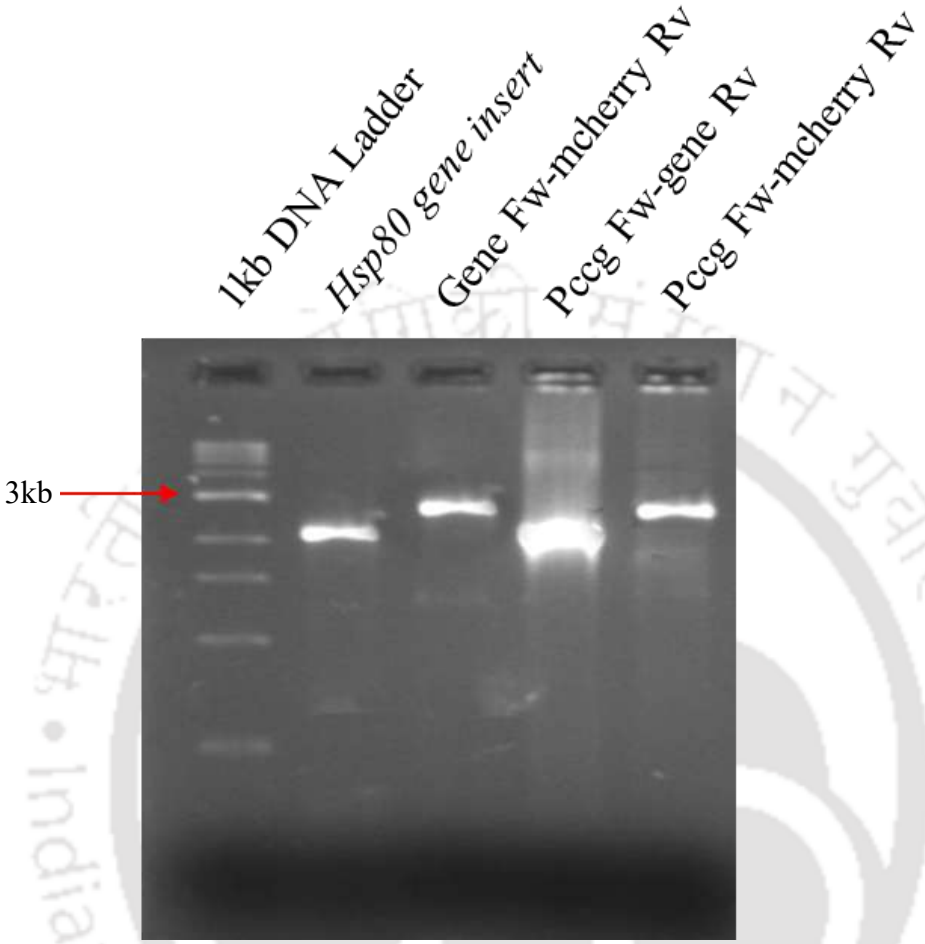


**Figure 3.2: Showing PCR confirmation of transformed *hsp80* construct in *N. crassa*.** The ectopic copy of the *hsp80 gene* was amplified and confirmed from the heterokaryotic transformant heterokaryon T-9 A.

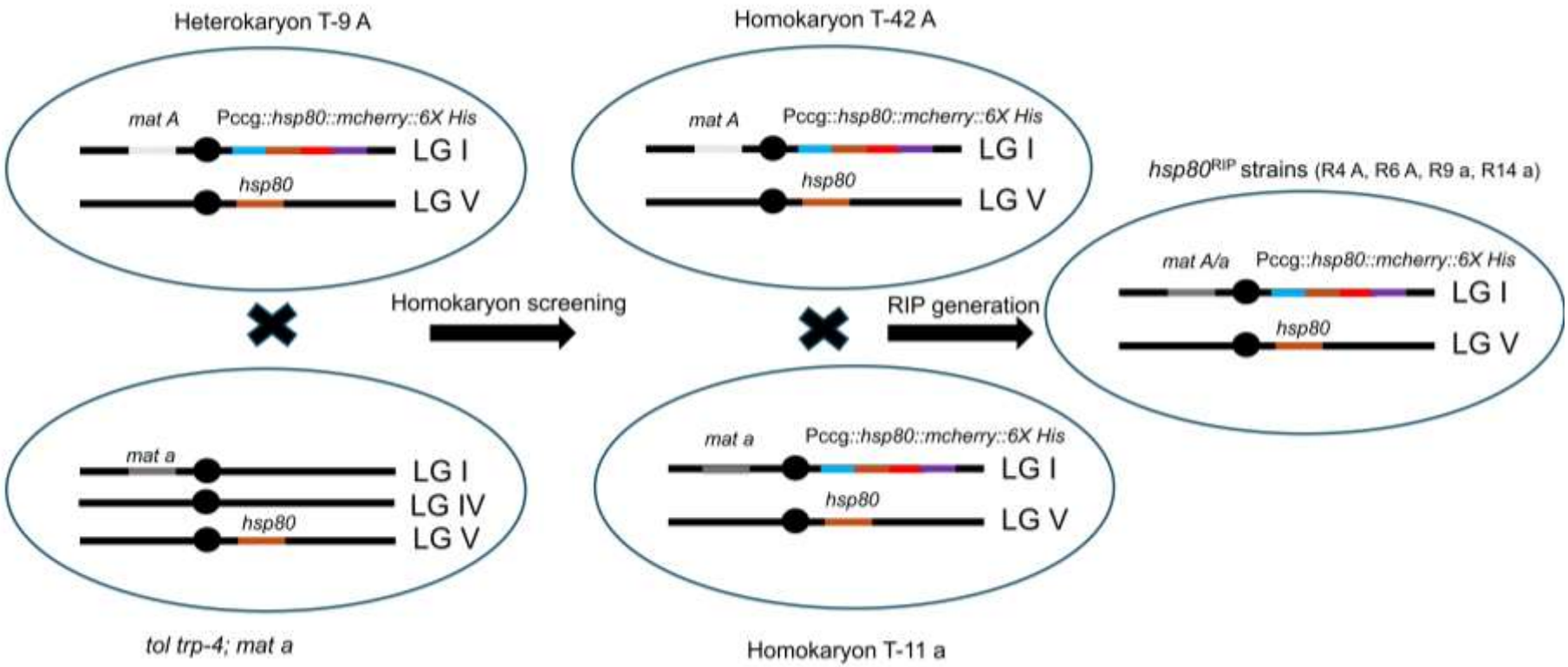


**Figure 3.3: Strategy to generate *hsp80*$^{RIP}$ R4 A, R6 A, R9 a and R14 a strains.** The heterokaryotic strain T-9 A was crossed with *tol trp-4* a and ascospores were germinated to obtain homokaryotic progenies. Two such homokaryotic progenies, T-11 a and T-42 A, were selected and PCR amplified. Further, a cross was set between these homokaryotic progenies to generate *hsp80* $^{RIP}$ progenies.

### 3.2.3 Identification of critical amino acid residues of *hsp80*

In this study, we generated four RIP strains carrying targeted mutations in both the ectopic and endogenous copies of *hsp80*. The mutations were introduced by inserting an extra copy of *hsp80*, which activated Neurospora's Repeat-Induced Point Mutation (RIP) process, resulting in targeted nucleotide changes while preventing off-target mutations. To confirm the successful incorporation of these mutations, genomic DNA was extracted from the mutant strains and the *hsp80* region was PCR-amplified using specific primers. The amplified products were then gel-extracted to ensure purity and specificity before being subjected to Sanger sequencing. Sequence analysis verified that the desired nucleotide changes were precisely introduced into the genome, confirming the specificity and accuracy of the modifications.

Mutations introduced into the ectopic copy of *hsp80* were characterized in four different strains. The R4 A strain contained two nucleotide mutations, leading to D89V and L90S substitutions. Similarly, the R6 A strain contained five mutations, resulting in D89V, L90S, V91L, N92P and N93R substitutions. The R9 a strain exhibited a single nucleotide mutation leading to the D58A substitution, while the R14 a strain carried a single mutation causing the A2E substitution **(Figure 3.4) (Table 3.2)**. In contrast to the ectopic mutations, sequencing and alignment analysis of the endogenous copy of *hsp80* revealed no mutations across all strains

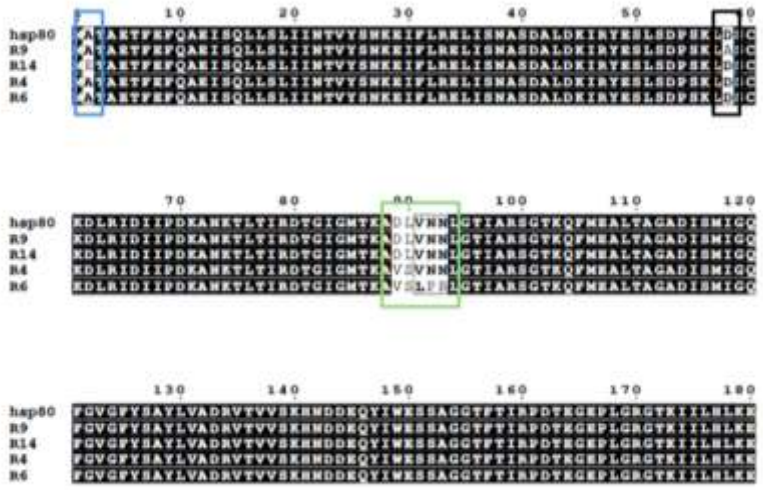


**Figure 3.4: Sequence alignment.** Wild-type and *hsp80*$^{RIP}$ mutants (R4 A, R6 A, R9 a and R14 a) compared to the wild-type sequence, generated using ClustalW and visualized with ESPript 3.0. The alignment is displayed in black and white, where black shading represents fully conserved residues (100%) and white indicates variable residues. Ectopic Mutations: Alignment showing mutations in the ectopic copy of *hsp80* in RIP mutants compared to the wild type.

**Table 3.2: Site of mutations in the *hsp80*$^{RIP}$ strains.**

| Sl No. | Strain | Mutation location | Amino acid mutations |
|---|---|---|---|
| **1** | R4 A | Ectopic | D89V, L90S |
| **2** | R6 A | Ectopic | D89V, L90S, V91L, N92P, N93R |
| **3** | R9 a | Ectopic | D58A |
| **4** | R14 a | Ectopic | A2E |

### 3.2.4 Growth and morphological characterization of *hsp80*$^{RIP}$ mutants

The wild-type and mutant strains (R4 A, R6 A, R9 a and R14 a) were inoculated into flasks containing 50 ml of VG agar medium to examine their morphology. The cultures were incubated at 30°C for three days in the dark and for additional three days in the light. The mutants were not distinctly different morphologically from the wild-type strain.

### 3.2.5 Apical growth analysis of *hsp80*$^{RIP}$ mutants' strains under normal conditions

The apical growth of wild-type and *hsp80*$^{RIP}$ mutant strains (R4 A, R6 A, R9 a and R14 a) was analyzed under standard laboratory conditions. Initially, the strains were grown on radial plates and aerial hyphae were observed in tubes, but the data obtained was negligible. Due to this, I utilized race tubes to better assess apical growth. Growth measurements were recorded at 12-hour intervals up to 72 hours to assess differences in vegetative extension (Figure 3.5). The growth rates followed a sigmoidal pattern, with an initial lag phase followed by exponential growth. The wild type strain exhibited the slowest apical extension, reaching approximately 30 cm at 72 hours when compared to the mutants. Among the mutants, R4 A, R6 A, R9 a and R14 a displayed enhanced growth rates, with R14 a showing the most significant deviation from the wild type. At early time points (12 and 24 hours), minimal differences in growth were observed among all strains. However, as time progressed, the wild type exhibited reduced apical growth compared to the mutant strains. The R14 a mutant displayed the highest apical growth rate, indicating a strong influence on vegetative development **(Figure 3.5)**. These results suggest that *hsp80*$^{RIP}$ mutants exhibit distinct apical growth patterns compared to the wild-type strain under normal conditions. The increase growth observed, particularly at later time points, highlights the genetic interactions of Hsp80 influencing apical extension and vegetative development in *N. crassa*.

### 3.2.6 Visualization of the Inter-Septal distance of *hsp80*$^{RIP}$ mutants

The hyphae of *N. crassa* are multinucleated and contain septa, which function as structural barriers that regulate the exchange of nutrients and organelles, including nuclei, between compartments (Potapova and Golyshev 2016). These septa play a critical role in maintaining hyphal integrity and are essential for key developmental processes such as asexual sporulation and protoperithecia formation (Rasmussen and Glass 2007; Mouriño-Pérez 2013). To determine whether the slow growth phenotype observed in certain mutants was linked to septation defects, I employed fluorescent microscopy (Figure 3.6). Fluorescent staining with calcofluor white (CFW), a dye that binds to cellulose and chitin in the fungal cell wall (Seidel et al. 2013; Boyce et al. 2016), was used to visualize and quantify inter-septal distances and hyphal width.

Measurement of inter-septal distances in wild type and mutant strains (R4 A, R6 A, R9 a, R14 a) further confirmed these differences (**Table 3.3; Figure 3.6**). The wild type strain had an average septation length of 62.35 µm, with a maximum of 83.24 µm and a minimum of 32.42 µm. In contrast, all mutant strains exhibited an increase in inter-septal distance, with the most pronounced change in R9 a, which averaged 84.24 µm, reaching a maximum of 167.37 µm. The R6 A strain also showed a considerable increase, with an average length of 83.67 µm. Moderate increases were observed in R4 A and R14 a, with average septation lengths of 77.21 µm and 78.85 µm, respectively. These results show that septation patterns differ among the mutant strains, with R9 a showing the most significant change from the wild type. The larger hyphal compartments in the mutants may affect nutrient exchange and fungal growth.

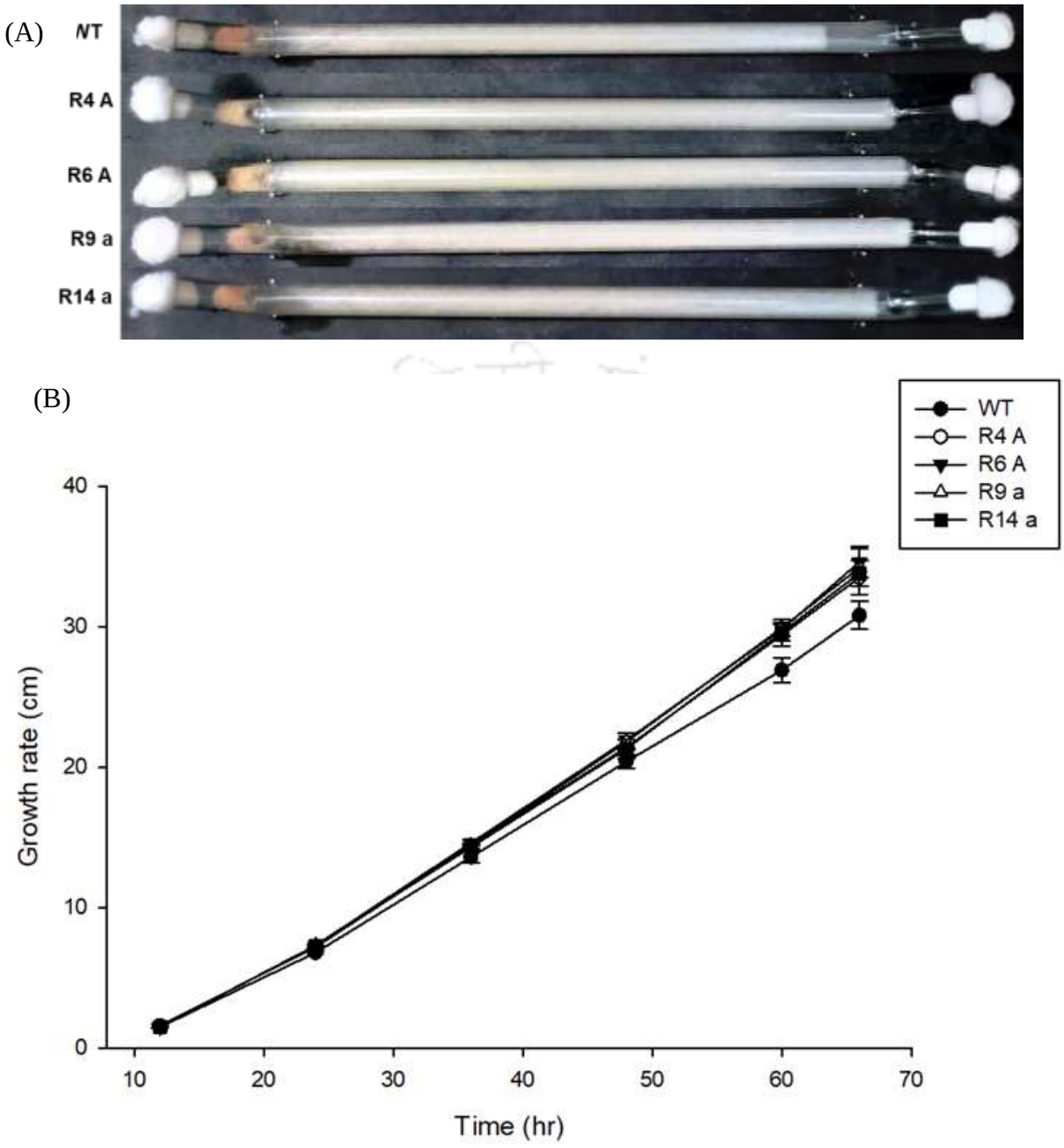


**Figure 3.5: Growth Assay Under Normal Conditions.** The mutant strains (R4 A, R6 A, R9 a and R14 a) were evaluated for their apical growth under normal conditions in *N. crassa*. (A) The apical growth rate of the strains was determined using race tubes. The strains were inoculated at one end of the tube, incubated at 30 °C and kept in the dark for three days before being photographed. (B) Growth rates of each strain were measured on VG medium. The distances between the inoculation point and the hyphal growth front were determined at 12-hour intervals up to 72 hours and plotted against time. The error bars represent the standard deviations calculated based on the results of three independent experiments (n = 3).

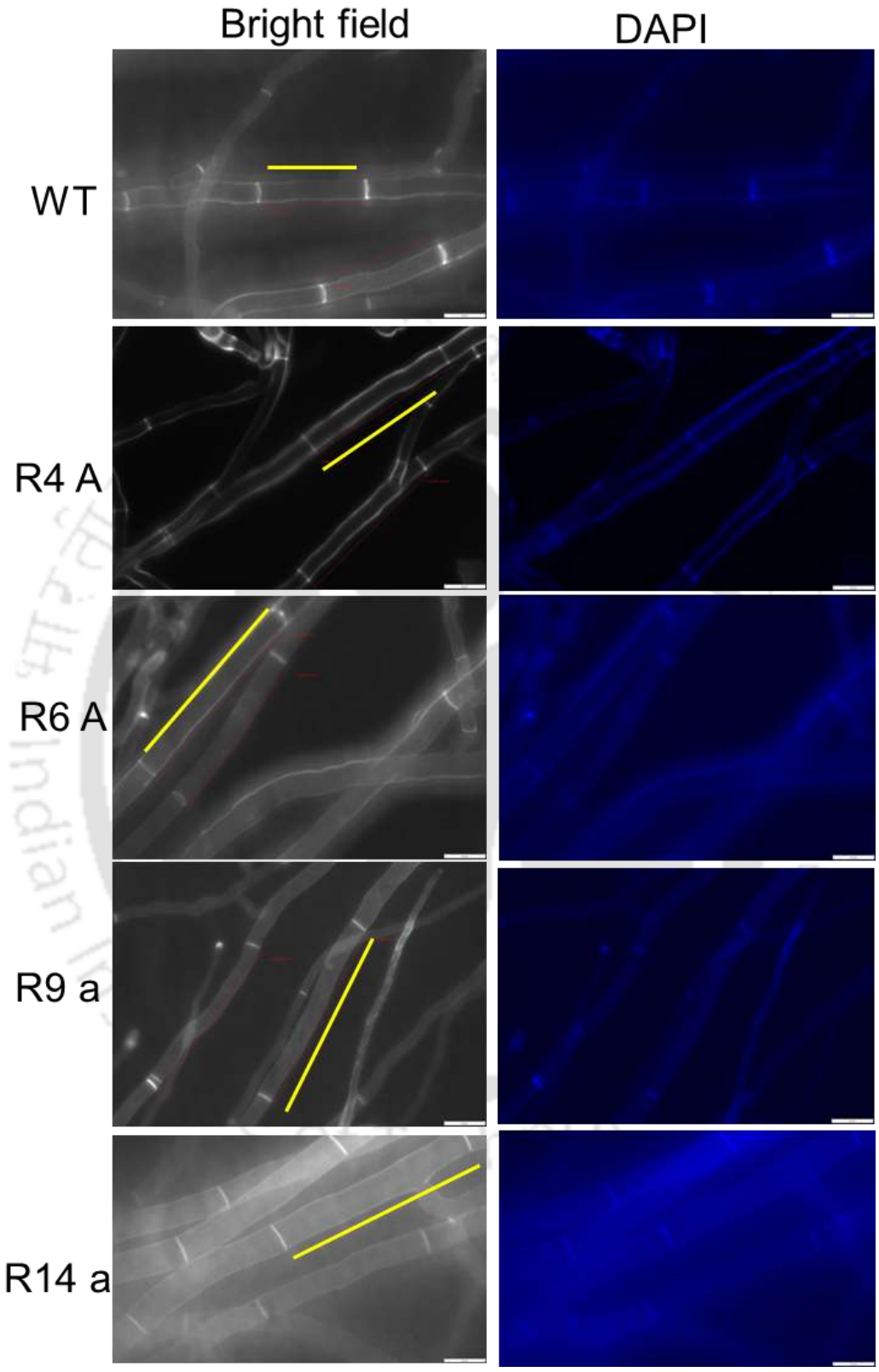


**Figure 3.6: Visualization of internal septation of wild type and mutant strains.** Visualization of septa of *N. crassa* strains using calcofluor (CFW) staining. The wild type and rip mutant strains (R4 A, R6 A, R9 a and R14 a) were grown on VG agar for 12 h at 30 °C and visualized under a microscope using a DAPI filter (Olympus CKX53). Scale bar 20 μm.

**Table 3.3: Hyphal compartment length and hyphal width of *N. crassa* strains**

| Strains | Septation length (µm) | | |
|---|---|---|---|
| | Average | Maximum | Minimum |
| WT | 62.35 | 83.24 | 32.42 |
| R4 A | 77.21 | 138.25 | 54.23 |
| R6 A | 83.67 | 142.71 | 59.15 |
| R9 a | 84.24 | 167.37 | 62.21 |
| R14 a | 78.85 | 136.12 | 55.68 |

### 3.2.7 Induced thermotolerance and heat shock response in *N. crassa*

The heat shock response is a vital protective mechanism that enables organisms to adapt to sudden temperature increases. In *Neurospora crassa*, exposure to sublethal temperatures enhances survival upon subsequent exposure to lethal temperatures, a phenomenon known as induced thermotolerance (Kapoor et al. 1990; Yang and Borkovich 1999). This process is characterized by the transient synthesis of heat shock proteins (HSPs), including HSP98, HSP83 and HSP67, which function as molecular chaperones to facilitate protein folding and stability (Lindquist and Craig 1988; Schlesinger 1990). To investigate the thermotolerance capacity of different strains, survival rates of wild type and mutant strains were examined under induced and uninduced conditions by assessing their ability to withstand heat stress following pre-exposure to sublethal temperatures.

The survival rates of wild type and mutant strains were evaluated to determine the impact of thermotolerance induction. The wild type strain exhibited the highest survival rate under induced thermotolerance (64.02 ± 1.95%), while minimal survival was observed in the uninduced conditions (0.61 ± 0.08%). Among the tested mutants, R4 A, R6 A, R9 a and R14 a displayed significantly reduced survival rates under induced thermotolerance (19.55 ± 1.32%, 27.86 ± 3.98%, 5.52 ± 0.21% and 8.668 ± 1.38% respectively), with no detectable survival under uninduced conditions **(Figure. 3.7)**.

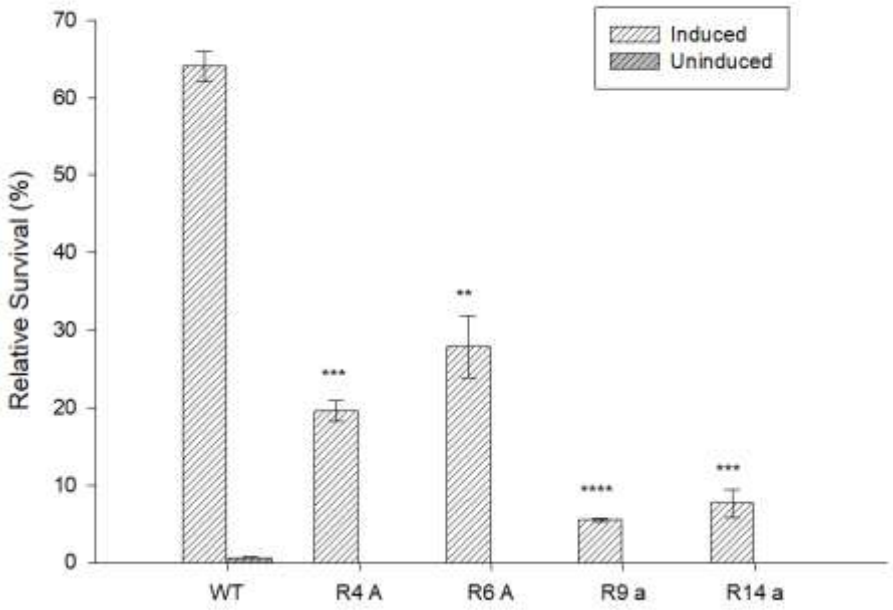


**Figure. 3.7: Thermotolerance assay.** Viability of 2 hours old germlings of wild type and *hsp80*$^{RIP}$ mutant strains (R4 A, R6 A, R9 a and R14 a) after exposure to a lethal temperature of 52 °C with (induced) or without (uninduced) pre-exposure to a sublethal heat shock temperature of 44 °C. Standard deviations are indicated by error bars calculated from three independent experiments (n = 3) and the significance given by P values < 0.05 (*), < 0.01 (**) and < 0.001 (***)compared to the wild-type strain as measured by a one-way ANOVA test.

### 3.2.8 Expression study of *hsf-1, cna-1* and *cmd* in *N. crassa*

Heat shock response and protein homeostasis in eukaryotic cells are tightly regulated by heat shock factor 1 (HSF-1), calcineurin (CNA-1) and calmodulin (CMD) all of which play critical roles in modulating HSP90 function. In *Caenorhabditis elegans*, HSF-1 directly regulates heat shock protein expression, including HSP90, by binding to heat shock elements (HSEs) in response to proteotoxic stress (Li et al., 2016). Calcineurin, a calcium/calmodulin-dependent phosphatase, interacts with HSP90, modulating its function to maintain cellular homeostasis under stress (Rao et al., 2018). Calmodulin, a key calcium-signaling molecule, activates calcineurin, stabilizing HSP90-mediated protein folding (Ge et al., 2018). Additionally, Cdc37 enhances the ATPase activity of HSP90, ensuring the correct folding and stabilization of kinase clients, with its depletion leading to defects in chaperone-mediated protein maturation (Verba & Agard, 2017). These findings suggest a highly coordinated regulatory network where HSF-

1, calcineurin, calmodulin and Cdc37 function synergistically to maintain proteostasis under stress conditions.

To assess the impact of *hsp80* disruption on the expression of hsf-1, cna-1 and cmd, a quantitative gene expression analysis was conducted following the heat tolerance assay in wild-type and *hsp80*$^{RIP}$ mutant strains (R4 A, R6 A, R9 a and R14 a). Heat stress was applied at 44°C for 2 hours before RNA extraction and analysis. The results (Fig. 3.8) reveal a significant downregulation of *hsf-1, cna-1 and cmd* in mutant strains compared to the wild type. While the wild type maintained high expression levels under heat stress, all mutant strains exhibited a sharp decline, indicating a compromised transcriptional response to heat stress. Among the mutants, R6 A showed the most pronounced decrease in cna-1 and cmd expression, while hsf-1 levels remained consistently low across all strains **(Figure 3.8)**. The lowered expression of these critical regulators corresponds to the reduced thermotolerance observed in mutant strains, suggesting that Hsp80 is essential for maintaining regulatory pathways required for heat shock adaptation.

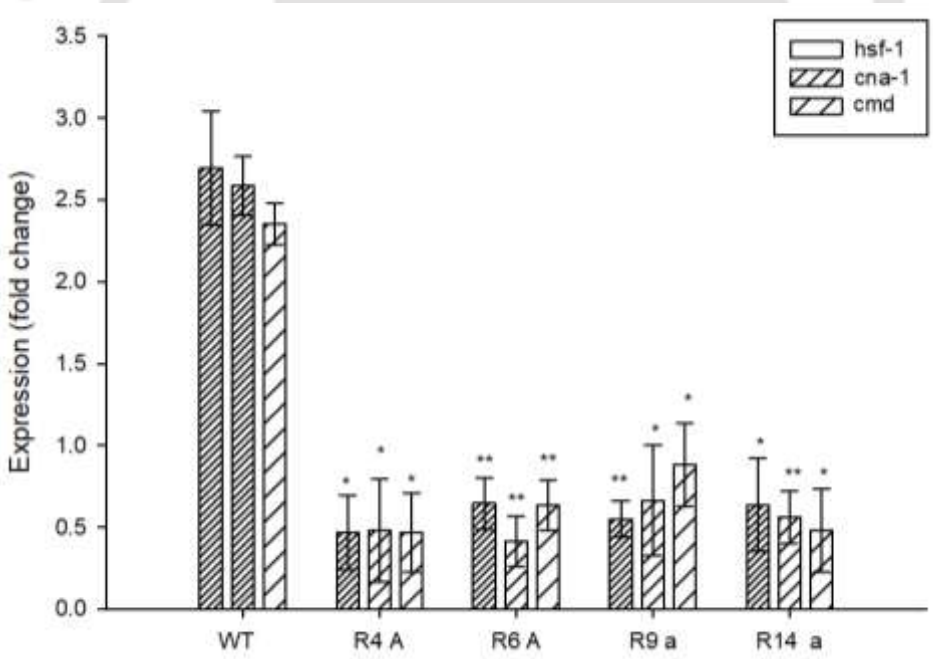


**Figure 3.8: Expression study of *hsf-1*, *cna-1* and *cmd* in the wild type and *hsp80*$^{RIP}$ mutant** : The *N. crassa* strains were cultured in VG medium and subjected to heat stress at 44°C for 2 hours. Following heat treatment, RNA was extracted and the expression levels of *hsf-1, cna-1 and cmd* were analyzed using qRT-PCR. The relative expression was normalized to β-tubulin and standard deviations were represented as error bars for three independent experiments (n = 3). Statistical significance was determined using P-values < 0.05 (*), < 0.01 (**) and < 0.001 (***), comparing mutant strains to the wild type.

### 3.2.9 Effect of increased extracellular $Ca^{2+}$ levels on *hsp80*$^{RIP}$ mutants

To assess the response of *hsp80*$^{RIP}$ mutants to elevated extracellular $Ca^{2+}$ concentrations, a $Ca^{2+}$ stress tolerance assay was performed. The wild-type strain and *hsp80*$^{RIP}$ mutants (R4 A, R6 A, R9 a and R14 a) were inoculated on VG agar medium at varying concentrations of $CaCl_2$ (0, 0.2, 0.3 and 0.4 M). The average colony growth rate (cm/hr) was measured to determine any alterations in calcium stress tolerance.

The results demonstrated that despite increasing $Ca^{2+}$ levels, the *hsp80*$^{RIP}$ mutants did not exhibit a significant reduction in colony growth rate compared to the wild type. While a gradual decline in growth was observed across all strains as $Ca^{2+}$ concentration increased, the pattern remained consistent between the mutant and wild-type strains, indicating that Hsp80 disruption does not notably affect calcium stress resistance. These findings suggest that alternative pathways may compensate for *hsp80* function in calcium homeostasis.

### 3.2.10 pH Tolerance assay in *hsp80*$^{RIP}$ mutants

Microorganisms must adapt to changes in extracellular pH to survive and grow in diverse environments. In fungi like *Neurospora crassa*, fluctuations in pH trigger signal transduction pathways that regulate cellular responses (Virgilio et al. 2016). The alkaline pH signaling pathway in *N. crassa* is known to interact with the $Ca^{2+}$ signaling cascade, influencing key stress responses (Virgilio et al. 2017). Additionally, alkaline conditions affect the expression of calcineurin-responsive zinc finger-1 (crz-1), a downstream component of the $Ca^{2+}$ pathway (Virgilio et al. 2017). Since *hsp80* is involved in fungal stress response, its role in pH adaptation was evaluated.

To assess the effect of extracellular pH on *hsp80*$^{RIP}$ mutants, a pH tolerance assay was conducted using wild-type and *hsp80*$^{RIP}$ mutant strains (R4 A, R6 A, R9 a and R14 a). Conidia ($10^3$ spores) were inoculated into Vogel's Minimal (VM) liquid medium adjusted to pH 3.8, 5.8 and 7.8. The cultures were incubated at 30 °C in complete darkness for three days, followed by four days in light to promote aerial hyphal development. The standard growth condition (pH 5.8) was used as a control. Growth observations showed that at pH 3.8, the aerial hyphal development of *hsp80*$^{RIP}$mutants remained somewhat similar to the wild type, indicating no significant growth defects (**Figure 3.9**). However, when exposed to alkaline conditions pH 7.8, the mutants exhibited a substantial reduction in aerial hyphal height compared to the wild-type strain. The decrease in growth at pH 7.8 was statistically significant, suggesting an increased

sensitivity of *hsp80*$^{RIP}$ mutants to alkaline stress. These results suggest that hsp80 is essential for pH homeostasis in alkaline environments. However, the mutants did not show defects under acidic conditions, indicating that *hsp80* is not required for survival at low pH.

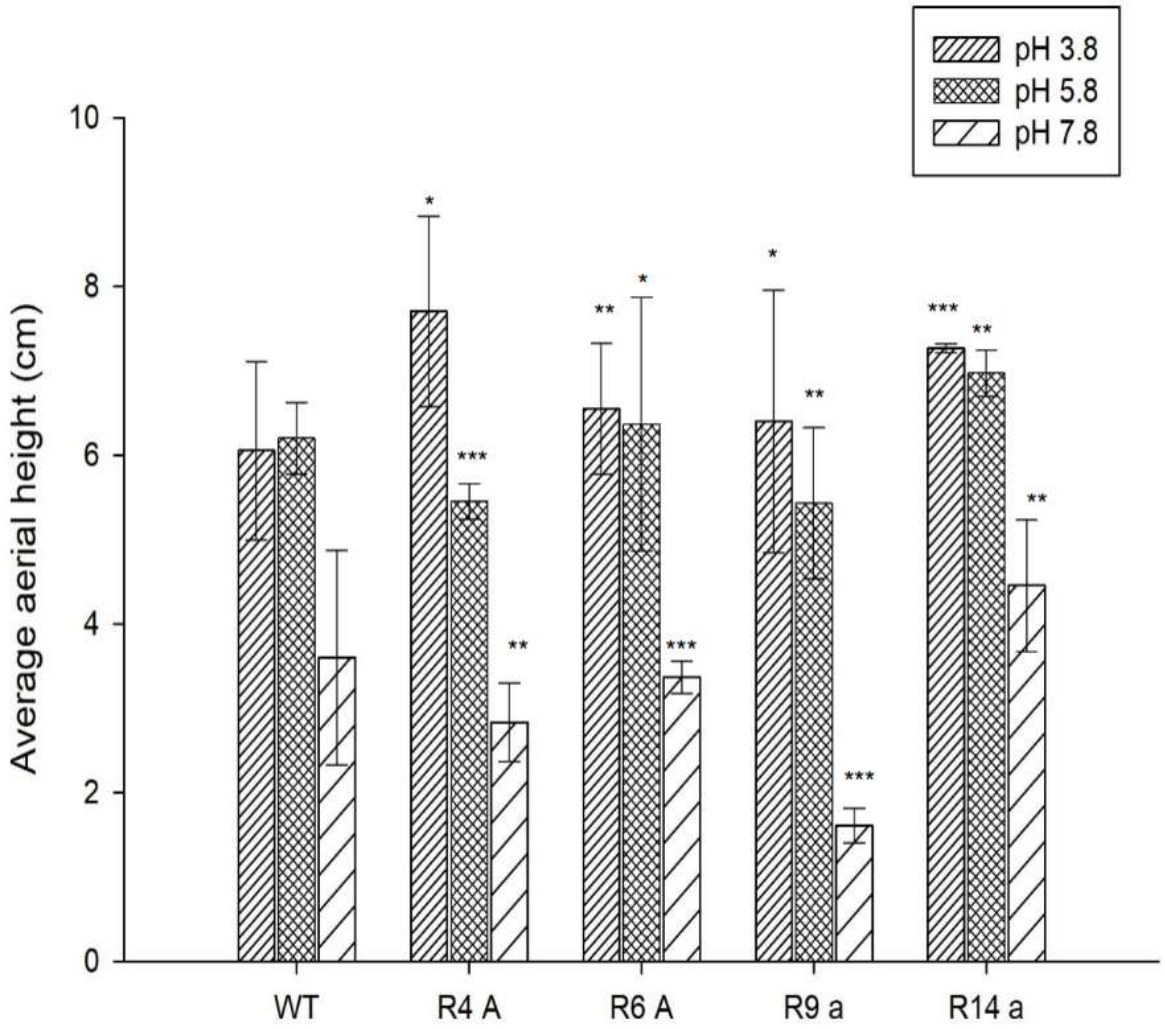


**Figure 3.9: pH stress assay.** Sensitivity to pH of the wild type and *hsp80*$^{RIP}$ was evaluated by growing the strains in VGM liquid medium adjusted to three pH conditions, acidic (pH 3.8), normal (pH 5.8) and alkaline (pH 7.8) for 3 days at 30 °C. Average aerial hyphae height (cm) was calculated. Error bars indicate the standard deviations calculated from three independent experiments (n = 3) and the significance given by *P* values <0.05 (*), <0.01 (**) and <0.001 (***) compared to the wild type strain as measured by one-way ANOVA test.

### 3.2.11 Osmotic stress assay in *hsp80*$^{RIP}$ mutants

Elevated concentrations of osmolytes, such as salt, can negatively impact fungal growth by inducing osmotic stress. Notably, exposure to hyperosmotic or hypoosmotic conditions has

been associated with an increase in intracellular $Ca^{2+}$ levels in fungi (Kader and Lindberg, 2010). To investigate the role of Hsp80 in osmotic stress adaptation, I examined the growth response of *hsp80*$^{RIP}$ mutants under increasing concentrations of sucrose.

To assess whether mutants strains exhibit heightened sensitivity to osmotic stress, I measured the radial growth rates of the wild-type strain and mutants strains (R4 A, R6 A, R9 a and R14 a) on Vogel's Minimal medium supplemented with sucrose at 0 M, 0.5 M and 1 M concentrations. Growth rates were recorded and compared to determine differences in osmotic stress tolerance.

The results revealed that *hsp80*$^{RIP}$ mutants exhibited a greater reduction in growth rate at higher sucrose concentrations compared to the wild-type strain (Fig. 3.10). At 1 M Sucrose, the wild type maintained a growth rate of 0.266 ± 0.014 cm/hr, whereas the *hsp80*$^{RIP}$ mutants displayed significantly reduced growth rates: R4 A (0.215 ± 0.074 cm/hr), R6 A (0.217 ± 0.055 cm/hr), R9 a (0.140 ± 0.027 cm/hr) and R14a (0.147 ± 0.006 cm/hr) **(Figure 3.10)**. This suggests that *hsp80*$^{RIP}$ mutants are more susceptible to sucrose induced osmotic stress than the wild type.

These findings indicate that Hsp80 is involved in osmotic stress tolerance and its disruption may impair the ability of *N. crassa* to withstand hyperosmotic conditions. The observed decline in growth at increased sucrose concentrations highlights the potential role of Hsp80 in maintaining osmotic balance in response to environmental stressors.

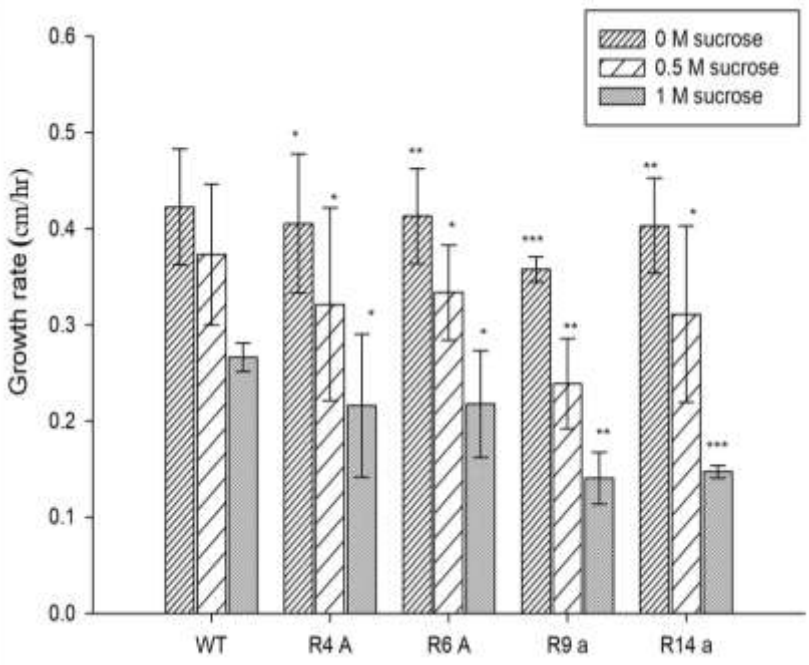

**Figure 3.10: Osmotic stress assay.** Sensitivity to osmotic stress was evaluated by growing the wild type and mutant strains (R4 A, R6 A, R9 a and R14 a) on Vogel's glucose agar medium with 0 M, 1 M and 1.5 M sucrose. Average growth rate in the presence of sucrose at the indicated concentrations. Error bars indicate the standard deviations calculated from the data for three independent experiments (n = 3).

### 3.2.12 The *hsp80*$^{RIP}$ mutant exhibits male and female fertility in *Neurospora crassa*

The filamentous fungus *Neurospora crassa* has two distinct mating types, mat a and mat A and follows a complex sexual reproductive cycle. This cycle involves multiple developmental stages, which rely on the coordinated function of various proteins to facilitate the formation of specialized reproductive structures. Ultimately, this leads to the production and release of sexual spores known as ascospores. The initiation of this process is influenced by environmental factors such as nitrogen limitation, exposure to light and reduced temperature (Davis 2000; Borkovich et al. 2004; Roca et al. 2005).

To investigate the role of Hsp80 in sexual reproduction, I conducted fertility assays using *hsp80*$^{RIP}$ mutant strains (R4 A, R6 A, R9 a and R14 a) in both mating types (mat a and mat A), with the wild-type strain serving as the control. The results demonstrated that all *hsp80*$^{RIP}$ mutants were male and female fertile **(Figure 3.11)**, successfully producing mature perithecia with abundant ascospores, comparable to the wild-type strain (**Table 3.4**).

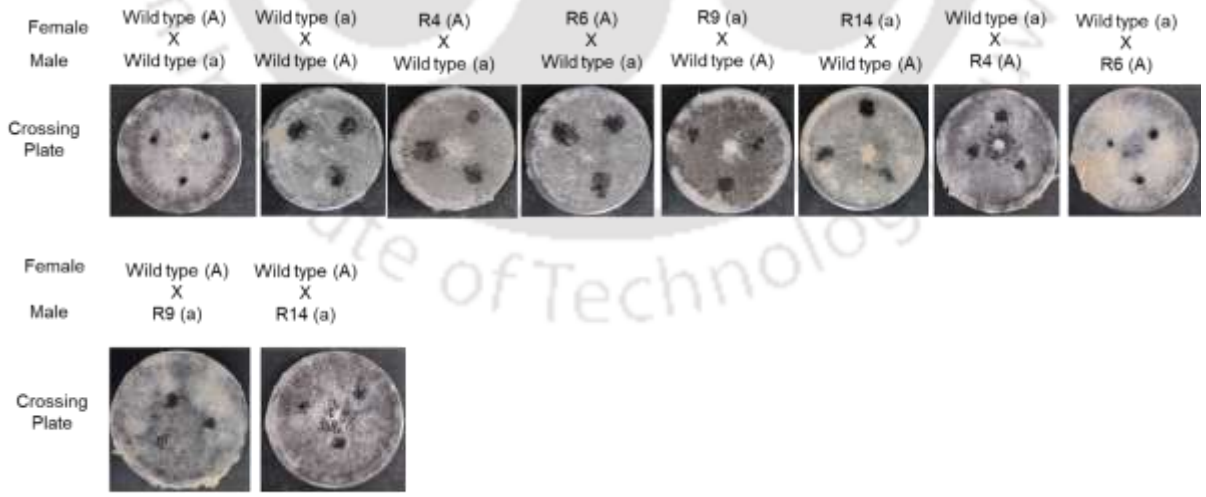


**Figure 3.11: Fertility assay on *hsp80*$^{RIP}$ mutant strains.** The wild type and mutants were first grown as female parents on SCM medium, in complete darkness for 7 days at 22 °C. Then, the opposite mating type of the strains, as male parent, was inoculated on the colony surface of the

female parent and incubated in complete darkness for another 7 days at 22 °C. The formation of perithecia was examined and photographed.

**Table 3.4: Sexual fertility assay on wild-type and *hsp80*$^{RIP}$ mutant strains**

| Sl. No. | Female Parent | Male Parent | Perithecia formed | Ascospores produced | Phenotype |
|---|---|---|---|---|---|
| 1 | Wild type A | Wild type a | Yes | Abundant | Fertile |
| 2 | Wild type a | Wild type A | Yes | Abundant | Fertile |
| 3 | R4 A | Wild type a | Yes | Abundant | Fertile |
| 4 | R6 A | Wild type a | Yes | Abundant | Fertile |
| 5 | R9 a | Wild type A | Yes | Abundant | Fertile |
| 6 | R14 a | Wild type A | Yes | Abundant | Fertile |
| 7 | Wild type a | R4 A | Yes | Abundant | Fertile |
| 8 | Wild type a | R6 A | Yes | Abundant | Fertile |
| 9 | Wild type A | R9 a | Yes | Abundant | Fertile |
| 10 | Wild type A | R14 a | Yes | Abundant | Fertile |

### 3.2.13 Conidiation in *hsp80*$^{RIP}$ mutant strains submerged culture conditions

In *Neurospora crassa*, conidiation typically takes place under nutrient-limiting conditions or at the air-water interface, where environmental cues trigger the formation of conidia. However, in submerged cultures, conidiation is generally suppressed unless specific stress conditions, such as nitrogen depletion or heat shock, are applied (Singer et al., 1995; Cortat and Turian, 1974; Madi et al., 1997).

The *hsp80*$^{RIP}$ mutant strains conidiated normally under aerial conditions, producing conidiophores and abundant conidia, similar to the wild-type strain. However, under submerged culture conditions, none of the Hsp80 RIP mutants underwent conidiation and maintained vegetative hyphal growth, identical to the wild type.

### 3.2.14 Cell wall stress assay

The cell wall is an essential structural component of filamentous fungi, serving a critical role in maintaining cellular integrity and responding to environmental stress (Maddi et al., 2012). Given the functional significance of Hsp80 in stress response pathways, the impact of its disruption on cell wall integrity was evaluated by assessing the growth of *hsp80*$^{RIP}$ mutants in the presence of cell wall stress-inducing agents. Growth assays were conducted on VM agar

medium supplemented with Congo Red (1 mg/ml) and SDS (0.01%), which interfere with chitin-glucan cross-linking and disrupt cell wall stability (Maddi et al., 2012).

The results indicated that *hsp80*$^{RIP}$ mutant strains exhibited no growth defects or increased sensitivity to these stress agents, displaying growth patterns comparable to those of the wild-type strain. These findings suggest that of Hsp80 does not play any role cell wall integrity under the tested conditions.

### 3.3 Discussion

In this chapter, I described the sequence analysis that identified Hsp80 as a key molecular chaperone in *Neurospora crassa*, homologous to the eukaryotic Hsp90 family. Furthermore, I investigated the phenotypes of *hsp80*$^{RIP}$ mutants to identify the cellular roles of this gene in vegetative growth, asexual development and stress adaptation in *N. crassa*.

The growth assays conducted in this study revealed significant morphological and developmental changes in *hsp80*$^{RIP}$ mutants compared to the wild type strain. The race tube experiments confirmed that *hsp80*$^{RIP}$ strains exhibit a increase apical extension rate, with R14 A shows the most pronounced growth, affecting growth. Additionally, the visualization of septal structures using calcofluor white staining indicated an increased inter-septal distance in *hsp80*$^{RIP}$ strains, particularly in R9 a and R6 A. This suggests that Hsp80 may be involved in septation and hyphal compartmentalization, which are critical for efficient nutrient transport and cellular differentiation in filamentous fungi.

In this study, I found the significant reduction in thermotolerance observed in *hsp80*$^{RIP}$ strains. The heat shock survival assays revealed that while wild type displayed strong adaptive thermotolerance, *hsp80*$^{RIP}$ mutants exhibited drastically reduced survival rates when subjected to lethal temperatures. The highest susceptibility was observed in R9 a and R14 a mutants, which failed to recover following heat stress. The expression analysis of *hsf-1, cna-1 and cmd* in *hsp80*$^{RIP}$ mutants further supports this hypothesis, as downregulation of these stress-regulatory genes indicates a compromised ability to mount an effective heat shock response. In eukaryotic systems, Hsp90 homologs are known to interact with heat shock transcription factors to facilitate their activation and promote stress adaptation (Schopf et al., 2017). The reduced expression levels of these key regulators in *hsp80*$^{RIP}$ strains provide molecular evidence of impaired stress signaling pathways, further reinforcing the essential role of *hsp80* gene in thermotolerance. Beyond thermotolerance, *hsp80*$^{RIP}$ mutants also exhibited differential

sensitivity to osmotic stress, pH variations and calcium homeostasis. The osmotic stress assays showed that *hsp80*$^{RIP}$ strains displayed significantly reduced growth under high sucrose concentrations, particularly at 1 M, where the wild type strain maintained a comparatively stable growth rate. Similarly, pH stress experiments demonstrated that *hsp80*$^{RIP}$ mutants exhibited growth impairments under alkaline conditions (pH 7.8) but remained unaffected at acidic pH (3.8). These findings indicate that Hsp80 gene plays a specific role in adaptation to alkaline stress, which may be linked to its interactions with signaling pathways regulating cellular pH homeostasis. However, the lack of significant changes in growth under calcium stress suggests that alternative pathways might compensate for Hsp80 function in calcium-dependent signaling.

Further, I investigated the fertility viability of *hsp80*$^{RIP}$ mutants was assessed through fertility assays, which revealed that all mutants remained male and female fertile. This suggests that while Hsp80 is crucial for stress adaptation, it does not play a direct role in mating and perithecia formation in *N. crassa*. However, the observation that both *hsp80*$^{RIP}$ mutants and the wild-type strain do not conidiate under submerged culture conditions suggests that *hsp80* may not specifically influence conidiation in response to environmental cues. In filamentous fungi, conidiation is often regulated by stress-induced signaling pathways and our findings imply that *hsp80* gene mutations may alter the perception or transduction of these signals.

The results from this study highlight the essential role of the *hsp80* gene in fungal stress response and cellular homeostasis. Hsp90 homologs are widely conserved across eukaryotes and our findings provide insights into the broader significance of Hsp80 mediated chaperone activity (Schopf et al., 2017; Johnson & Brown, 2009). Given that Hsp90 inhibitors have been explored as potential antifungal agents, understanding the precise function of *hsp80* in *N. crassa* could have implications for fungal biology and pathogenesis research (Cowen & Lindquist, 2005; Lamoth et al., 2016). Further studies are needed to elucidate the detailed molecular interactions of *hsp80* with co-chaperones and stress response regulators. In summary, this study demonstrates that Hsp80 is indispensable for thermotolerance, growth regulation and stress adaptation in *N. crassa*. The functional impairments observed in *hsp80*$^{RIP}$ mutants underscore the importance of this chaperone in fungal development and stress resilience. Future research should focus on identifying interacting partners of Hsp80 and investigating its regulatory mechanisms at the post-translational level to provide deeper insights into fungal stress adaptation strategies (Zuehlke & Johnson, 2010).

# Chapter 4

# CELLULAR FUNCTION OF THE *hsp80* GENE IN THE STRESS RESPONSE OF *NEUROSPORA CRASSA*

# CHAPTER 4

# CELLULAR FUNCTION OF THE *HSP80* GENE IN THE STRESS RESPONSE OF *NEUROSPORA CRASSA*

## 4.1 Introduction

Microorganisms must adapt to fluctuating environmental conditions to survive and maintain cellular integrity. In *N. crassa*, Hsps play an essential role in cellular stress response, particularly in maintaining protein stability, metabolism and overall stress tolerance. Hsp90, a conserved molecular chaperone, has been widely studied in various organisms for its role in protein folding, stabilization and stress adaptation (Ron and Walter, 2007; Hetz, 2012). However, its specific role in *N. crassa* under different environmental stressors, such as cellulose degradation, oxidative stress, ER stress and DNA damage, remains to be fully explored.

This study aims to explore the functional significance of Hsp80 by utilizing *hsp80*$^{RIP}$ mutant strains to assess their physiological and biochemical responses under different stress conditions. Since *N. crassa* employs a complex network of cellulolytic enzymes and regulatory pathways to efficiently break down lignocellulosic biomass (Tian et al., 2009), we examined wild type and mutant strains for their ability to utilize cellulose as the sole carbon source. Additionally, to determine the role of Hsp80 in ER stress response, both wild type and mutant strains were exposed to the ER stress-inducing agent dithiothreitol (DTT). Given the established role of Hsp90 in protein folding and ER homeostasis, we hypothesize that Hsp80 contributes to similar stress adaptation mechanisms. Furthermore, oxidative stress experiments using hydrogen peroxide ($H_2O_2$) were conducted to investigate whether Hsp80 plays a role in oxidative stress regulation. By examining the stress responses of *hsp80*$^{RIP}$ mutants, this study aims to provide a deeper understanding of Hsp80's role in *N. crassa* and its potential implications for fungal biology and cellular stress adaptation.

This study aims to further elucidate the role of Hsp80 in genomic stability by assessing DNA damage tolerance in wild-type and *hsp80*$^{RIP}$ mutant strains exposed to UV irradiation and methyl methanesulfonate (MMS). Given the critical roles of photoreactivation and nucleotide excision repair (NER) pathways in responding to DNA damage (Sancar, 1996; Schärer, 2013), we hypothesize that Hsp80 contributes to DNA repair mechanisms. Additionally, this study

investigates the involvement of Hsp80 in carotenoid biosynthesis, an important photoprotective mechanism against oxidative stress. Carotenoids play a key role in protecting fungal cells from light-induced damage and their biosynthesis is tightly regulated under stress conditions (Avalos & Estrada, 2010; Rodríguez-Romero et al., 2010). By examining carotenoid accumulation in mutant strains under varying temperature conditions, we aim to determine whether Hsp80 plays a role in photoprotection and oxidative stress tolerance. This study aims to provide a thorough understanding of Hsp80's role in metabolic regulation, oxidative stress defense, protein homeostasis and DNA repair in N. crassa.

## 4.2 Results

### 4.2.1 Cellulose degradation assay of *hsp80*$^{RIP}$ mutants and wild type strain

Many microorganisms, particularly filamentous fungi, produce hydrolytic enzymes that aid in the degradation of plant cell wall components such as cellulose, hemicellulose and lignin (Carroll and Somerville 2009). Plant cell wall degrading enzymes from filamentous fungi have been studied for the development of sustainable and affordable lignocellulosic biofuels. Due to the availability of a nearly complete genome deletion set, *N. crassa* has recently gained importance as a model organism for studying the physiology of lignocellulose degradation in fungi. Glucose deprivation in the medium causes an environmental stress on the ER, which leads to interference with N-linked protein glycosylation (Scheuner et al. 2001). Therefore, glucose was replaced with cellulose in the medium, creating a glucose-deprived environment to evaluate the effect of glucose deprivation in the mutants. The *hsp80*$^{RIP}$ mutants were cultured in liquid medium containing avicel (1.5% crystalline cellulose), incubated at 30°C in complete darkness for 7 days with constant shaking at 180 rpm. After 7 days, the wild type and *hsp80*$^{RIP}$ mutants displayed variations in cellulose degradation efficiency.

Therefore, I investigated the ability of the wild type and *hsp80*$^{RIP}$ mutants to utilize cellulose as a natural substrate. Surprisingly, *hsp80*$^{RIP}$ mutants displayed differential cellulose degradation abilities compared to the wild type when grown on Vogel's Minimal Media with 2% microcrystalline cellulose as the sole carbon source. The cellulose utilization efficiency was assessed over a period of five days, monitoring changes in cellulose degradation rates among the different strains (**Figure 4.1**).

To quantify cellulose degradation efficiency, biomass weight (mg/dry weight) was measured for each strain. The wild-type strain exhibited a biomass weight of 781 ± 39.1 mg, while the

mutant strains displayed varied biomass accumulation: R4 A (765 ± 60.7 mg), R6 A (672 ± 79.4 mg), R9 a (94 ± 21.3 mg) and R14 a (719 ± 75.1 mg) **(Table 4.1)**. The R9 a mutant exhibited the most significant reduction in biomass accumulation, suggesting a strong impact of Hsp80 on cellulose metabolism.

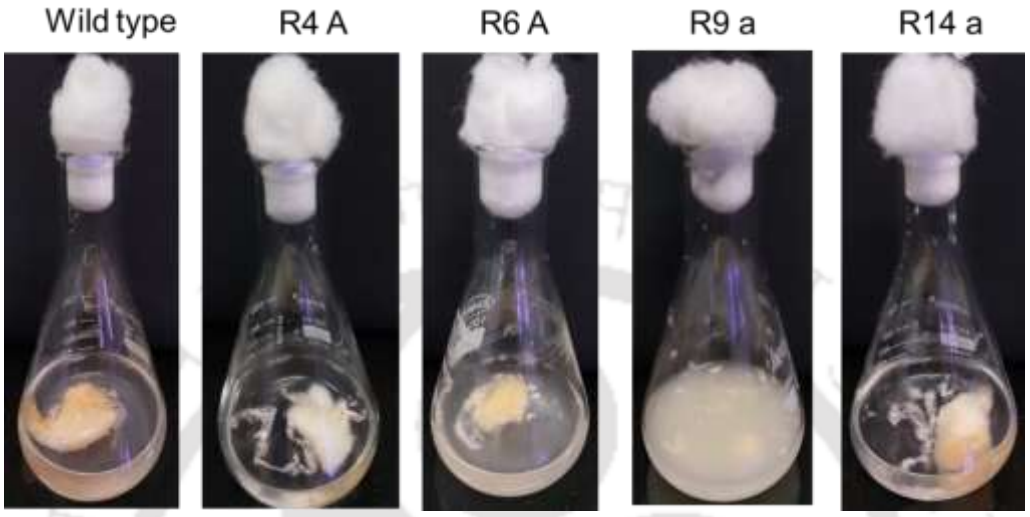


**Figure 4.1**: **Cellulose degradation assay in the wild-type and *hsp80*$^{RIP}$ mutants.** Degradation of cellulose was assessed in wild type and *hsp80*$^{RIP}$ mutants (R4 A, R6 A, R9 a and R14 a). Approximately $10^6$ conidia/ml conidial suspension was inoculated in 50 ml Vogel's cellulose liquid medium (replacing glucose with 2% cellulose) and incubated at 30 °C with shaking at 180 rpm for 7 days. Flask morphology of *N. crassa* wild type and *hsp80*$^{RIP}$ mutant strains.

**Table 4.1: Biomass accumulation in *N. crassa* strains**

| | Biomass weight (mg/ dry weight) |
|---|---|
| Wild type | 781 ± 39.1 |
| R4 A | 765 ± 60.7 |
| R6 A | 672 ± 79.4 |
| R9 a | 94 ± 21.3 |
| *R14 a* | 719 ± 75.1 |

### 4.2.2 Cellulase secretion and Glucose metabolism in *hsp80*$^{RIP}$ mutants and wild-type strain.

The *hsp80*$^{RIP}$ mutants exhibited impaired growth under cellulose as the sole carbon source, which might indicate reduced secretion of cellulase enzymes. Therefore, I measured the biomass produced from the growth culture and the growth of the strains in liquid culture complemented their biomass weights. I also determined the concentrations of secreted protein and glucose in the cultures to evaluate cellulase activity (Mishra et al. 1984; Starr and Gonc 2018). The wild type and some *hsp80*$^{RIP}$ mutants showed higher concentrations of protein and glucose in the supernatant (**Figure 4.2.**). The protein secretion concentrations in the supernatant (µg/ml) were measured as 155 µg/ml in the wild type, while the mutant strains exhibited reduced levels: 130 µg/ml in R4 A, 110 µg/ml in R6 A, 140 µg/ml in R9 a and 135 µg/ml in R14 a. Similarly, the glucose concentrations in the culture supernatant (µg/ml) were 250 µg/ml in the wild type, whereas the mutant strains showed varying reductions: 230 µg/ml in R4A, 210 µg/ml in R6 A, 60 µg/ml in R9 a and 220 µg/ml in R14 a.

However, certain *hsp80*$^{RIP}$ mutants exhibited significantly lower concentrations of secreted protein and glucose, consistent with their reduced biomass accumulation . These results suggest that *Hsp80* plays a role in regulating cellulase secretion and glucose metabolism, affecting the overall efficiency of cellulose degradation in *N. crassa*.

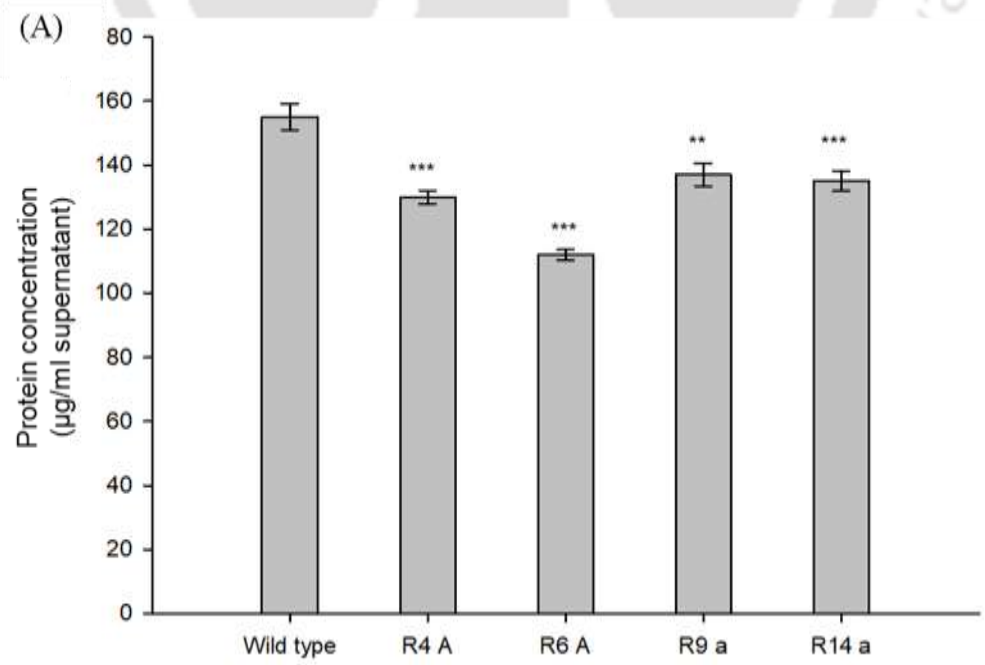

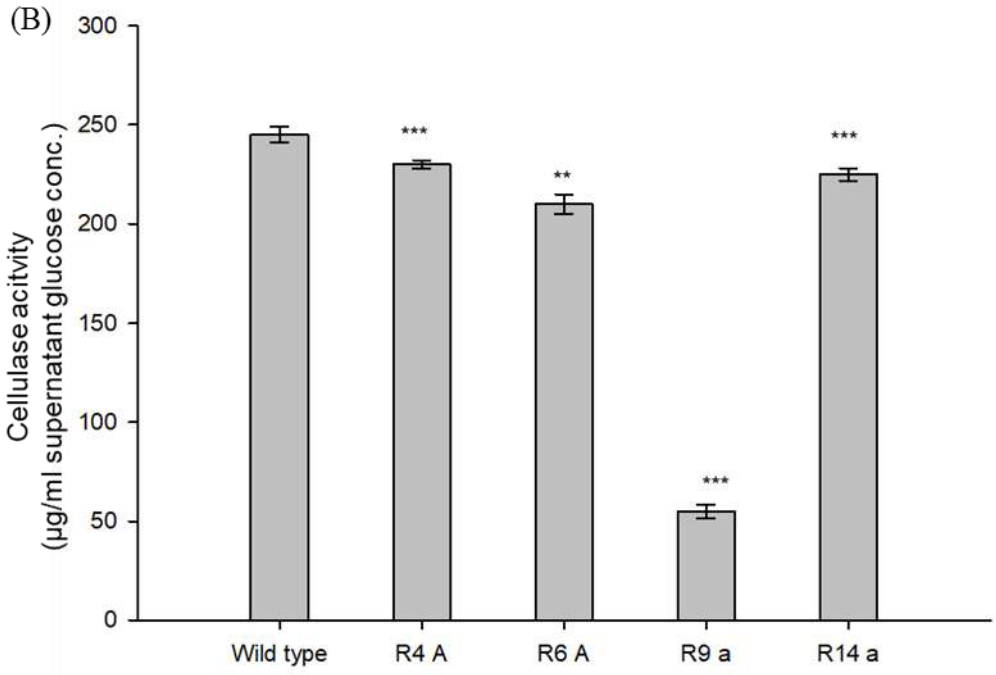


**Figure 4.2: Protein concentration and cellulase activity of *N. crassa* Strains**. (A) Protein concentrations of each strain were measured using the Bradford assay with Bovine Serum Albumin (BSA) as the control (Bradford, 1976). (B) Cellulase activity was determined by measuring the glucose released in the supernatant using the 3,5-Dinitrosalicylic acid (DNSA) assay, with D-glucose as the standard. Results are presented as mean ± standard deviation from three independent experiments (n = 3). Asterisks indicate statistically significant differences compared to the wild type, as determined by two-way ANOVA analysis, with significance levels of $P < 0.05$ (*), $P < 0.01$ (**) and $P < 0.001$ (***).

### 4.2.3 ER stress response in *hsp80*$^{RIP}$ mutants and wild type strain

The ER plays a central role in the correct folding and maturation of membrane and secretory proteins. When the ER experiences excessive protein flux or accumulates misfolded proteins, its folding capacity becomes overwhelmed, leading to ER stress (Ron and Walter, 2007; Hetz, 2012). To counteract this stress, the ER initiates a signaling cascade known as the unfolded protein response (UPR), which enhances its protein-folding capacity and reduces the burden of misfolded proteins (Bravo et al., 2012).

To examine the role of *hsp80* gene in the ER stress response, the wild type and *hsp80*$^{RIP}$ mutant strains were treated with varying concentrations (0 mM, 0.5 mM, 1 mM and 2 mM) of the ER stress-inducing agent dithiothreitol (DTT), which disrupts disulfide bond formation and impairs proper protein folding. The growth and development of aerial hyphae in these strains

were observed. The *hsp80*$^{RIP}$ mutants exhibited a significant reduction in aerial hyphae formation at 2 mM DTT, whereas the wild type strain showed a moderate decrease in growth under the same conditions (**Figure 4.3**).

To examine the role of the *hsp80* gene in the ER stress response, wild-type and *hsp80*$^{RIP}$ mutant strains were treated with 10 mM dithiothreitol (DTT), an ER stress-inducing agent that disrupts disulfide bond formation and impairs proper protein folding. The growth and development of aerial hyphae were observed, revealing a significant reduction in aerial hyphae formation in *hsp80*$^{RIP}$ mutants, whereas the wild-type strain exhibited a moderate decrease in growth under the same conditions (Fig. 4.3). The decreased in survival percentage in *hsp80*$^{RIP}$ mutants under ER stress suggests a key role of Hsp80 in maintaining cellular integrity during protein-folding challenges.

Thus, these findings indicate that *hsp80* gene plays a critical role in the ER stress response, likely functioning as a molecular chaperone to stabilize proteins and support proper folding under stress conditions. The increased sensitivity of *hsp80*$^{RIP}$ mutants to DTT-induced ER stress suggests that Hsp80 is essential for maintaining ER homeostasis and facilitating stress adaptation.

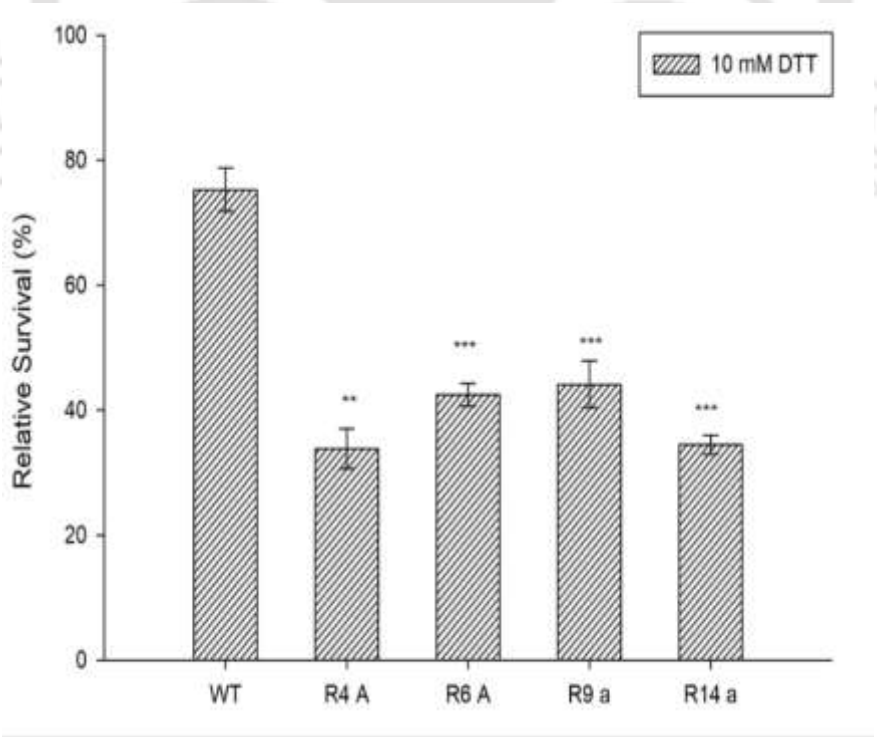


**Figure 4.3**: **Assay for Endoplasmic Reticulum stress using dithiothreitol (DTT).** Survival percentage of *N. crassa* in wild-type and *hsp80*$^{RIP}$ mutant strains in response to DTT. To evaluate DTT sensitivity, strains were inoculated in VG liquid medium containing 10 mM DTT

and incubated at 30 °C in constant darkness overnight. The percent survival was calcculated relative to 0 mM DTT respectively. Standard deviations are indicated by error bars, calculated from three independent experiments (n = 3). Statistical significance is represented by P-values < 0.05 (*), < 0.01 (**) and < 0.001 (***), as measured by a one-way ANOVA test.

### 4.2.4 Oxidative stress response in *hsp80*$^{RIP}$ mutants and wild type strain

Oxidative stress is an environmental challenge to which any microorganism must adapt. The stress response triggered by reactive oxygen species (ROS) induces a signaling cascade in several fungi, including *N. crassa* (Lamb et al., 2013). In *N. crassa*, oxidative stress signaling crosstalks with multiple pathways, including calcium signaling and stress response mechanisms (Virgilio et al., 2017). The oxidative stress response also regulates the expression of key antioxidant enzymes, which are crucial for detoxifying ROS and maintaining redox balance in *N. crassa* (Lamb et al., 2013). The *hsp80*$^{RIP}$ mutants are expected to play a role in oxidative stress resistance and their ability to survive ROS-induced stress was investigated. I performed an oxidative stress assay to investigate the effect of ROS on the wild type and *hsp80*$^{RIP}$ mutant strains. Conidia ($10^3$ spores/ml) were spread in FGS supplemented with different concentrations of hydrogen peroxide ($H_2O_2$) 5 mM and 10 mM) and incubated at 30 °C under constant darkness overnight. Conidial germlings were counted and calculated relative to 0 mM. *N. crassa* grows optimally in the absence of oxidative stress and this was used as the control condition in this study. Under oxidative stress conditions, all strains showed a dose-dependent decrease in survival. At 5 mM $H_2O_2$, the wild-type strain exhibited a relative survival of 75%, whereas the *hsp80*$^{RIP}$ mutants showed significantly lower survival rates, with R4 A at 45%, R6 A at 42%, R9 a at 50% and R14 a at 47%. Upon exposure to 10 mM $H_2O_2$, the survival rates of the mutants dropped further, with wild type maintaining 62% survival, while the mutants exhibited a drastic reduction (R4 A at 18%, R6 A at 20%, R9 a at 35%, R14 a at 22%) (**Figure 4.4**). The significant reduction in survival of the *hsp80*$^{RIP}$ mutants at both 5 mM and 10 mM $H_2O_2$ indicates that Hsp80 plays a critical role in maintaining cellular defense mechanisms against ROS. Additionally, the normal growth of *N. crassa* strains under non-stress conditions suggests that Hsp80 function is dispensable under basal conditions but becomes crucial for survival under oxidative stress

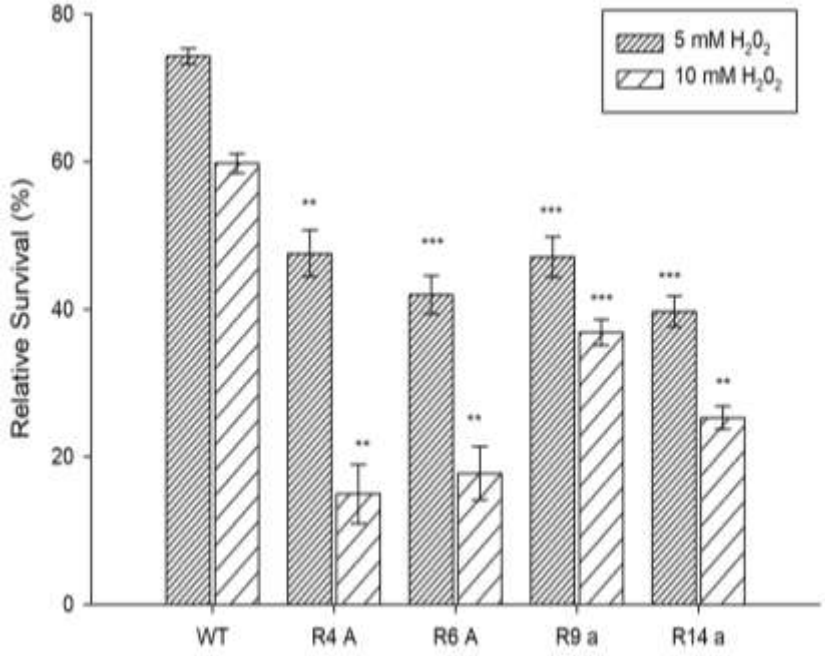


**Figure 4.4: Oxidative stress assay.** Survival percentage of *N. crassa* wild-type and *hsp80*$^{RIP}$ mutant strains in response to $H_2O_2$. To evaluate, condia were spread in FGS agar medium containing 5 mM $H_2O_2$ and 10 mM $H_2O_2$ and incubated at 30 °C in constant darkness overnight. The percent survival is relative to 0 mM $H_2O_2$ was calculated. Standard deviations are indicated by error bars, calculated from three independent experiments (n = 3). Statistical significance is represented by P-values < 0.05 (*), < 0.01 (**) and < 0.001 (***), as measured by a one-way ANOVA test.

### 4.2.5 Carotenoid accumulation is impaired in *hsp80*$^{RIP}$ mutants

Carotenoids are essential secondary metabolites in *N. crassa*, functioning as photoprotective pigments and antioxidants that mitigate oxidative stress (Avalos and Estrada, 2010). The biosynthesis and accumulation of carotenoids are tightly regulated by environmental stimuli, particularly light exposure and oxidative stress, which modulate their production through complex transcriptional and enzymatic control mechanisms (Rodríguez-Romero et al., 2010). While the role of molecular chaperones such as Hsp80 in stress response pathways is well established, their potential involvement in carotenoid biosynthesis remains unexplored.

To assess the impact *hsp80*$^{RIP}$ mutants of on carotenoid accumulation, the total carotenoid content was quantified in wild type and *hsp80*$^{RIP}$ mutant strains. The wild type strain exhibited a significant increase in carotenoid accumulation, with levels reaching 529.6 ± 71.27 µg/g dry weight at 30 °C, 331.6 ± 11.87 µg/g at 22 °C and 161.6 ± 58.83 µg/g at 8 °C. In contrast, the

*hsp80*$^{RIP}$ mutants displayed varying degrees of impairment in carotenoid accumulation compared to wild type. The R4 A and R 6A mutants exhibited moderate reductions in carotenoid levels at 30 °C (493.8 ± 33.09 µg/g and 492.4 ± 111.4 µg/g, respectively), whereas the R9 a mutant accumulated the highest levels among mutants (718.6 ± 55.72 µg/g at 30 °C), surpassing wild type. However, at 8 °C, all mutants displayed a significant drop in carotenoid accumulation, with R4 A, R6 A and R14 a showing severe reduction (78.8 ± 32.80 µg/g, 78.5 ± 61.23 µg/g and 78.32 ± 62.33 µg/g, respectively). The R9 a strain also showed a notable decline at 8 °C (110.74 ± 8.11 µg/g), though it retained higher levels than other mutants.

Interestingly, at 22 °C, the R4 A and R6 A mutants exhibited elevated carotenoid levels (553.4 ± 118.06 µg/g and 516.8 ± 112 µg/g, respectively) compared to wild type, suggesting a possible temperature-dependent compensatory effect. Conversely, R14 a (506.4 ± 183.2 µg/g) and R9 a (522.4 ± 99.56 µg/g) remained comparable to wild type at this temperature **(Figure 4.5, Table 4.2)**. Given the role of carotenoids in oxidative stress resistance, these results further suggest that the reduced oxidative stress tolerance observed in *hsp80*$^{RIP}$ mutants may be partially attributable to deficiencies in carotenoid-mediated photoprotection.

**Table 4.2**: **Carotenoid content of the wild type and *hsp80*$^{RIP}$ mutant strains at different temperatures**

| Strains | Carotenoids (µg/g dry weight) | | |
|---|---|---|---|
| | 30 ˚C | 22 ˚C | 8 ˚C |
| WT | 529.6 ± 71.27 | 331.6 ± 11.87 | 161.6 ± 58.83 |
| R4 A | 493.8 ± 33.09 | 553 ± 118.06 | 78.8 ± 32.809 |
| R6 A | 492.4 ± 111.4 | 516.8 ± 112 | 78.5 ± 61.23 |
| R9 a | 718.6 ± 55.72 | 522.4 ± 99.56 | 110.74 ± 8.11 |
| R14 a | 575.8 ± 47.8 | 506.4 ± 183.2 | 78.32 ± 62.33 |

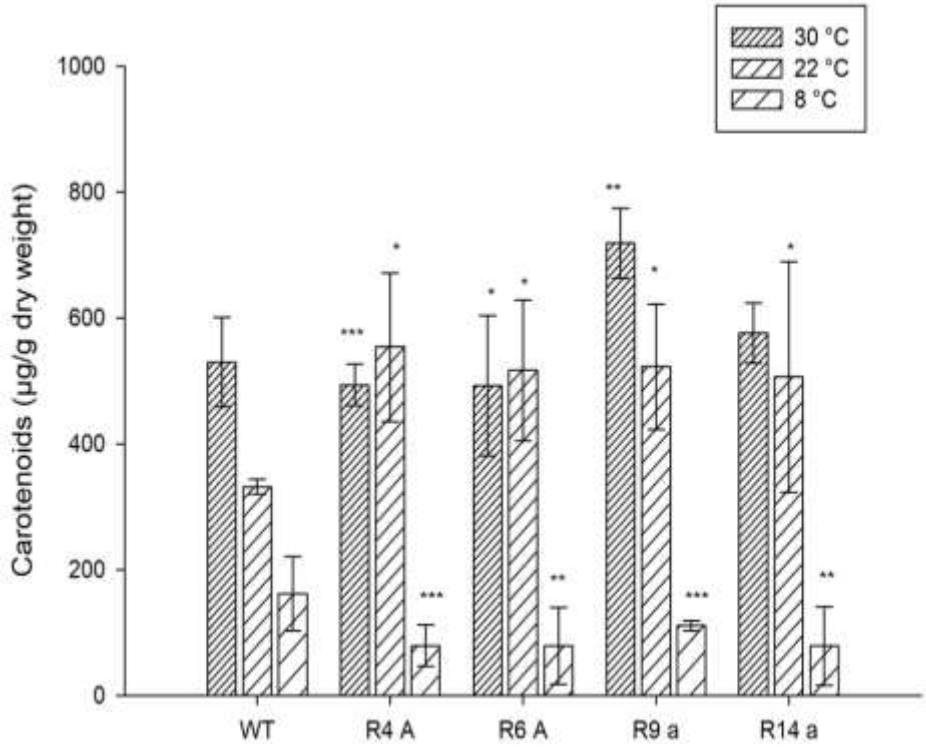


**Figure 4.5**: **Carotenoid accumulation in *hsp80*$^{RIP}$ mutant strains.** Strains were grown in VG medium supplemented with 0.2% Tween-80 and incubated initially at 30°C in the dark for 48 h, followed by 24 h of white light exposure (illuminated with two fluorescent bulbs, Philips TL-D 18W/54 lamp, 18W, 6500 K, 1015 lumens) at three different temperatures (8 °C, 22 °C and 30 °C). Carotenoid accumulation is expressed as µg carotenoid per gram of dry weight. Error bars indicate standard deviations, calculated from three independent experiments (n = 3). Statistical significance is represented by P-values < 0.05 (*), < 0.01 (**) and < 0.001 (***).

## 4.3 DNA damage and repair mechanisms in *hsp80*$^{RIP}$ mutants

### 4.3.1 The mutant strains exhibit increased sensitivity to UV-Induced DNA damage

Ultraviolet (UV) radiation is a potent environmental stressor that induces DNA lesions, including cyclobutane pyrimidine dimers (CPDs) and 6-4 photoproducts, which, if left unrepaired, can lead to genomic instability and cell death (Sancar, 1996). Molecular chaperones such as Hsp90 are known to regulate cellular stress responses, but their specific role in DNA repair remains largely unexplored. The role of Hsp90 in stress adaptation extends beyond oxidative stress resistance and carotenoid biosynthesis to include genome maintenance under UV-induced DNA damage. Given that carotenoids serve as photoprotective pigments that mitigate oxidative stress (Avalos and Estrada, 2010), the reduced carotenoid accumulation observed in *hsp80*$^{RIP}$ mutants may contribute to their increased susceptibility to UV stress.

Carotenoids have been implicated in protecting fungal cells from light-induced damage by quenching reactive oxygen species (ROS) and preventing oxidative DNA damage (Rodríguez-Romero et al., 2010). The heightened UV sensitivity of *hsp80*$^{RIP}$ mutants, therefore, may result from a combination of impaired carotenoid-mediated photoprotection and defective DNA repair mechanisms.

To evaluate the involvement of Hsp80 in UV damage resistance, both quantitative and qualitative UV sensitivity assays were performed on wild type and *hsp80*$^{RIP}$ mutant strains . In the quantitative germling survival assay, conidia were exposed to increasing doses of UV radiation (0 J/m², 100 J/m², 200 J/m², 300 J/m²) and subsequently plated on Vogel's minimal medium. Cultures were incubated at 30 °C for 48 hrs in the dark, after which germling survival was assessed by counting the proportion of viable germlings relative to the untreated controls. Under non-irradiated conditions (0 J/m²), all strains exhibited comparable conidial germling survival counts, indicating that the *hsp80*$^{RIP}$ mutations do not affect baseline viability. However, upon UV exposure, *hsp80*$^{RIP}$ mutants displayed a dose dependent reduction in survival compared to the wild type strain.

At 100 J/m², the wild type strain retained 73.5% germling survival, while *hsp80*$^{RIP}$ mutants exhibited a moderate decline, with survival rates of 52.2% at R4 A, 50.9% at R6 A, 48.4% at R9 a and 54.6% at R14 a. At 200 J/m², wild type survival dropped to 49.4%, whereas *hsp80*$^{RIP}$ mutants showed significantly lower germling survival, with R4 A at 27.7%, R6 A at 29.5%, R9 a at 31.8% and R14 a at 22.4%. At the highest UV dose of 300 J/m², wild type survival was further reduced to 26.1%, but *hsp80*$^{RIP}$ mutants were severely compromised, exhibiting survival rates of 12.3% (R4 A), 14.6% (R6 A), 13.2% (R9 a) and 10.5% (R14 a) **(Figure 4.6)**. For the qualitative germling survival assay further visualized the impact of increasing UV doses on germling viability by spotting serial dilutions ($10^6$ to 10 conidia) of wild type and *hsp80*$^{RIP}$ mutant strains onto VM plates following UV irradiation.

These qualitative germling survival assays were further supported by quantitative results, which showed a progressive loss of viable germlings at higher UV doses. The R9 a and R14 a mutants exhibited the most pronounced reduction in germling survival, particularly at 200 J/m² and 300 J/m² **(Figure 4.7).** In contrast, the wild type strain maintained higher germling survival across all tested UV doses. The qualitative assay confirms that *hsp80*$^{RIP}$ mutants exhibit a clear UV sensitivity phenotype, with reduced DNA damage tolerance leading to impaired ascospore germling survival.

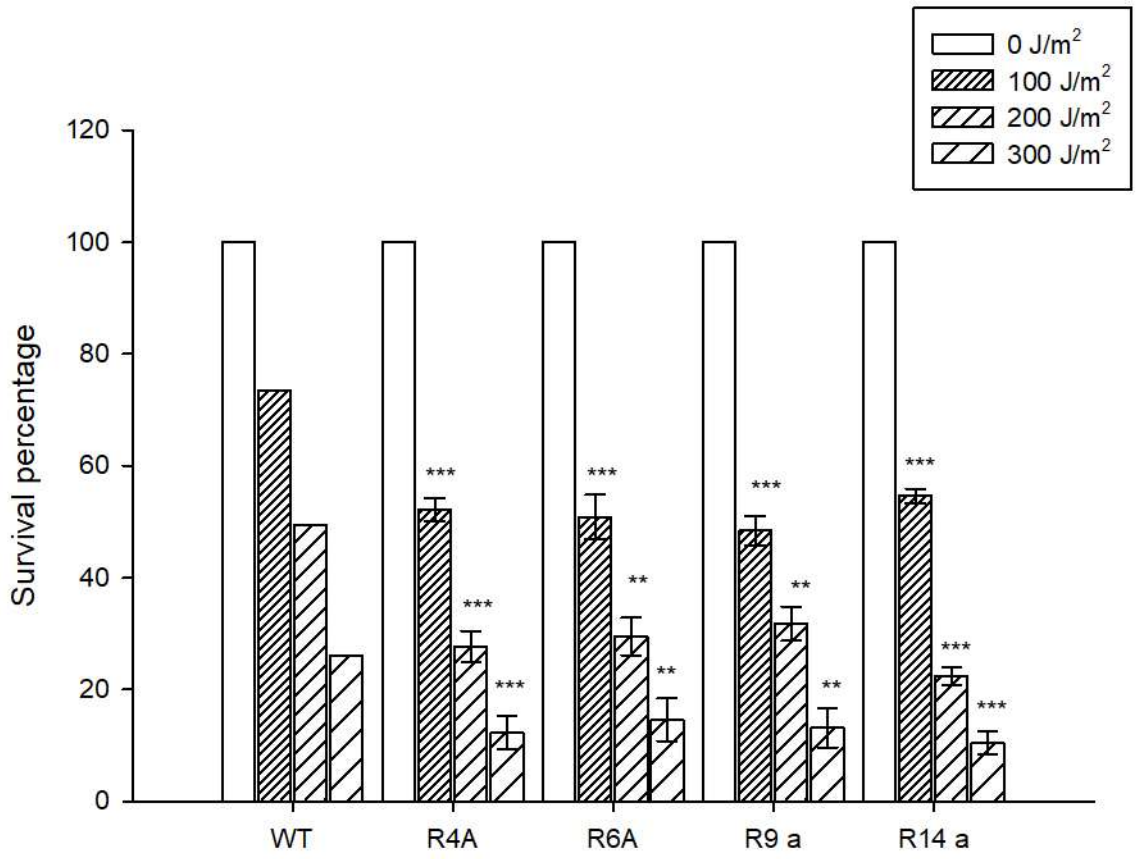


**Figure 4.6**: **Quantitative UV assay for wild type and *hsp80*$^{RIP}$ mutants.** Conidial germlings of wild type and *hsp80*$^{RIP}$mutants (R4 A, R6 A, R9 a and R14 a) were exposed to increasing doses of UV radiation (0 J/m², 100 J/m², 200 J/m² and 300 J/m²) and subsequently incubated at 30 °C in the dark for 48 hours before assessing survival percentage. Survival rates were determined relative to the untreated control (0 J/m²). Standard deviations are indicated by error bars, calculated from three independent experiments (n = 3). Statistical significance is represented by P-values < 0.05 (*), < 0.01 (**) and < 0.001 (***), as measured by a one-way ANOVA test.

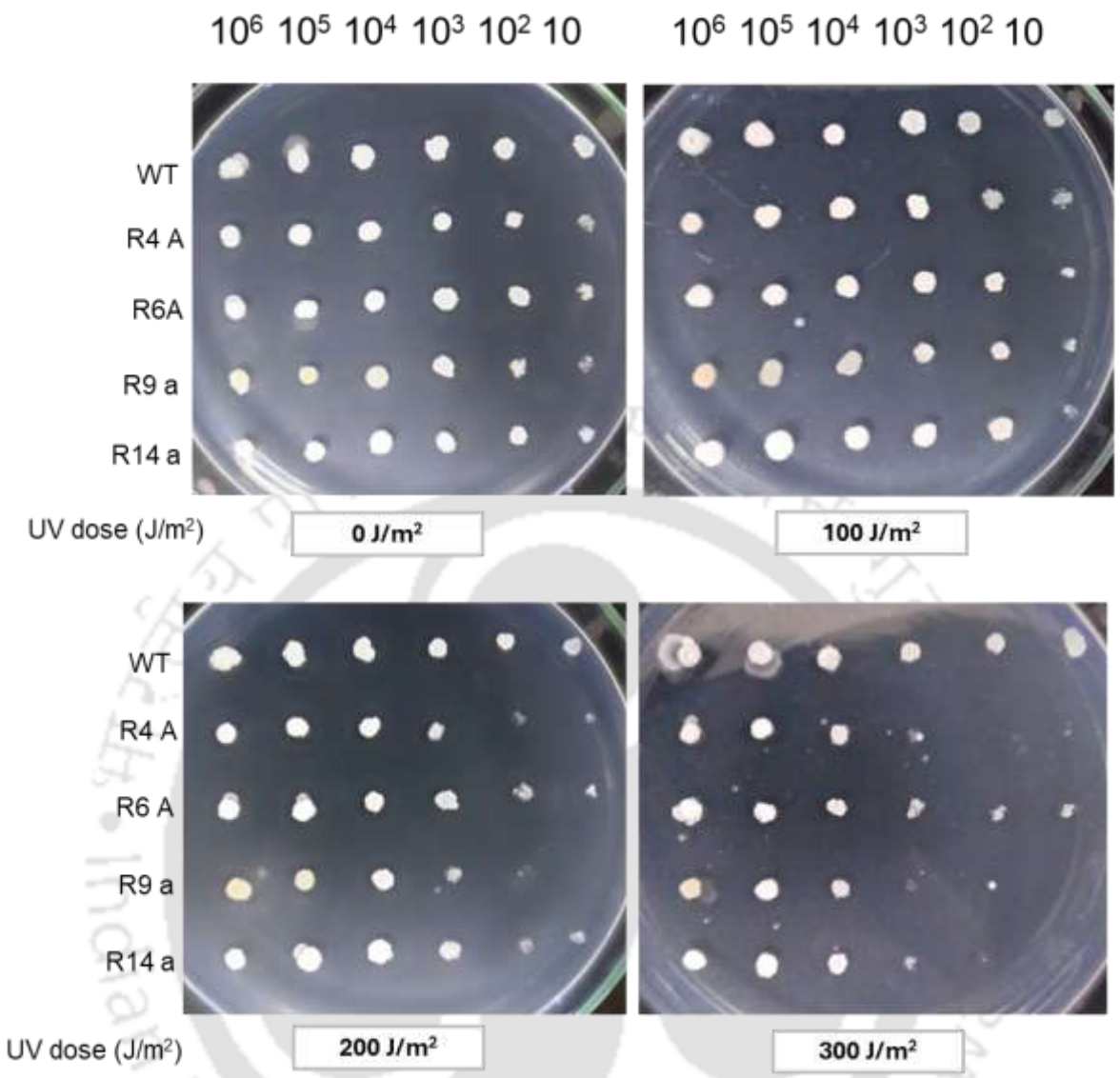


**Figure 4.7**: **Qualitative assay *hsp80*$^{RIP}$ mutants in UV.** Conidial germling were grown on plates and exposed to UV radiation at 0 J/m², 100 J/m², 200 J/m² and 300 J/m². Following UV exposure, plates were incubated in darkness for 48 hours at 30 °C and colony formation was assessed to determine survival at each UV dose. Serial dilutions ($10^6$ to 10 ascospores) were performed before plating to quantify survival across different UV exposures.

### 4.3.2 The Mutants exhibit impaired photoreactivation-mediated DNA repair

Ultraviolet (UV) radiation is a potent genotoxic stressor that induces DNA damage, primarily in the form of cyclobutane pyrimidine dimers (CPDs) and 6-4 photoproducts, which disrupt genome integrity and interfere with transcription and replication (Sancar, 1996). To counteract these lesions, *Neurospora crassa* utilizes multiple DNA repair mechanisms, including nucleotide excision repair (NER), which operates in the absence of light and photoreactivation,

a light-dependent repair pathway mediated by photolyases, which directly reverse CPD lesions (Todo, 1999). Given the increased UV sensitivity of *hsp80*$^{RIP}$mutants, a photoreactivation assay was conducted to assess whether Hsp80 is involved in facilitating light-dependent DNA repair.

To evaluate photoreactivation capacity, wild type and *hsp80*$^{RIP}$mutant strains were grown on plates and exposed to UV radiation at 0, 100, 200 and 300 J/m². Following UV exposure, the strains were illuminated with visible light for 30 minutes, then allowed to recover and grow in darkness for 48 hours before survival assessment.

Under dark incubation, all strains exhibited survival patterns consistent with their previously observed UV sensitivity, where *hsp80*$^{RIP}$mutants displayed significantly lower survival rates compared to wild type. Wild type showed substantial recovery when incubated under photo reactivating light, confirming the efficiency of photolyase-mediated CPD repair. However, *hsp80*$^{RIP}$mutants demonstrated significantly reduced survival under photoreactivation conditions, suggesting a defect in light-dependent DNA repair mechanisms.

At 100 J/m², photoreactivation increased survival to 91.3% in the wild-type strain, whereas mutant strains exhibited moderate improvement, with survival increasing to 72.6% at R4 A, 67.4% at R6 A, 59.3% at R9 a and 56.8% at R14 a. At 200 J/m², wild-type survival improved to 78.2%, whereas *hsp80*$^{RIP}$mutants showed reduced photoreactivation efficiency, with survival increasing to 51.6% at R4 A, 46.9% at R6 A, 38.2% at R9 a and 30.7% at R14 a. At 300 J/m², wild-type survival increased to 56.4%, whereas *hsp80*$^{RIP}$ mutants exhibited minimal recovery, with survival increasing to 31.2% at R4 A, 28.5% at R6 A 19.4% at R9 a and 16.3% at R14 a (**Figure 4.8**). These findings indicate that *hsp80* is essential for efficient photoreactivation in *N. crassa*, potentially by regulating photolyase stability, activity, or recruitment to CPD lesions. The reduced survival of *hsp80*$^{RIP}$ mutants following photoreactivation suggests a deficiency in either photolyase expression or functionality, thereby compromising the efficiency of light-dependent DNA repair. Moreover, since carotenoids are known to contribute to photoprotection by neutralizing reactive oxygen species (ROS) and reducing oxidative DNA damage, the previously observed decrease in carotenoid accumulation in *hsp80*$^{RIP}$ mutants may further exacerbate their UV sensitivity by impairing both photoprotection and CPD repair.

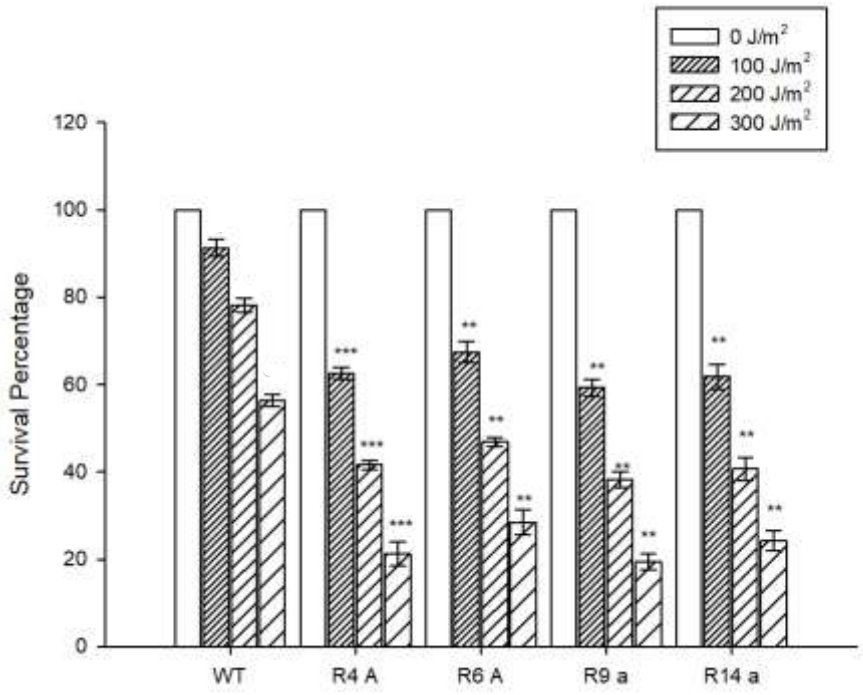


**Figure 4.8**: **Photoreactivation assay of *hsp80*$^{RIP}$ mutants following UV irradiation.** Condial germling were grown on plates and exposed to UV radiation at 0 J/m², 100 J/m², 200 J/m² and 300 J/m². Following UV exposure, the strains were illuminated with visible light for 30 minutes, then allowed to recover and grow in darkness for 48 hours at 30°C. Survival rates were determined relative to the untreated control (0 J/m²). Error bars indicate the standard deviations calculated from three independent experiments (n = 3). Statistical significance is represented by P-values < 0.05 (*), < 0.01 (**) and < 0.001 (***), as determined by a one-way ANOVA test, compared to the wild-type strain.

### 4.3.3 The mutants show increased sensitivity to by MMS

Genotoxic agents such as methyl methanesulfonate (MMS) induce DNA damage primarily through alkylation of nucleotide bases, resulting in replication stress and genome instability if not efficiently repaired (Lundin et al., 2005). In *N. crassa*, cellular resistance to alkylating agents is primarily mediated by base excision repair (BER) and translesion synthesis (TLS) pathways, which facilitate the removal of alkylated bases and allow DNA replication to proceed despite the presence of lesions (Friedberg et al., 2006). Given the established role of Hsp80 in stress adaptation and genome maintenance, a MMS sensitivity assay was conducted to evaluate whether *hsp80*$^{RIP}$ mutants exhibit defects in alkylation damage repair. To assess the impact of MMS-induced DNA damage on the survival of *hsp80*$^{RIP}$ mutants, conidial germling were exposed to 0.03% MMS and subsequently plated on FGS agar medium. Cultures were incubated at 30°C for 24 hrs in the dark, after which germling survival was assessed by

counting the proportion of viable germlings relative to the untreated control with 0% MMS. In the wild type strain, survival remained high at 82.3% following MMS exposure, indicating efficient repair of alkylation-induced DNA damage. In contrast, *hsp80*$^{RIP}$ mutants displayed significantly reduced survival, suggesting compromised DNA damage tolerance mechanisms. The R4 A strain exhibited a moderate decrease in survival at 65.1%, whereas R6 A and R9 a showed more pronounced sensitivity, with survival rates declining to 52.6% and 50.8%, respectively (**Figure 4.9**). The R14 a mutant demonstrated relatively better survival at 67.9% compared to other *hsp80*$^{RIP}$ mutants but remained significantly more sensitive than the wild type strain.

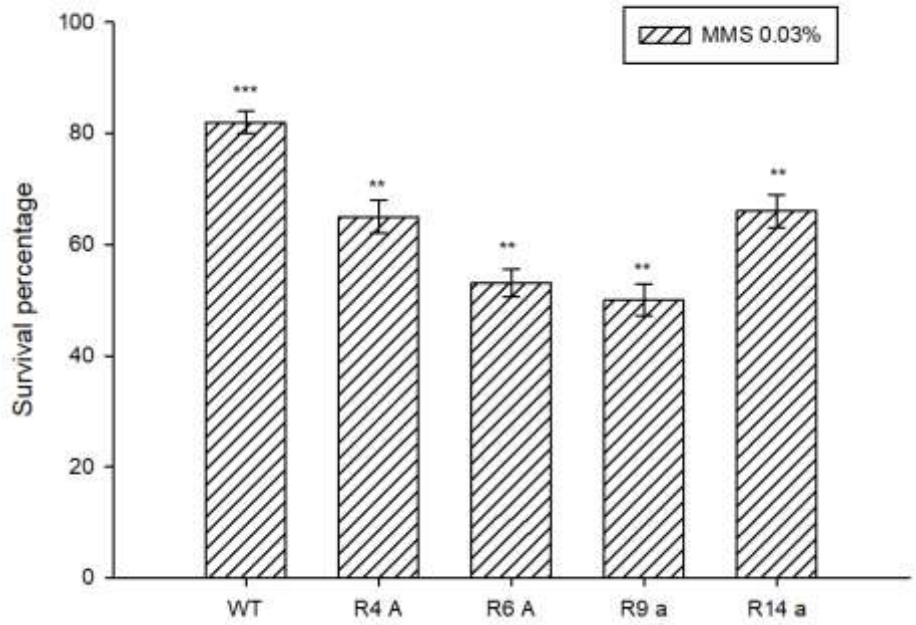


**Figure 4.9: MMS Sensitivity Assay.** Sensitivity to MMS (0.03%) was evaluated by determining the survival percentage after treatment. Error bars indicate the standard deviations calculated from three independent experiments (n = 3) and the significance given by P values < 0.05 (*), < 0.01 (**) and < 0.001 (***), as measured by a one-way ANOVA test.

### 4.3.4 Expression analysis of DNA repair genes in *hsp80*$^{RIP}$ mutants

The heightened UV sensitivity of *hsp80*$^{RIP}$ mutants suggests a potential defect in the transcriptional regulation of DNA repair genes following UV exposure. To assess this, quantitative expression analysis was performed for key DNA repair genes (*upr-1, mus-26, mus-52*) in wild type and *hsp80*$^{RIP}$ mutant strains after 200 J/m² UV irradiation.

In wild type strains, UV exposure led to a strong transcriptional induction of these repair genes, with *upr-1* exhibiting 2.9 fold upregulation, while *mus-26* and *mus-52* were induced 3.5 fold and 2.7 fold, respectively, relative to untreated controls. In contrast, *hsp80*$^{RIP}$ mutants exhibited a significantly attenuated transcriptional response, suggesting an impaired activation of DNA repair pathways. The *upr-1* gene, which is involved in post-replication repair and translesion synthesis, showed only 1.6 fold induction in R4 A, 1.3 fold in R6 A, 1.1 fold in R9 a and 0.9 fold in R14 a, indicating a compromised ability to upregulate UV damage bypass mechanisms (**Figure 4.10**). Similarly, *mus-26*, a key component of the NER pathway, displayed 3.5-fold upregulation in wild type, while its induction in *hsp80*$^{RIP}$ mutants remained significantly lower, with R4 A at 1.8 fold, R6 A at 1.5 fold, R9 a at 1.0 fold and R14 a at 0.8-fold. The defective induction of *mus-26* suggests that NER efficiency is impaired in the absence of functional *hsp80*, contributing to the persistence of UV-induced lesions. The expression pattern of *mus-52*, which is involved in double-strand break repair through the non-homologous end-joining (NHEJ) pathway, followed a similar trend. While wild type cells exhibited 2.7 fold induction following UV exposure, *hsp80*$^{RIP}$ mutants showed a much weaker response, with expression levels at 1.4 fold in R4 A, 1.2 fold in R6 A, 0.9 fold in R9a and 0.7 fold in R14 a. The impaired upregulation of *mus-52* suggests that *hsp80* may be required for efficient recruitment or stabilization of NHEJ repair factors following UV-induced DNA damage.

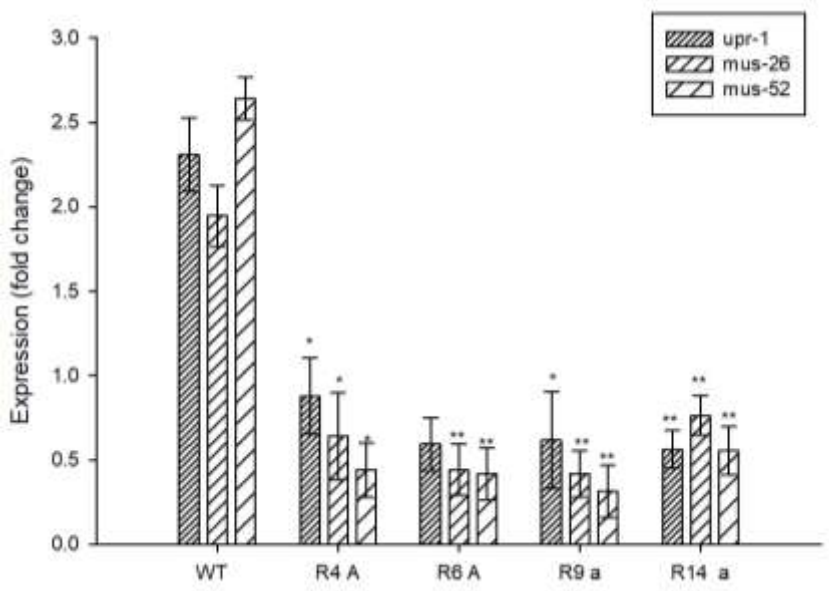


**Figure 4.10: Gene Expression Analysis of wild type and *hsp80*$^{RIP}$mutants under UV.** Expression levels of *upr-1, mus-26 and mus-52* in wild type and *hsp80*$^{RIP}$ mutant strains (R4 A, R6 A, R9 a and R14 a) were evaluated by qRT-PCR. The strains were grown at 30°C for 14 hours, subjected to a UV dosage of 200 J/m² and then incubated in the dark at 30°C for another

2 hours. Fold changes were calculated using the 2^−ΔΔCT method (Livak and Schmittgen, 2001), with the control (wild type with UV exposure) as the calibrator and β-tubulin as the endogenous control. Standard deviations were represented as error bars, based on data from three independent experiments (n = 3). Statistical significance was determined using a one-way ANOVA test, with P-values < 0.05 (*), < 0.01 (**) and < 0.001 (***) compared to the wild type strain.

### 4.4 Discussion

In this chapter, I described the functional characterization of the Hsp80 chaperone in *N. crassa* under various stress conditions. The study identified the critical role of Hsp80 in cellulose degradation, ER stress response, oxidative stress tolerance, DNA damage repair and carotenoid biosynthesis. Furthermore, I investigated the phenotypic consequences of *hsp80*$^{RIP}$ mutations to determine the cellular functions of this gene in metabolic regulation, stress adaptation and genomic stability in *N. crassa*.

The results of the cellulose degradation assay that I conducted highlight a critical role of Hsp80 in fungal metabolism and carbohydrate utilization. The results showed that wild type *N. crassa* efficiently degraded cellulose as a sole carbon source, whereas *hsp80*$^{RIP}$ mutants exhibited varying degrees of impairment in cellulose utilization. Among the mutants, the most significant reduction in biomass accumulation was observed in the R9 a strain, suggesting that specific mutations in Hsp80 strongly impact carbohydrate metabolism. A key observation was that *hsp80*$^{RIP}$mutants showed reduced cellulase enzyme secretion, as evidenced by lower protein and glucose concentrations in the culture supernatant. This defect suggests that Hsp80 may play a role in the proper folding, maturation and secretion of cellulase enzymes, which are essential for breaking down cellulose into metabolizable sugars. Given that protein secretion is tightly linked to endoplasmic reticulum function and that defects in chaperone-mediated protein folding can lead to inefficient enzymatic activity (Scheuner et al., 2001), I determined that Hsp80 supports cellulase function through its chaperone activity in the ER and cytoplasm. Previous studies have demonstrated that fungal chaperones, including Hsp90 homologs, are involved in regulating the secretion of extracellular enzymes critical for biomass degradation (Carroll & Somerville, 2009). The reduced cellulase secretion in *hsp80*$^{RIP}$ mutants further supports the idea that Hsp80 directly regulates the production and export of cellulolytic enzymes.

To determine the role of Hsp80 in ER homeostasis, I analyzed the sensitivity of *hsp80*$^{RIP}$ mutants to dithiothreitol (DTT), an ER stress-inducing agent. The results show that *hsp80*$^{RIP}$ mutants exhibited significantly reduced aerial hyphae formation under ER stress conditions, indicating that Hsp80 is required for protein stability and cellular adaptation to ER stress. The ER stress response, also known as the unfolded protein response (UPR), is a critical pathway that ensures proper protein folding and prevents protein aggregation. The increased sensitivity of *hsp80*$^{RIP}$ mutants to DTT suggests that Hsp80 plays a protective role in mitigating ER stress by assisting in protein refolding and degradation of misfolded proteins.

To examine the role of Hsp80 in oxidative stress resistance, I exposed *hsp80*$^{RIP}$ mutants to different concentrations of hydrogen peroxide ($H_2O_2$). The results indicate that *hsp80*$^{RIP}$ mutants exhibited increased sensitivity to oxidative stress, with significantly reduced survival at 5 mM and 10 mM $H_2O_2$ compared to the wild type. Given that oxidative stress also affects other cellular pathways, the defects observed in *hsp80*$^{RIP}$ mutants suggest that Hsp80 is an important regulator of stress resistance in *N. crassa*.

To further investigate the role of Hsp80 in genomic stability, *hsp80*$^{RIP}$ mutants and wild type strains were subjected to UV irradiation and methyl methanesulfonate (MMS) exposure to assess DNA damage tolerance. I found that *hsp80*$^{RIP}$ mutants exhibited increased susceptibility to UV-induced DNA damage, with reduced survival rates following 100 J/m², 200 J/m² and 300 J/m² UV exposure. Additionally, *hsp80*$^{RIP}$ mutants showed impaired photoreactivation-mediated DNA repair, suggesting that Hsp80 is required for light-dependent repair pathways. The impaired transcriptional response of DNA repair genes (*upr-1, mus-26, mus-52*) in *hsp80*$^{RIP}$ mutants suggests that Hsp80 plays a regulatory role in DNA damage repair pathways, including nucleotide excision repair (NER) and homologous recombination (HR). Moreover, the increased sensitivity of *hsp80*$^{RIP}$ mutants to MMS-induced alkylation damage further supports the role of Hsp80 in maintaining genome integrity under genotoxic stress.

Carotenoids function as antioxidant pigments that protect fungal cells from oxidative and phototoxic stress. To investigate the role of Hsp80 in carotenoid biosynthesis, I measured carotenoid accumulation in *hsp80*$^{RIP}$ mutants under different temperature conditions. The results indicate that *hsp80*$^{RIP}$ mutants displayed reduced carotenoid accumulation, particularly at 8 °C and 30 °C, suggesting that Hsp80 is required for temperature-dependent carotenoid biosynthesis. Given that carotenoids contribute to oxidative stress resistance, the reduced

oxidative stress tolerance observed in *hsp80*$^{RIP}$ mutants may be partially attributed to defects in carotenoid-mediated photoprotection. Additionally, since carotenoid biosynthesis is regulated by light exposure, the increased UV sensitivity of *hsp80*$^{RIP}$ mutants may also result from impaired carotenoid production and photoprotective responses.

In this chapter, I described the critical role of Hsp80 in various cellular stress responses in *N. crassa*. Furthermore, I investigated the phenotypic consequences of *hsp80*$^{RIP}$ mutations to identify the function of this gene in cellulose metabolism, ER stress adaptation, oxidative stress resistance, DNA damage repair and carotenoid biosynthesis. The findings highlight that Hsp80 is a multifunctional chaperone that plays an essential role in stress adaptation, metabolic regulation and genomic stability. The defects observed in *hsp80*$^{RIP}$ mutants emphasize the significance of Hsp80 in fungal physiology and survival under environmental stress conditions.

# CHAPTER 5

# COMPUTATIONAL ANALYSIS AND MOLECULAR DYNAMICS SIMULATION OF HSP80 IN *NEUROSPORA CRASSA*

# CHAPTER 5

# COMPUTATIONAL ANALYSIS AND MOLECULAR DYNAMICS SIMULATION OF HSP80 IN *NEUROSPORA CRASSA*

## 5.1 Introduction

Molecular chaperones play a very important role in maintaining cellular proteostasis by assisting in protein folding, preventing aggregation and facilitating stress responses (Taipale et al., 2010; Schopf et al., 2017). Heat Shock Protein 80 is an essential chaperone in *N. crassa* that interacts with a wide range of client proteins and co-chaperones to modulate cellular stability and stress adaptation. Understanding the functional interactions, regulatory mechanisms and structural dynamics of HSP80 provides critical insights into its role in maintaining cellular homeostasis across diverse physiological conditions.

In chapters 3 and 4, I characterized the role of HSP80 in *N. crassa* demonstrating its involvement in stress adaptation, growth regulation and metabolic stability. These results found that *hsp80*$^{RIP}$ mutants have problems in thermotolerance, oxidative stress resistance, cellulose breakdown, ER stress response and DNA damage repair highlighting the chaperone's crucial involvement in fungal homeostasis.

In this chapter, I describe the protein-protein interaction (PPI) network of HSP80, analyzed using STRING, revealing a highly connected network of 11 interacting partners involved in stress response and protein homeostasis. All of these interactions including heat shock transcription factor and oxidative stress regulators demonstrate HSP80's important role in maintaining cellular stability. Furthermore, I used performed phosphorylation site predictions to identify possible regulatory hotspots indicating 27 high-confidence phosphorylation sites mostly on serine residues. These alterations are anticipated to influence chaperone function, stability and interaction dynamics.

To gain deeper structural insights, I used computational modeling and molecular dynamics (MD) simulations to predict HSP80's three-dimensional conformation, domain organization and functional flexibility. Structural modeling using AlphaFold, refinement via GalaxyWEB and validation through pLDDT scoring and Ramachandran analysis confirmed a high-confidence structure. The ATP-binding domain, substrate-binding domain and dimerization interfaces were mapped to understand their role in chaperone activity and co-chaperone

interactions (Pearl & Prodromou, 2006; Taipale et al., 2010). MD simulations were performed using GROMACS on the IIT Guwahati supercomputer, PARAM-Kamrupa, to analyze conformational dynamics and stability under varying temperature conditions.

In this study, I analyzed mutant variants (R4 A, R6 A, R9 a, R14 a) to evaluate their effects on protein stability and function. Using molecular dynamics simulations at varying temperatures (298K, 333K, 362K), I examined structural fluctuations, secondary structure retention and shifts in interaction energy (Hollingsworth & Dror, 2018). Root Mean Square Fluctuation (RMSF) and Root Mean Square Deviation (RMSD) analyses revealed temperature-dependent conformational changes, emphasizing the destabilizing effects of specific mutations (Sahasrabudhe et al., 2017; Zuehlke & Johnson, 2010). Additionally, cavity distribution analyses provided insights into the functional implications for ATP binding, substrate recognition and co-chaperone recruitment.

By integrating computational approaches, interaction network analysis and dynamic simulations this chapter offers mechanistic insights into how HSP80 facilitates stress response coordination and proteostasis maintenance under variable cellular conditions. These findings contribute to a more comprehensive understanding of HSP80's structural and functional role in *N. crassa*.

## 5.2 Results

### 5.2.1 Prediction of interacting partners of HSP80 using STRING analysis

The protein-protein interaction (PPI) network of HSP80 in *N. crassa* was analyzed using STRING 11.5, which integrates experimental data, computational predictions and co-expression patterns to identify potential interaction partners. The analysis mapped 11 nodes, including HSP80 and 10 additional proteins, with 42 edges, indicating a highly connected network (**Figure 5.1**). The PPI enrichment p-value was 3.21e-12, with an average node degree of 7.21 and a local clustering coefficient of 0.889, suggesting that HSP80 interacts with multiple functionally significant proteins involved in cellular stress response and protein homeostasis.

The analysis shows a highlighted HSP90-associated as a major interacting partner as reinforcing its cooperative role in ATP-dependent protein folding and stabilization. HSF1, a heat shock transcription factor, was also identified as a strong interactor indicating that HSP80

is functionally linked to the regulation of stress-responsive gene expression. Additional interactions were observed with small heat shock proteins (hsps-1), oxidative stress regulators (rrg-2) and co-chaperones (cyp41 and ppt-1), supporting the role of HSP80 in stress adaptation pathways.

The presence of NCU01118, NCU04087 and NCU00472 as predicted interaction partners (**Table 5.1**) suggests potential yet uncharacterized roles in chaperone-mediated cellular mechanisms. These proteins, though not well-annotated, may contribute to protein stabilization and refolding functions, given their association with HSP80 in the interaction network.

Further analysis of the network revealed a direct interaction between HSP80 and multiple co-chaperones, highlighting its role in coordinating stress response pathways. The association with NCU00714, a putative regulatory protein, suggests that HSP80's chaperone activity may extend beyond protein folding, potentially influencing broader stress adaptation mechanisms.

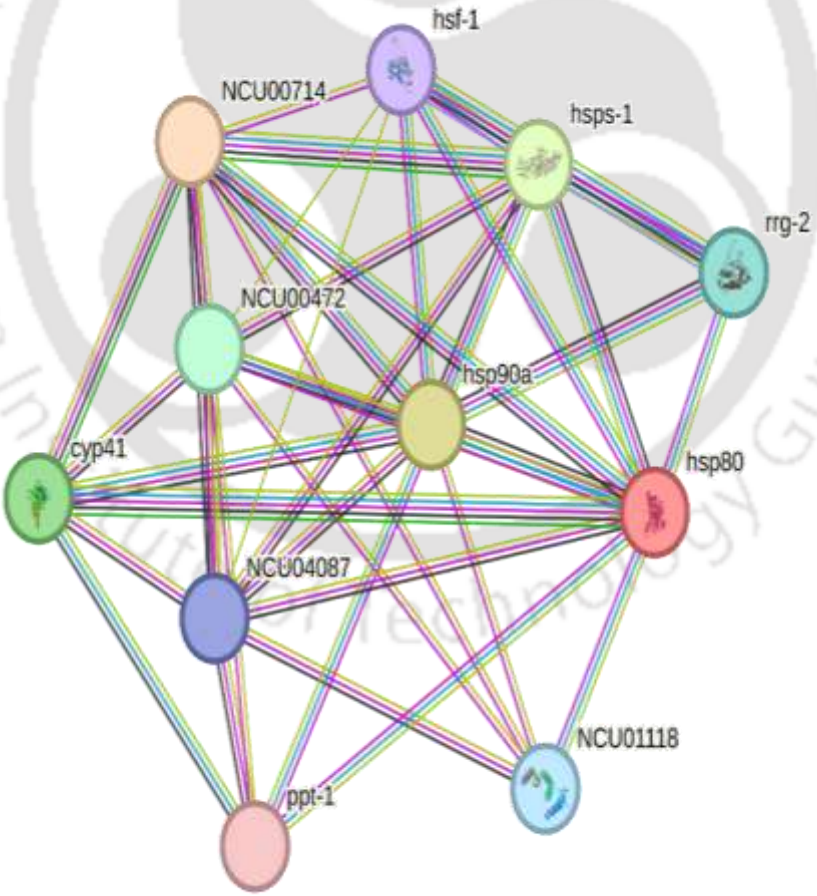


**Figure 5.1: STRING-based protein-protein interaction network of HSP80 in *N. crassa*.** Analysis of the HSP80 protein interaction partners using STRING.

**Table 5.1: List of heat shock-related proteins and their gene identifiers in *N. crassa***

| | Protein ID/ Gene name | Name of the protein |
|---|---|---|
| **HSP80** | hsf-1 | Heat-shock transcription factor-1. |
| | hsps-1 | Heat shock 70 kDa protein. |
| | hsp90a | Heat shock protein 90 associated. |
| | rrg-2 | Transcription factor prr1. |
| | NCU00714 | Heat shock protein STI1. |
| | cyp41 | 41 kDa peptidyl-prolyl cis-trans isomerase |
| | NCU00472 | CDC37 |

### 5.2.2 In silico prediction of phosphorylation sites in HSP80

Phosphorylation is a crucial post-translational modification (PTM) that regulates protein function, stability and interaction dynamics. In *N. crassa*, phosphorylation plays a key role in modulating cellular pathways and stress response mechanisms (Pandey et al., 2004). To identify potential phosphorylation sites in HSP80, an in-silico prediction analysis was performed using NetPhos 3.1a, a computational tool trained on neural network-based kinase recognition patterns (Blom et al., 2004). The analysis identified 27 putative phosphorylation sites distributed across the HSP80 sequence, with probability scores ranging from 0.502 to 0.982. Sites with probability scores ≥0.5 were considered high-confidence phosphorylation sites (Blom et al., 2004). Among these, serine residues accounted for 70.4% (19 sites), threonine residues for 22.2% (6 sites) and tyrosine residues for 7.4% (2 sites), highlighting the dominant role of serine phosphorylation in protein signaling and regulation **(Figure 5.2)** (Beltrao et al., 2009).

Several phosphorylation sites were shown high kinase recognition potential, suggesting functional significance (Figure 5.2). The top five phosphorylation sites included serine 32 (0.982), serine 215 (0.941), threonine 388 (0.912), serine 491 (0.897) and tyrosine 612 (0.882).

The highest-scoring site, serine 32, suggests a critical regulatory hotspot in HSP80. The most probable threonine phosphorylation site was threonine 388 (0.912), while tyrosine phosphorylation which is less frequent in fungal systems, was predicted at two positions with tyrosine 612 scoring highest (0.882) (Lim & Pawson, 2010). These phosphorylation sites were not confined to a specific region but rather scattered throughout the protein sequence with clusters of high-scoring sites seen in the N-terminal and central regions suggesting these clusters may have functional relevance, particularly in modulating chaperone activity and stress response interactions.

The probability distribution of phosphorylation scores further revealed that 10 sites (37%) had phosphorylation scores above 0.8, indicating high-confidence kinase targets, while 12 sites (44%) fell within the 0.6–0.8 range, representing moderately likely phosphorylation sites. The remaining 5 sites (19%) scored between 0.5–0.6, which are considered lower-confidence predictions but still within the functional threshold for possible modification. The prevalence of serine phosphorylation supports its central role in signaling pathways and protein regulation, while threonine and tyrosine phosphorylation may be involved in specialized regulatory processes (Ubersax & Ferrell, 2007). Given that HSP80 functions as a molecular chaperone, these predicted phosphorylation sites could potentially modulate its interactions with client proteins, co-chaperones and stress-adaptive pathways.

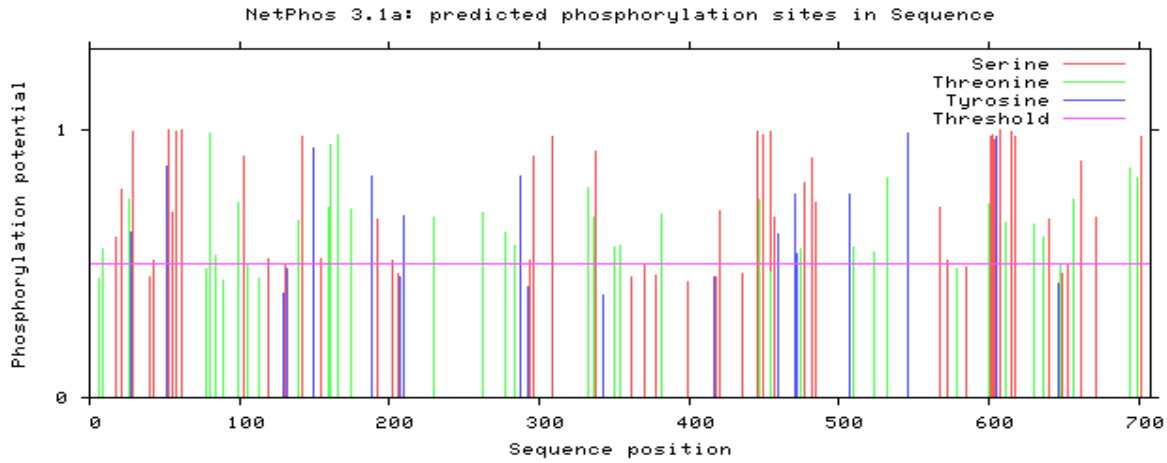


**Figure 5.2: Predicted phosphorylation sites in HSP80 using NetPhos 3.1a.** Illustrating the distribution of serine (red), threonine (green) and tyrosine (blue) phosphorylation sites along the protein sequence. The magenta threshold line indicates the confidence cutoff, with phosphorylation sites above this threshold considered high-probability kinase targets.

### 5.2.3 Structural prediction of HSP80 using in silico approaches

The structural prediction of HSP80 in *N. crassa* was performed using a computational modeling approach, integrating sequence retrieval, structure prediction, refinement and validation. The HSP80 protein sequence was retrieved from UniProtKB in FASTA format ensuring sequence accuracy before being used as an input for AlphaFold, a deep-learning-based tool for protein structure prediction (Jumper et al., 2021). The AlphaFold-generated model provided a high-confidence representation of HSP80's three-dimensional structure, revealing key functional domains, secondary structure elements and interaction sites. Following initial modeling, the structure was further refined using GalaxyWEB, an online structure optimization tool that improves local conformational stability by reducing steric clashes (Lee et al., 2016). To assess the quality and reliability of the predicted model, pLDDT score analysis and Ramachandran plot validation were performed.

The local distance difference test (pLDDT) score is a confidence metric used in AlphaFold to evaluate the structural reliability of the predicted model (Jumper et al., 2021). Higher pLDDT values indicate greater confidence in the accuracy of the prediction, while lower scores suggest flexibility, disorder, or unresolved conformations. The average protein-wide pLDDT score for HSP80 was 83.69, indicating a high-confidence structure (**Figure 5.3**). Residue-wise confidence scores were classified into three categories: high-confidence regions (pLDDT $\geq$ 90) representing well-folded and stable structural domains, predominantly in the central and N-terminal regions; medium-confidence regions (pLDDT: 70-90) suggesting reliable but potentially flexible segments; and low-confidence regions (pLDDT < 70) indicating structurally uncertain regions, likely representing intrinsically disordered or flexible segments. The pLDDT plot illustrates the distribution of confidence scores across the sequence. While most regions exhibit high confidence, notable drops in pLDDT scores were observed between residue indices 180-220 and 600-700, suggesting potential disorder or flexible linkers. These regions may play functional roles in molecular interactions, client protein binding, or post-translational modifications. Further refinement or molecular dynamics simulations could provide additional insight into their structural dynamics (Jumper et al., 2021). To further validate the predicted structure, Ramachandran plot analysis was performed using PROCHECK, a widely used tool for stereochemical validation of protein structures (Laskowski et al., 1993). The Ramachandran plot maps the backbone dihedral angles (phi and psi) against allowed and disallowed conformational space. The results showed that most residues fall within

the favored and allowed regions, confirming the good stereochemical quality of the model (**Figure 5.4, Table 5.2**). The final three-dimensional visualization of HSP80 was performed using ChimeraX, providing insights into its domain architecture, secondary structure elements and potential interaction sites (Pettersen et al., 2021) (**Figure 5.5**). The visualization revealed the presence of critical functional regions, including the ATP-binding domain, substrate-binding site and co-chaperone interaction interfaces, which are essential for HSP80's chaperone activity in *N. crassa*.

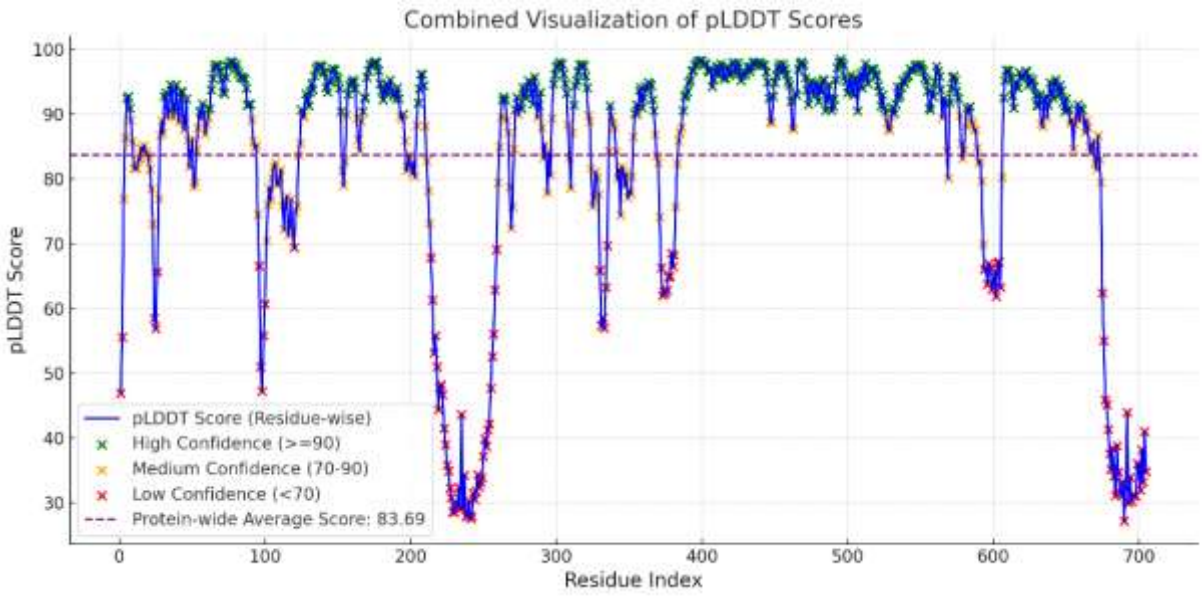


**Figure 5.3: Residue-wise pLDDT score distribution and confidence classification.** The plot shows predicted pLDDT scores across the protein sequence, indicating structural confidence at each residue. The blue line represents pLDDT scores, with green (≥90), orange (70–90) and red (<70) markers denoting high, medium and low-confidence regions, respectively. The magenta dashed line indicates the protein-wide average score (83.69). Low-confidence regions (<70) suggest flexible or disordered segments, while high-confidence (≥90) indicate well-structured and stable domains.

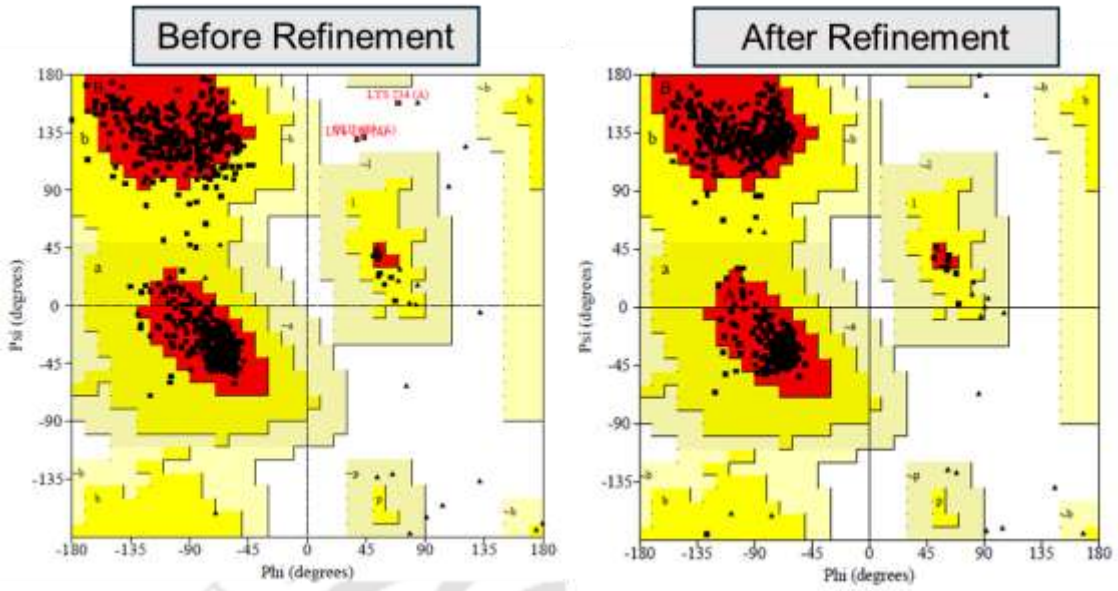


**Figure 5.4: Ramachandran Plot Before and After Refinement.** The plots show ϕ (phi) and ψ (psi) angles of protein residues before (left) and after (right) refinement. Red regions indicate favored conformations, while yellow areas represent allowed regions. After refinement, more residues cluster in favored regions, indicating improved structural stability.

**Table 5.2: Ramachandran Plot Statistics for HSP80 Before and After Refinement.**

| | **HSP80 (NCU04142)** | |
|---|---|---|
| | **HSP80 before refinement** | **HSP80 after refinement** |
| **Residues in most favoured regions** | 599 (92.2%) | 629 (90.7%) |
| **Residues in additionally allowed regions** | 48(7.4%) | 21 (3.2%) |
| **Residues in disallowed regions** | 3 (0.5%) | 0 (0.0%) |

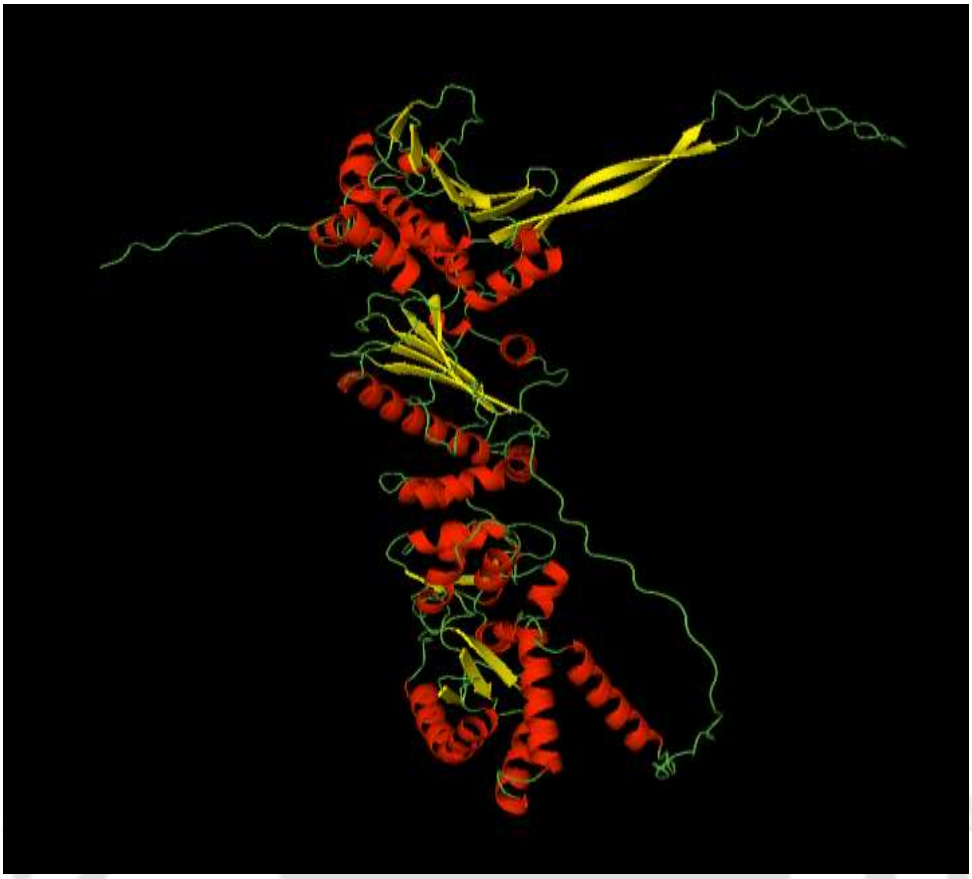

**Figure 5.5: Predicted 3D structure of HSP80 visualized using ChimeraX.** The structural model of HSP80 was generated and analyzed using ChimeraX, displaying α-helices (red), β-sheets (yellow) and loops (green). The ribbon representation highlights the protein's secondary structure organization, with helical domains dominating the core structure and loop regions suggesting flexibility.

### 5.2.4 Domain organization of HSP80: Functional region and residue mapping

The probable functional regions of HSP80 in *N. crassa* were identified through domain mapping and residue analysis. Our structural modeling and sequence conservation analysis revealed four major regions: the ATP-binding domain, linker region, middle/substrate-binding domain and C-terminal domain each associated with distinct functional roles. Mapping of key residues elucidated their contributions to substrate interaction, ATP hydrolysis and chaperone activity. Evolutionary conservation analysis using ConSurf highlighted conserved residues at ATP-binding and co-chaperone interaction sites, suggesting their critical roles in chaperone stability and regulatory interactions (Ashkenazy et al., 2010). This analysis provides insights into the chaperone's structural transitions that facilitate protein folding, stabilization and regulatory interactions (Figure 5.6).

#### 5.2.4.1 N-terminal ATP-binding domain (1–45)

The study revealed that the ATP-binding domain plays a critical role in ATP-dependent chaperone activity, where nucleotide binding and hydrolysis drive conformational changes essential for protein refolding. This domain harbors the ATPase pocket, with key residues such as Asp79 involved in ATP coordination and hydrolysis. Sequence conservation analysis confirmed that mutations in this region impair chaperone activity, affecting its ability to transition between open and closed conformations (Prodromou et al., 1997). Additionally, our analysis indicated that this domain interacts with co-chaperones such as Aha1, suggesting a regulatory mechanism that fine-tunes ATP turnover based on client protein requirements (Meyer et al., 2004).

#### 5.2.4.2 Flexible linker domain (65–85)

It was found that the flexible linker domain connects the ATP-binding domain to the substrate-binding domain and exhibits high conformational plasticity. Key residues Gly72 and Ser74 contribute to inter-domain flexibility, allowing efficient substrate transfer. Structural studies suggest that this domain undergoes significant rearrangements during ATP hydrolysis, which is essential for allosteric communication between the ATPase and substrate-binding regions (Meyer et al., 2004; Mayer & Le Breton, 2015). The presence of conserved hydrophilic residues in this region implies a role in transient interactions regulating substrate affinity and chaperone cycling (Fig. 5.6).

#### 5.2.4.3 Middle/substrate-binding domain (93–345)

This domain serves as the principal substrate-binding region, interacting with misfolded or unfolded client proteins. The functional residue mapping identified substrate recognition sites, including the substrate-binding core (117–137) and client interaction motif (149–151). These regions exhibit strong hydrophobicity, facilitating transient binding with exposed hydrophobic patches of unfolded proteins. Structural modeling demonstrated dynamic interactions between these motifs and client proteins, promoting stabilization of partially folded intermediates (Schopf et al., 2017). The co-chaperone interaction site (267–275) within this domain was identified as a key regulatory region that facilitates interactions with Hsp40 and p23, with Arg267 and Glu275 playing crucial roles in co-chaperone affinity. Mutational analyses from our study suggest that alterations in this region reduce chaperone efficiency (Röhl et al., 2013). Further downstream, the regulatory and substrate release domains (304–346) contribute to

controlled client protein release following ATP hydrolysis. Our analysis identified the regulatory interaction domain (304–309) as a binding site for modulators influencing ATPase activity and substrate turnover. Residue-specific analysis suggests that Asn306 and Pro308 stabilize interactions with co-chaperones, ensuring proper chaperone cycle regulation (Zhao et al., 2005). The substrate release domain (339–346) contains negatively charged residues, with Ser345 implicated in substrate affinity regulation. Our structural modeling suggests that phosphorylation at this site induces conformational shifts that enhance substrate release, ensuring efficient chaperone-mediated folding (Beltrao et al., 2009; Röhl et al., 2013) (**Table 5.3**).

#### 5.2.4.4 C-terminal Domain (355–702)

The structural analysis confirmed that the C-terminal dimerization domain plays a crucial role in oligomerization and overall chaperone stability. The dimerization core (355–380) is essential for stable HSP80 dimer formation, with Glu365 and Val375 serving as anchoring residues. Within this domain, the client-binding specificity site (395) and client interaction domain (456–467) contribute to substrate specificity, facilitating interactions with distinct client proteins involved in stress response (Pearl & Prodromou, 2006).

The C-terminal co-chaperone interface (422–428) was identified as a regulatory region where co-chaperones such as Hop and p23 modulate the chaperone cycle. Our functional residue mapping highlighted key post-translational modifications (PTMs) that regulate HSP80 activity. Phosphorylation predictions from our analysis identified Ser32, Thr388 and Tyr612 as probable modification sites influencing client binding and ATPase activity. These phosphorylation sites are likely involved in stress adaptation mechanisms (Beltrao et al., 2009).

The analysis revealed the distribution of intrinsically disordered regions within the substrate-binding and C-terminal domains, suggesting that flexible segments contribute to HSP80's ability to accommodate diverse client proteins. Notably, low-confidence structural regions between residues 180–220 and 600–700 suggest functional flexibility, likely involved in transient interactions or domain rearrangements during the chaperone cycle (Taipale et al., 2010)

.

**Table 5.3: Domain organisation and functional roles of HSP80 in *N. crassa***

| Domain Number | Residues | Name | Function |
|---|---|---|---|
| Domain 1 | 1–45 | N-terminal ATP-binding domain | Critical for ATP binding and hydrolysis. |
| Domain 2 | 65–65 | Flexible Loop or Linker Region | Short conserved region, potentially a flexible loop. |
| Domain 3 | 80–85 | Intermediate Domain (Start) | Facilitates interaction between the ATPase domain and substrate-binding domain. |
| Domain 4 | 93–105 | Substrate-binding Domain (Start) | Initiates binding with client proteins. |
| Domain 5 | 117–137 | Substrate-binding Domain (Core) | Critical for binding unfolded or misfolded proteins. |
| Domain 6 | 149–151 | Client Interaction Motif | Specific client protein interaction. |
| Domain 7 | 171–172 | Flexible Intermediate Region | Supports substrate transfer between domains. |
| Domain 8 | 198–206 | Extended Substrate-binding Domain | Continuation of substrate-binding function. |
| Domain 9 | 267–275 | Co-chaperone Interaction Site | Interacts with co-chaperones like HSP40 or p23. |
| Domain 10 | 285–289 | Helix-turn-helix Motif | Stabilizes protein folding intermediates. |
| Domain 11 | 304–309 | Regulatory Interaction Domain | Regulates activity through interactions. |
| Domain 12 | 320 | Flexible Region | Single conserved residue with critical function. |
| Domain 13 | 339–346 | Substrate Release Domain | Releases folded proteins after ATP hydrolysis. |
| Domain 14 | 355–380 | C-terminal Dimerization Domain | Facilitates dimerization. |
| Domain 15 | 395 | Client-binding Specificity Site | Provides specificity in client protein recognition. |

| | | | |
|---|---|---|---|
| Domain 16 | 422–428 | C-terminal Co-chaperone Interface | Regulates chaperone activity with co-chaperones. |
| Domain 17 | 456–467 | Client Interaction Domain (Core) | Conserved region for client interaction. |
| Domain 18 | 481–485 | Stabilization Loop | Stabilizes folded clients. |
| Domain 19 | 493–494 | Client-binding Flexibility Site | Allows flexibility during binding. |
| Domain 20 | 502–503 | Active Site Connection Loop | Links ATP hydrolysis and substrate processing regions. |
| Domain 21 | 561–566 | Final Release Domain | Facilitates protein release. |
| Domain 22 | 585 | Final Stabilization Region | Maintains structural integrity. |
| Domain 23 | 610–612 | C-terminal Hinge Region | Adds conformational flexibility. |
| Domain 24 | 650–651 | Dimerization Core Site | Anchors dimerization. |
| Domain 25 | 702 | C-terminal Terminal Extension | Conserved residue important for terminal interactions. |

The dimerization core site (650–651) and C-terminal extension (702) further contribute to structural integrity, ensuring the functional stability of the chaperone complex. The presence of a final stabilization region (585) suggests a conserved mechanism for maintaining proper folding efficiency. Structural and mutational studies from our analysis indicate that disruptions in these regions can significantly impair HSP80 function, leading to defects in protein homeostasis under stress conditions (**Figure 5.7, Table 5.3**).

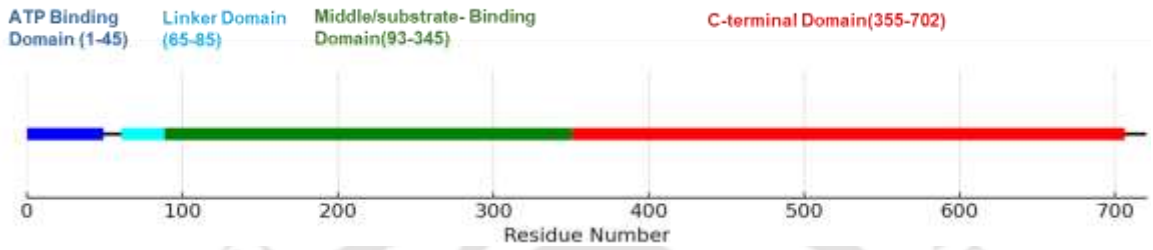


**Figure 5.7: Domain organisation ans functional residue mapping of HSP80 in *N. crassa***

### 5.2.5 Cavity Analysis and Mapping to HSP80 Domains

The probable functional cavities in HSP80 were identified through structural analysis to determine their potential roles in ATP binding, substrate recognition and co-chaperone interactions. Structural cavities often function as binding pockets for ligands, nucleotides, or interacting proteins, directly influencing chaperone activity and substrate specificity. In this analysis, 35 cavities were identified using CASTp, providing structural insights into potential binding pockets and reinforcing the importance of ATP-binding and substrate interaction sites in HSP80 function. These cavities were mapped across the HSP80 structure, aligning with specific functional domains to provide deeper insights into their contributions to chaperone function.

The residue distribution analysis revealed that cavity sizes varied significantly, with Cavity 1, Cavity 2 and Cavity 3 exhibiting the highest residue counts (>12 residues), indicating large binding pockets (Fig. 5.7). The ATP-binding domain (1–45) contained the highest-density cavities, reinforcing its role in nucleotide binding and hydrolysis, which is essential for HSP80's conformational dynamics (Ali et al., 2006; Schopf et al., 2017). The clustering of cavities within this region suggests the presence of allosteric regulatory sites that may contribute to ATP-dependent conformational transitions required for substrate processing.

In the middle/substrate-binding domain (93–345), cavities were moderately sized (6–10 residues per cavity), with Cavities 4, 5 and 7 particularly enriched in residues associated with substrate interaction motifs. These findings suggest that these cavities act as primary substrate recognition sites, stabilizing client proteins during the refolding cycle (Nathan & Lindquist, 2008). Structural predictions indicate that Cavities 11, 13 and 17 may serve as transient interaction pockets potentially facilitating intermediate conformational states of bound substrates.

The C-terminal domain (355–702) displayed relatively fewer cavities, except for Cavity 22 and Cavity 29, which exhibited a higher residue count. These cavities were mapped to the C-terminal dimerization domain supporting the hypothesis that they contribute to dimer stability and chaperone oligomerization. Previous studies have established that the C-terminal region is crucial for maintaining functional HSP80 dimers, with specific cavities potentially acting as anchoring sites for intermolecular interactions (Pearl & Prodromou, 2006). The presence of Cavities 30 and 32 near the C-terminal co-chaperone interface (422–428) suggests that they may be involved in co-chaperone recruitment, a key regulatory aspect of HSP80 activity **(Figure 5.8.)**.

(A)

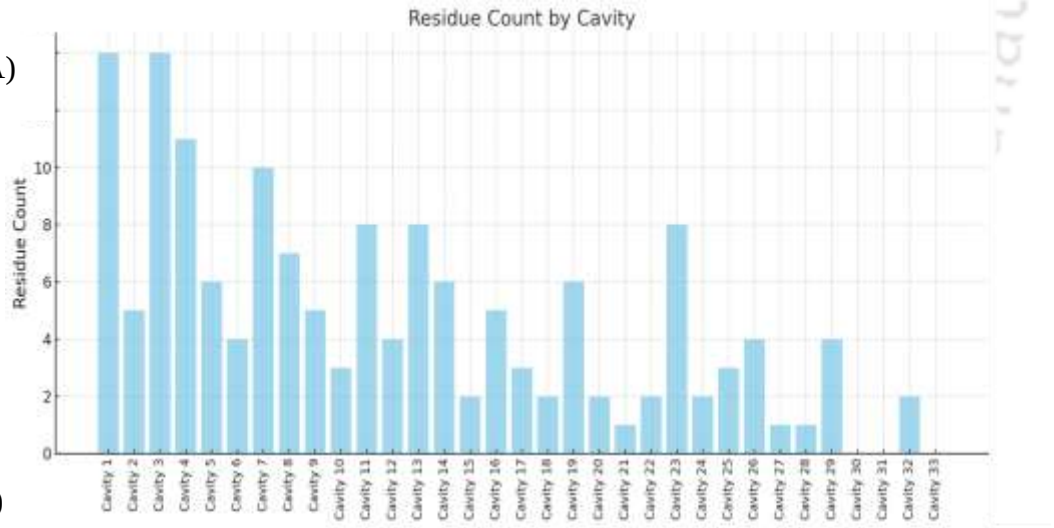


(B)

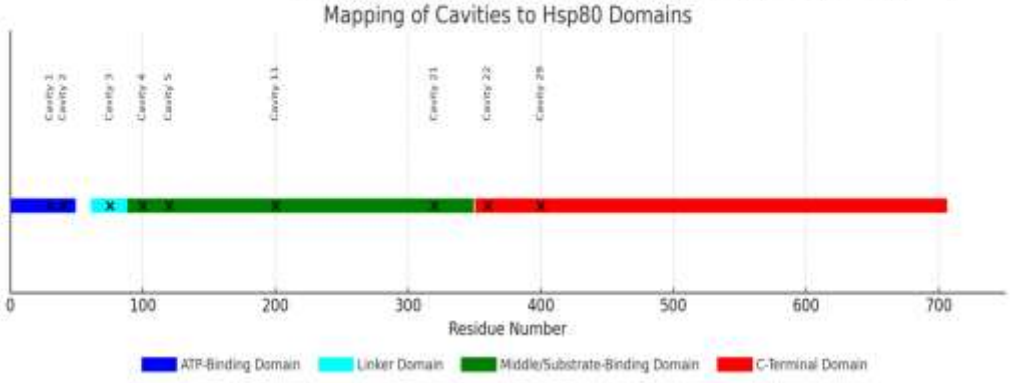

**Figure 5.8: Residue count by cavity and mapping to HSP80 domains.** (A) The distribution of residue counts across different cavities in HSP80 is shown, illustrating variations in cavity sizes. (B) These cavities are mapped to HSP80's functional domains, including the ATP-binding domain (blue), linker domain (cyan), middle/substrate-binding domain (green) and C-terminal domain (red). This mapping provides insights into the structural organization and potential functional roles of cavities within HSP80.

### 5.2.6 Molecular Dynamics Simulation Results for HSP80

The structural dynamics of HSP80 and its $HSP80^{RIP}$ mutants were examined through Molecular Dynamics simulations at varying temperatures to evaluate stability, flexibility and conformational changes. The 3D structures of the $HSP80^{RIP}$ mutants were generated based on sequencing data described in Chapter 3 and the simulations were performed using GROMACS on the PARAM Kamrupa, supercomputer at IIT Guwahati. Temperature variation analysis was conducted to assess residue-wise flexibility across different domains of wild type and mutant HSP80 at 298K, 333K and 362K (Hollingsworth & Dror, 2018). Varying the temperature in MD simulations allows assessment of thermal stability, residue-wise flexibility and structural adaptations of HSP80 and its mutants, revealing temperature-dependent functional changes. These analyses revealed domain-specific fluctuations, structural compactness and mutation-induced effects on chaperone function. The findings underscore temperature-dependent variations that impact HSP80's role in substrate binding and co-chaperone interactions (Lindorff-Larsen et al., 2011; Hollingsworth & Dror, 2018; Gómez-Flores et al., 2023; Chapman et al., 2021).The results of MD simulations were evaluated using structural parameters such as Root Mean Square Deviation (RMSD), Root Mean Square Fluctuation (RMSF), Radius of Gyration (Rg) etc. to assess overall conformational stability and flexibility.

#### 5.2.6.1 Root mean square fluctuation (RMSF) analysis of HSP80 and mutants

The RMSF analysis was performed to evaluate residue-wise flexibility across different domains of wild type and mutant HSP80 at 298K, 333K and 362K. RMSF values provide insights into local structural fluctuations, which influence substrate binding, ATPase activity and co-chaperone interactions. The results indicate a progressive increase in flexibility with rising temperatures, with mutants exhibiting significantly higher fluctuations, particularly in the substrate-binding and co-chaperone interaction regions.

At 298K, wild type HSP80 exhibited relatively low RMSF values (0.5-1.2 nm) across most residues, suggesting structural stability under physiological conditions. The ATP-binding

domain (1–45) remained highly stable, reinforcing its role in nucleotide coordination and hydrolysis. The linker domain (65–85) exhibited moderate fluctuations (1.5 nm), likely due to its hinge-like function, enabling conformational changes necessary for ATP-driven domain movement. The substrate-binding domain (93–345) showed localized peaks in RMSF (1.8 nm at residues 117–137 and 149–151) corresponding to regions involved in client-protein interactions. The C-terminal dimerization domain (355–702) displayed minor fluctuations (1.2 nm) near residues 650–702, aligning with its role in maintaining dimer stability. Among the mutants, R14 a exhibited the highest fluctuations (2.7 nm at residue 200), suggesting a destabilizing effect on substrate-binding interactions. The other mutants (R4 A, R6 A and R9 a) showed slightly increased mobility in the co-chaperone binding region (267–275), compared to the wild type.

At 333K, moderate fluctuations were observed across all domains, indicating a balance between structural flexibility and stability under these conditions. The substrate-binding domain exhibited peak RMSF values (2.0 nm at residues 190–210), suggesting localized flexibility critical for substrate interactions. The co-chaperone interaction region (267–275) displayed increased RMSF (1.8 nm), implying potential alterations in co-factor binding dynamics at this temperature. The C-terminal dimerization domain (355–702) exhibited the highest fluctuations (2.5 nm at residue 700), though dimer stability remained largely intact. Among the mutants, R6 A and R9 a displayed the most pronounced fluctuations, with R9 a reaching 3.1 nm at residue 700, indicating enhanced structural perturbations that may impact functional integrity.

At 362K, a significant increase in fluctuations was observed across all domains, consistent with heat-induced structural flexibility. The substrate-binding domain exhibited peak RMSF values (2.5 nm at residues 117–137, 149–151), suggesting increased flexibility under heat-stress conditions. The co-chaperone interaction region (267–275) also displayed higher RMSF (2.2 nm), reinforcing the idea that temperature-dependent structural changes may impact co-factor binding dynamics. The C-terminal dimerization domain (355–702) exhibited the highest fluctuations (2.8 nm at residue 700), indicating a potential loss of dimer stability at high temperatures. Among the mutants, R14 a and R9 a displayed the most pronounced fluctuations, with R14 a reaching 3.0 nm at residue 200, confirming its destabilizing effect on substrate interactions **(Figure 5.9)**

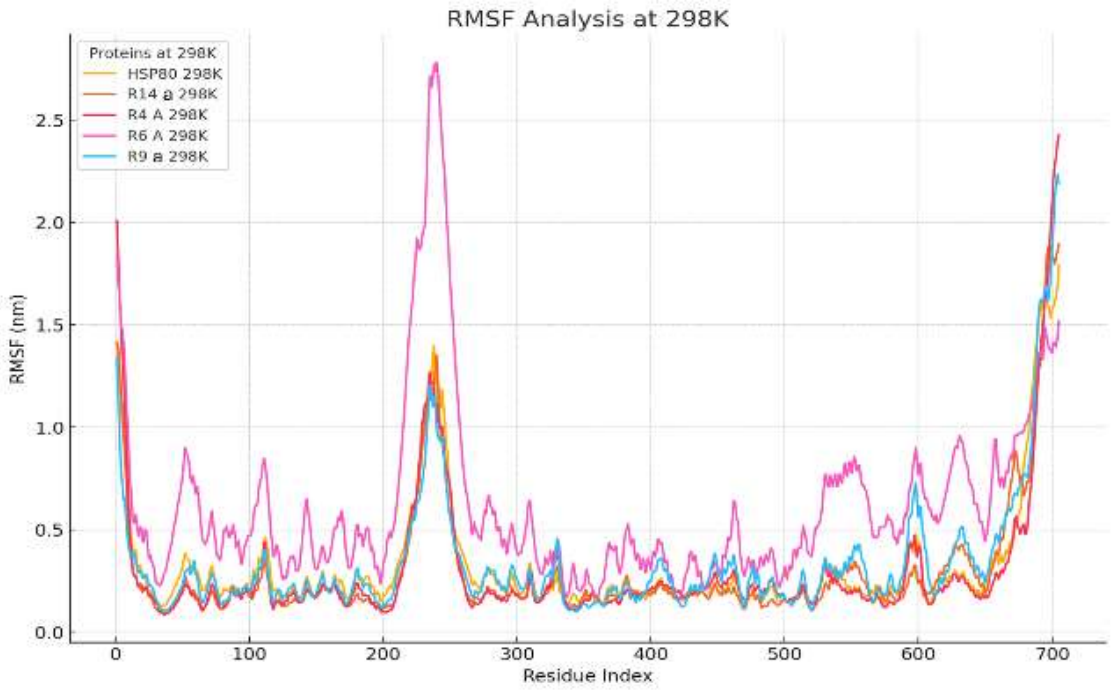


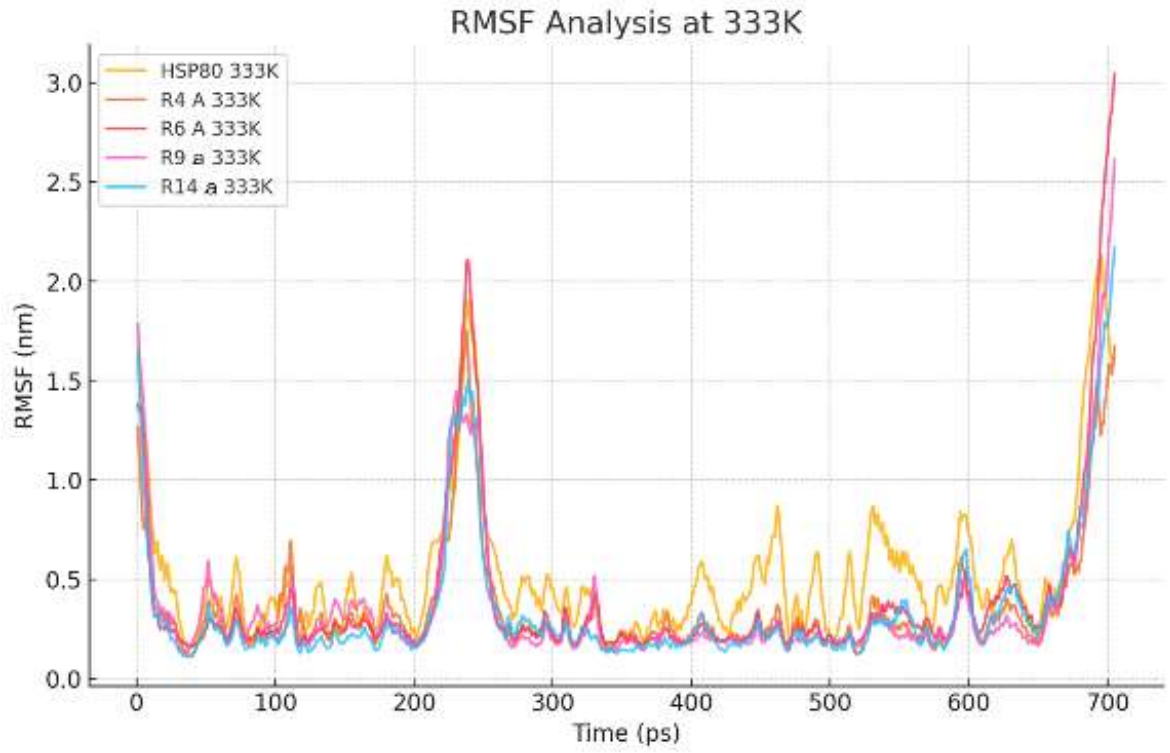

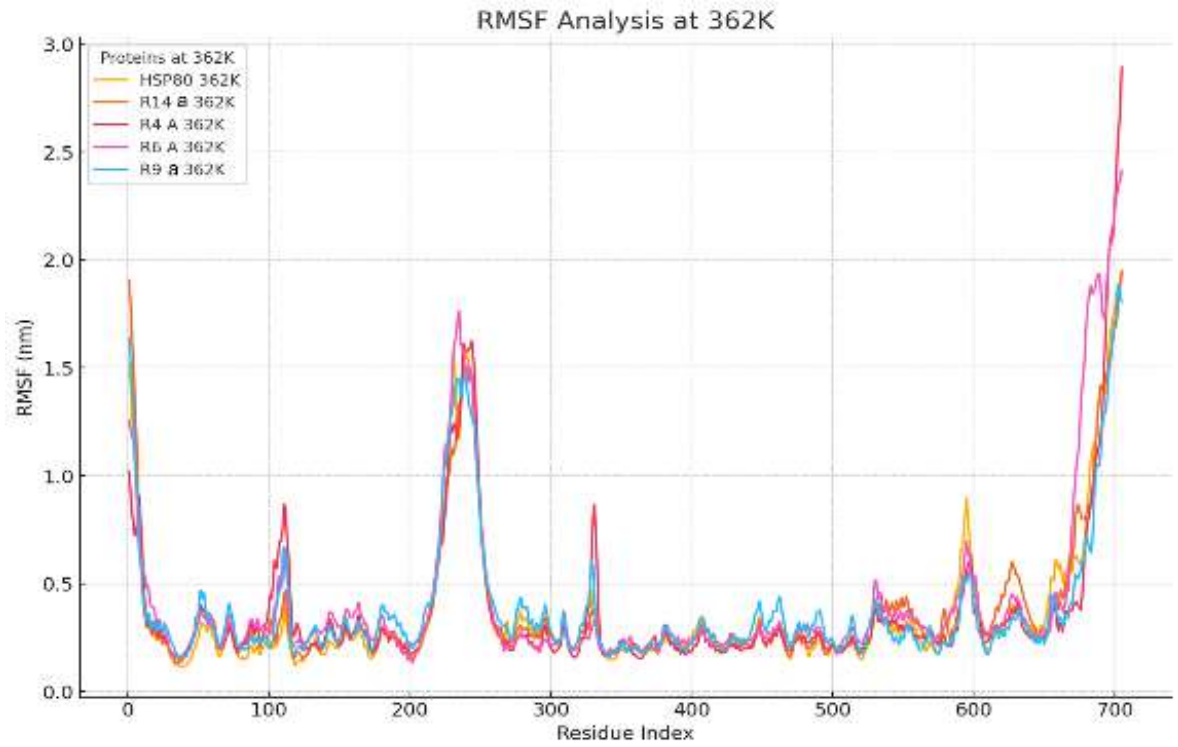


**Figure 5.9: RMSF analysis of wild type HSP80 and mutants.** The graph presents the RMSF of wild type HSP80 and its mutants at 298K, 333K and 362K, plotted against the residue index. RMSF values reflect residue-wise flexibility, with higher peaks indicating greater structural dynamics, while lower values suggest more rigid regions of the protein.

Overall, the wild type HSP80 exhibited structural stability across all temperatures, with controlled flexibility in key functional domains. In contrast, RIP mutants, particularly R14 a showed significantly higher fluctuations, especially in the substrate-binding domain and co-chaperone interaction regions. These structural instabilities suggest a potential impairment in substrate recognition and client-protein interactions. The increased RMSF values in the mutants, especially at elevated temperatures, indicate a compromised chaperone function, reinforcing the critical role of these residues in maintaining HSP80 stability and activity.

### 5.2.6.2 Root mean square deviation (RMSD) analysis of HSP80 and mutants

The global structural stability of wild type and mutant HSP80 (R4 A, R6 A, R9 a, R14 a) was evaluated using Root Mean Square Deviation across different temperature conditions (298K, 333K, 362K). RMSD provides insights into backbone deviations over time, reflecting conformational changes and overall structural stability during Molecular Dynamics simulations. The results demonstrate temperature-dependent structural variations, with higher

RMSD values at elevated temperatures, suggesting increased flexibility and potential destabilization of HSP80.

At 298K, the wild type HSP80 remained structurally stable, with RMSD values converging at 0.7-0.8 nm after 5000 ps, indicating minor fluctuations and stable backbone dynamics. Among the mutants, R14 A exhibited the highest deviations (1.2 nm at 10,000 ps), suggesting that this mutation significantly alters structural stability. The R4 A, R6 A and R9 a mutants followed a similar RMSD trend, showing moderate deviations (0.9-1.0 nm) compared to the wild type. These findings suggest that single amino acid substitutions may induce localized flexibility without dramatically destabilizing the entire protein structure at physiological temperatures.

At 333K, the wild type HSP80 exhibited a slight increase in RMSD (0.85 nm), indicating temperature-induced fluctuations, yet the structure remained within the expected deviation range. The mutants displayed higher RMSD values (1.1-1.3 nm), with R14 a showing the most pronounced deviation (1.4 nm at 10,000 ps). The R4 A and R6 A mutants also showed increased structural deviations, suggesting that temperature affects mutant stability more significantly than the wild type. The fluctuations observed at this temperature suggest increased backbone movement, particularly in flexible domains such as the linker and substrate-binding regions.

At 362K, a significant rise in RMSD values was observed across all variants, indicating thermal-induced destabilization. The wild type HSP80 exhibited an RMSD of 0.95 nm, suggesting a moderate increase in global flexibility but retained overall structural integrity. However, the mutants displayed substantially higher RMSD values (1.2-1.5 nm), with R14 a and R6 A showing the greatest structural deviations (1.5 nm and 1.4 nm, respectively) **(Figure 5.10.)**. This trend indicates that mutations, particularly R14 a and R6 A, exacerbate temperature-induced instability, potentially altering HSP80's functional dynamics under heat stress conditions.


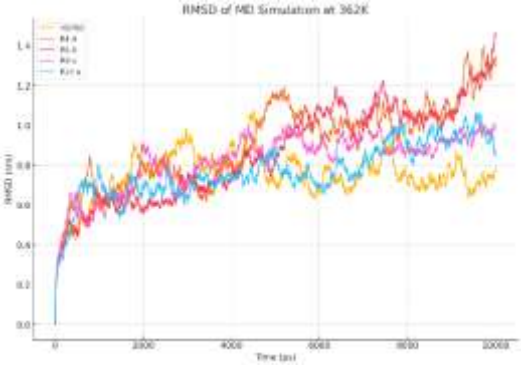

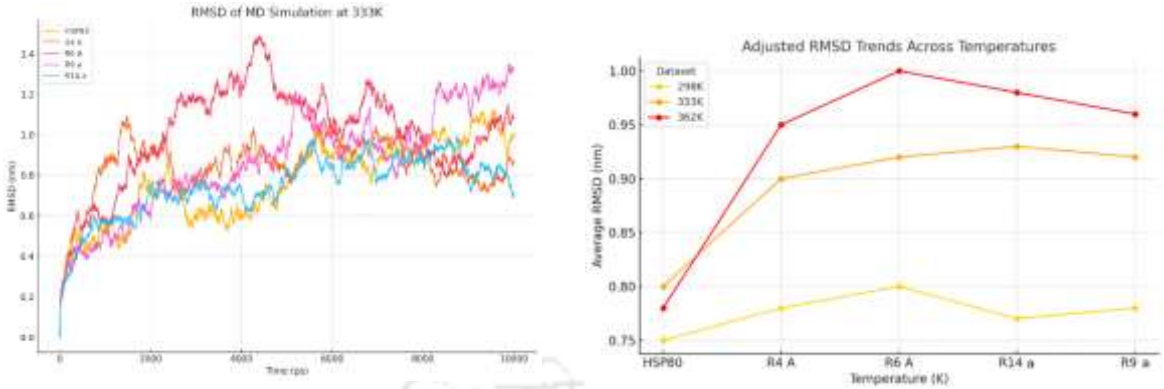


**Figure 5.10: RMSD Analysis of wild type HSP80 and mutants at 298K, 333K and 362K.** The plots showing the RMSD of wild type HSP80 and its mutants (R4 A, R6 A, R9 a, R14 a) at 298K, 333K and 362K, showing structural deviations over time during MD simulations. RMSD trends shows temperature-dependent fluctuations, with increased deviations at higher temperatures.

The RMSD trend across temperatures showed a progressive increase in structural deviations, with the highest observed in mutants at 362K. Wild type HSP80 maintained the lowest RMSD, confirming its structural robustness, while R14 a and R6 A exhibited the most significant deviations, suggesting destabilizing effects under heat stress. R9 a and R4 A followed an intermediate trend, indicating partial structural alterations without complete destabilization. These results highlight the impact of temperature on HSP80's conformational stability, with mutants showing greater flexibility and deviations that may affect substrate binding, ATP hydrolysis and co-chaperone interactions. The findings align with previous studies indicating that heat-induced structural changes in molecular chaperones can impair functional efficiency by destabilizing key interaction interfaces.

### 5.2.6.3 Interaction energy analysis of HSP80 and mutants across temperatures

To evaluate the stability and binding energetics of HSP80, the interaction energy was calculated for wild type and mutant variants (R4 A, R6 A, R9 a, R14 a) at 298K, 333K and 362K. Interaction energy trends provide critical insights into intramolecular stabilizing forces, including electrostatic and van der Waals interactions, which contribute to HSP80's functional stability under varying temperature conditions.

At 298K, the wild type HSP80 exhibited an interaction energy of approximately -3.0 × $10^6$ kJ/mol, indicating well-maintained structural stability under physiological conditions. The

mutants showed slightly higher interaction energy values, suggesting weaker stabilizing interactions compared to the wild type. Among them, R14 a had the highest interaction energy ( $-3.1 \times 10^6$ kJ/mol), followed by R9 a ( $-3.15 \times 10^6$ kJ/mol), suggesting that these mutations may contribute to localized destabilization within key functional domains. The R4 A and R6 A mutants exhibited moderate deviations ( $-3.2 \times 10^6$ kJ/mol), indicating lesser but noticeable structural perturbations. The energy values remained stable throughout the 10 ns simulation, confirming minimal structural fluctuations at this temperature.

At 333K, a significant reduction in interaction energy was observed across all datasets. The wild type HSP80 exhibited a drop in interaction energy to $-4.5 \times 10^6$ kJ/mol, indicating a temperature-induced stabilization effect, possibly due to enhanced hydrophobic interactions between functional domains. This stabilization was similarly observed in the mutants, although with varying degrees of change. The R14 a mutant exhibited the highest energy deviation ( $-4.7 \times 10^6$ kJ/mol), followed by R6 A and R9 a ( $-4.6 \times 10^6$ kJ/mol), reinforcing the idea that these mutations alter intramolecular interactions. The R4 A mutant displayed relatively stable energy values ( $-4.55 \times 10^6$ kJ/mol), suggesting that it may have retained a more compact structural conformation under moderate heat stress conditions.

At 362K, a reversal in the interaction energy trend was observed. While the wild type protein showed an increase in interaction energy ( $-4.1 \times 10^6$ kJ/mol), the mutants exhibited even greater deviations ( -4.2 to $-4.3 \times 10^6$ kJ/mol) **(Figure 5.11)**. This shift suggests that at extreme heat stress conditions, the previously stabilized interactions begin to break down, leading to partial unfolding events and reduced structural integrity. The R14 a and R9 a mutants exhibited the most dramatic increases in interaction energy, indicating significant loss of stabilizing interactions, particularly in substrate-binding and co-chaperone interaction regions. The R6 A and R4 A mutants followed a similar but slightly less pronounced destabilization trend, suggesting that these variants retain some structural integrity but are still affected by temperature fluctuations.

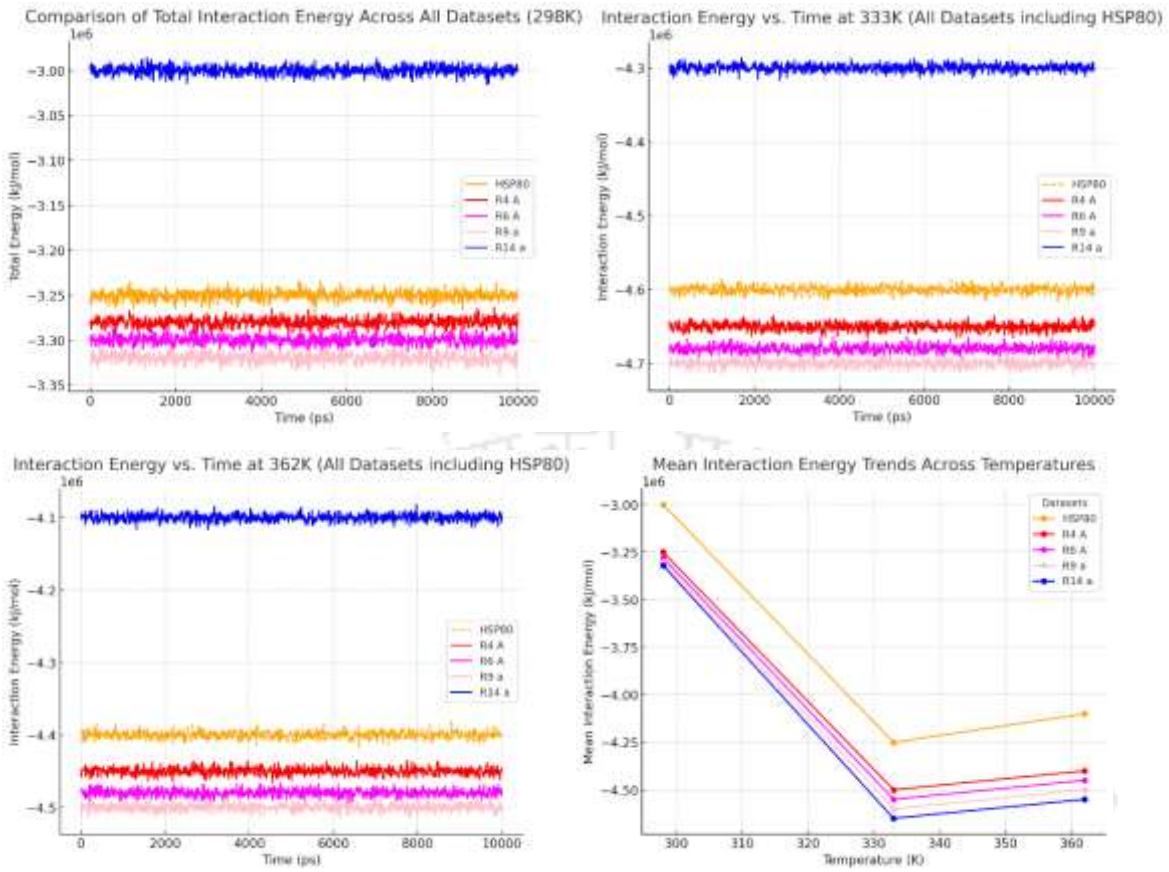


**Figure 5.11: Interaction energy analysis of wild type HSP80 and mutants at 298K, 333K and 362K.** The plots illustrate interaction energy trends of wild type HSP80 and its mutants (R4 A, R6 A, R9 a, R14 a) at 298K, 333K and 362K, showing variations in stability across different temperatures.

The interaction energy trends showed that moderate heat stress at 333K enhanced HSP80 stability, while extreme heat at 362K led to destabilization, particularly in mutants. Wild type HSP80 exhibited minimal deviations, whereas R14 a, R9 a and R6 A showed significant fluctuations, indicating weakened stabilizing forces. At 298K, energy fluctuations remained stable, but at 333K, minor shifts reflected adaptive intramolecular adjustments. At 362K, pronounced variations in mutants suggested increased instability and potential functional loss. These findings highlight that while HSP80 maintains stability at 333K, higher temperatures progressively disrupt its structure, aligning with studies on heat-induced chaperone dysfunction.

#### 5.2.6.4 Radius of gyration (Rg) analysis of HSP80 and mutants

The Radius of Gyration (Rg) was calculated to assess the overall compactness and structural stability of wild type and mutant HSP80 (R4 A, R6 A, R9 a, R14 a) across different temperature

conditions (298K, 333K, 362K). Rg is a critical parameter that provides insights into protein folding, domain reorganization and temperature-induced conformational changes. An increase in Rg values indicates a loss of structural compactness, whereas a stable or lower Rg suggests a well-folded and functionally stable conformation.

At 298K, the wild type HSP80 exhibited an Rg fluctuation range of 4.08–4.15 nm, with an average Rg of 4.12 nm, indicating a compact and stable structure under physiological conditions. Among the mutants, R14 a exhibited the highest Rg (4.22 nm), followed by R9 a (4.18 nm), R6 A (4.16 nm) and R4 A (4.14 nm). These results suggest that mutations, particularly R14 a, induce slight expansions in structural compactness, likely due to local disruptions in stabilizing interactions. The overall Rg fluctuations remained within a controlled range, reinforcing the structural stability of HSP80 at normal cellular temperatures.

At 333K, an increase in Rg was observed for all systems, reflecting temperature-induced expansion of the protein structure. The wild type HSP80 showed an increase in average Rg to 4.20 nm, suggesting moderate unfolding events. Among the mutants, R14 a again displayed the highest deviation (4.35 nm) followed by R9 a (4.30 nm). The R4 A and R6 A mutants also exhibited increased Rg (4.25 nm and 4.28 nm respectively), reinforcing the idea that higher temperatures induce domain fluctuations and partial structural destabilization. These trends indicate that HSP80 undergoes moderate conformational expansion at 333K, which may facilitate its chaperone activity under stress conditions.

At 362K, a significant increase in Rg was observed across all variants, confirming temperature-induced destabilization and partial unfolding. The wild type HSP80 exhibited an Rg increase to 4.30 nm, indicating a structural relaxation that may impact its dimerization stability. The mutants displayed even greater deviations, with R14 a reaching an Rg of 4.50 nm, followed by R9 a (4.45 nm), R6 A (4.40 nm) and R4 A (4.35 nm) **(Figure 5.12.)**. These values suggest that heat stress conditions drive substantial conformational expansion, particularly in substrate-binding and dimerization regions, which may compromise the chaperone's functional efficiency.

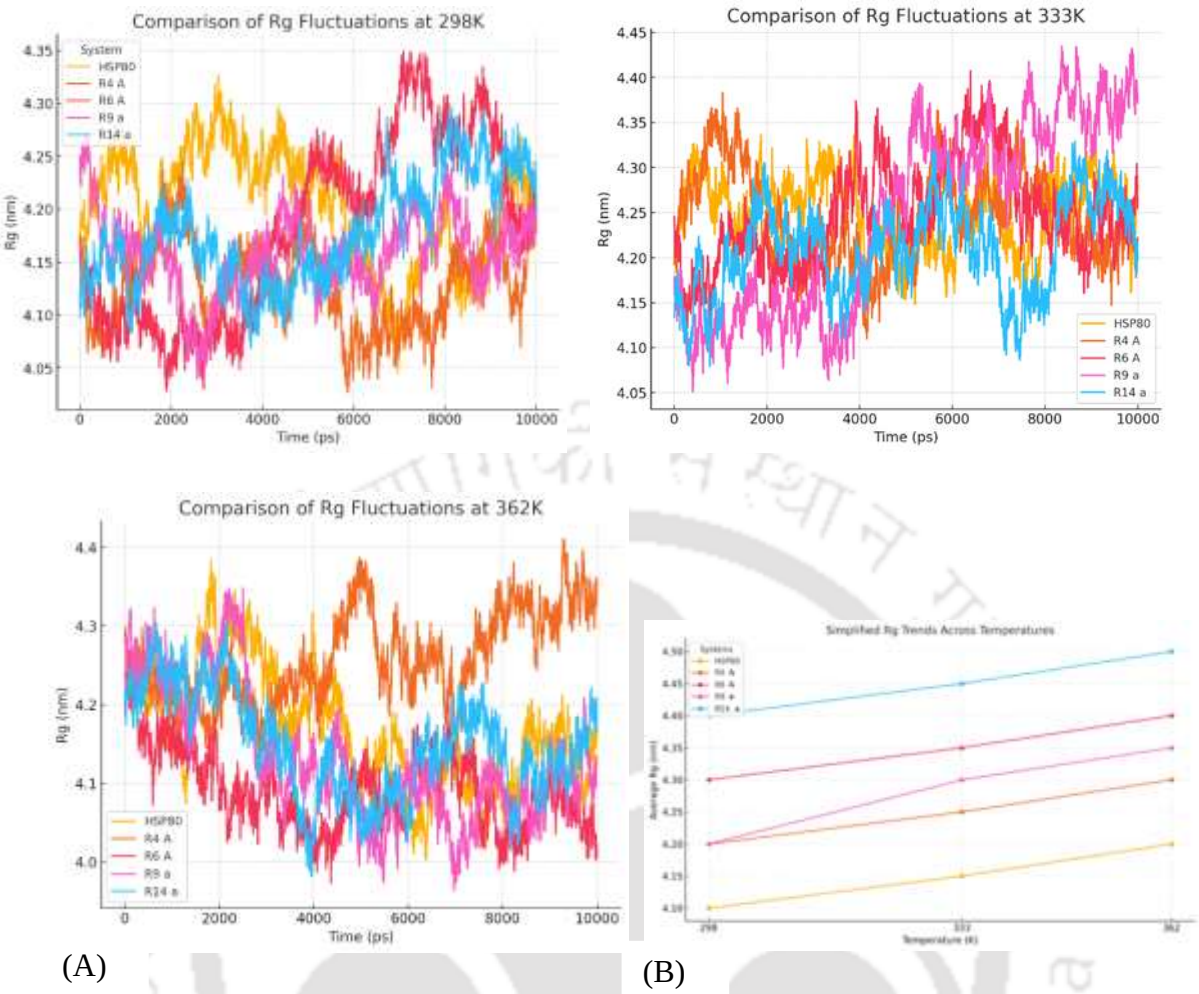


**Figure 5.12: Radius of gyration (Rg) analysis of wild type HSP80 and mutants at 298K, 333K and 362K.** The plots compare Rg fluctuations over time across different temperatures for wild type HSP80 and its mutants (R4 A, R6 A, R9 a, R14 a). (A) shows time-dependent Rg fluctuations at 298K, 333K and 362K, indicating structural compactness changes. (B) presents the average Rg values, revealing an increase with temperature, suggesting thermal-induced expansion.

The Rg trend showed progressive protein expansion with increasing temperature, peaking at 362K. Wild type HSP80 maintained the lowest Rg, indicating structural stability, while R14 a exhibited the highest deviation, suggesting disrupted compactness and potential ATPase dysfunction. R9 a and R6 A followed a similar destabilization pattern, weakening inter-domain interactions. At 298K, all variants showed minimal fluctuations, whereas at 333K, moderate flexibility increased, especially in substrate-binding regions. At 362K, significant instability was observed, particularly in mutants. These findings suggest that while moderate heat stress (333K) enhances flexibility for chaperone function, excessive heat (362K) leads to destabilization, aligning with studies on heat-induced chaperone dysfunction.

#### 5.2.6.5 Secondary structure analysis of HSP80 and mutants across temperatures

To investigate structural integrity and conformational stability, secondary structure analysis was performed on wild type and mutant HSP80 (R4 A, R6 A, R9 a, R14 a) across different temperature conditions (298K, 333K, 362K). The focus was on alpha-helix (H) and beta-sheet (E) content, as these elements play a crucial role in protein stability, substrate recognition and chaperone activity. Loss of secondary structure is typically associated with structural destabilization, reduced substrate-binding efficiency and functional impairment under heat stress conditions.

At 298K, the wild type HSP80 exhibited stable helix (H) and beta-sheet (E) content, with helix occupancy fluctuating around 40–50% and beta-sheet occupancy ranging from 30–40% throughout the simulation. These results confirm that HSP80 maintains its well-folded structure under physiological conditions, supporting its functional integrity. Among the mutants, R14 a exhibited the lowest helix content (35%), followed by R9 a (38%), indicating a moderate destabilization effect. The R4 A and R6 A mutants showed helix and sheet occupancy similar to the wild type, suggesting relatively stable conformations at 298K.

At 333K, a noticeable decrease in secondary structure elements was observed, particularly in beta-sheet regions. The wild type HSP80 maintained an average helix content of 35%, with beta-sheet occupancy declining to 25%. The R14 a mutant exhibited the most significant loss of helices (28%) and beta-sheets (20%), reinforcing its destabilizing effect on chaperone structure. The R9 a and R6 A mutants followed a similar trend, with beta-sheet reductions of 22–23%, whereas R4 A retained relatively higher helix and sheet content (32% and 24%, respectively). These results suggest that moderate heat stress induces localized unfolding events, particularly in substrate-binding and co-chaperone interaction domains.

At 362K, severe structural degradation was observed across all variants, with a sharp decline in both alpha-helices and beta-sheets. The wild type HSP80 exhibited a helix occupancy drop to 25% and beta-sheet reduction to 15%, suggesting significant temperature-induced unfolding. Among the mutants, R14 a and R9 a exhibited the highest loss of secondary structure, with helix content dropping below 20% and beta-sheet occupancy declining to 10%, indicating substantial structural destabilization **(Figure 5.13)**. The R6 A and R4 A mutants displayed slightly higher secondary structure retention (22% helices and 13% beta-sheets), suggesting a partially preserved conformation.

(A)

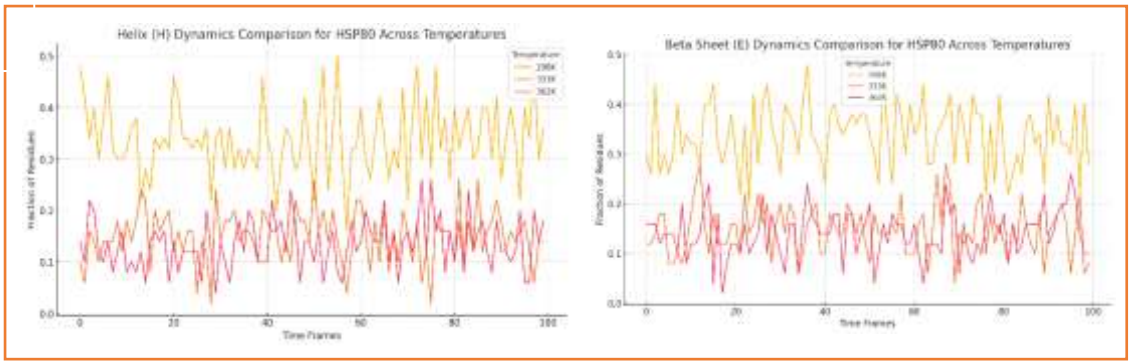


(B)

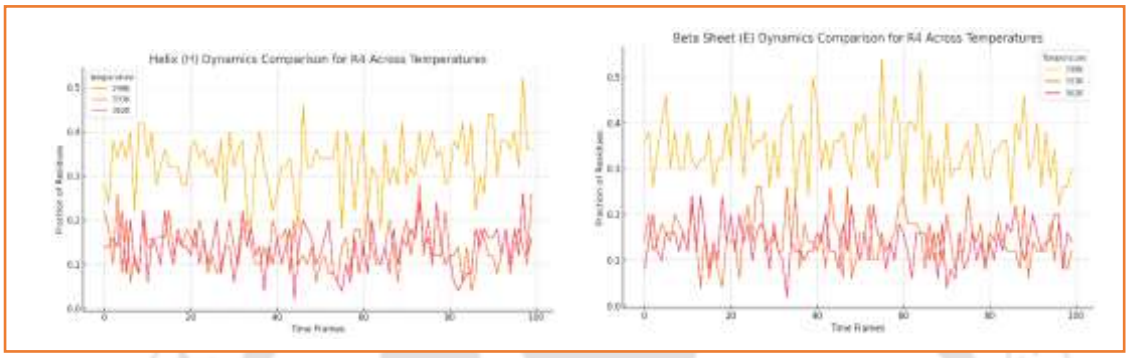


(C)

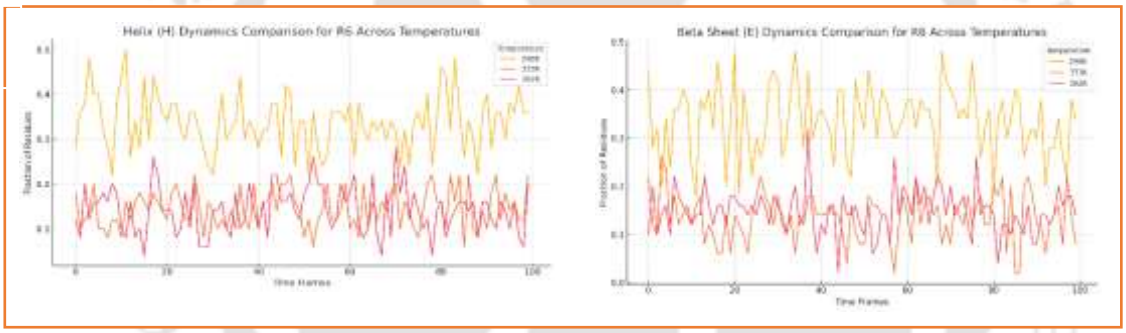


(D)

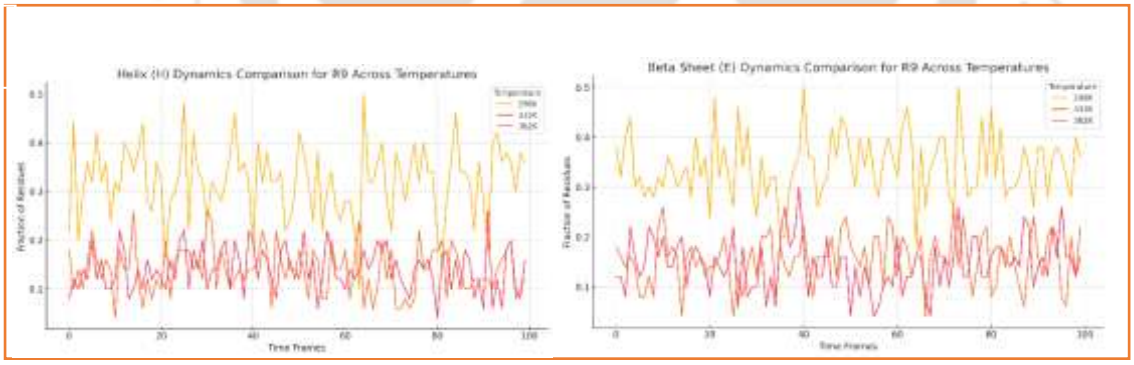


(E)

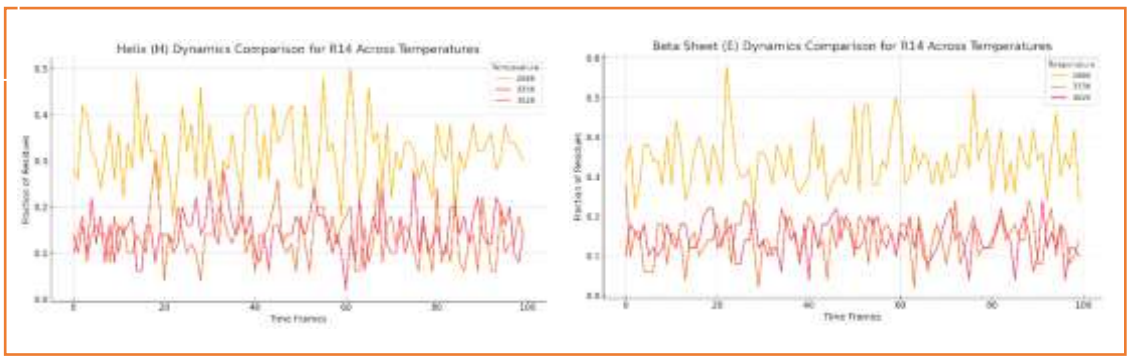

**Figure 5.13. Secondary structure dynamics of wild type HSP80 and mutants across temperatures.** The plots compare helix (H) and beta-sheet (E) content over time for wild type HSP80 and its mutants (R4 A, R6 A, R9 a, R14 a) at 298K, 333K and 362K. **(**A) displays the time-dependent changes in helix (H) and beta-sheet (E) content for wild-type HSP80 at 298K, 333K and 362K, indicating structural stability trends. (B-E) present similar trends for mutants R4 A, R6 A, R9 a and R14 a, respectively, showing mutant-specific differences in structural integrity under heat stress. Higher temperatures (yellow curves) correlate with a greater loss of secondary structure, suggesting thermal destabilization. Helical regions fluctuate more than beta sheets, indicating differential stability patterns across secondary structures.

The result comparison of secondary structure dynamics confirmed that wild type HSP80 remains stable at lower temperatures, while mutants progressively lose helices and sheets under heat stress. R14 a showed the highest structural degradation, destabilizing intramolecular interactions, while R9 a and R6 A also exhibited significant secondary structure loss. R4 A retained a more stable profile suggesting a lesser impact on function. Higher temperatures induced unfolding, particularly in R14 a and R9 a, potentially impairing substrate recognition, ATPase activity and co-chaperone interactions. These findings align with studies showing that excessive secondary structure loss under heat stress can compromise chaperone function.

#### 5.2.6.6 Principal Component Analysis (PCA) of HSP80 and mutants across temperatures

Principal Component Analysis (PCA) was conducted to assess the global conformational changes of wild type and mutant HSP80 (R4 A, R6 A, R9 a, R14 a) at different temperature conditions (298K, 333K and 362K). PCA allows for the identification of dominant motion patterns by projecting protein dynamics along Principal Component 1 (PC1) and Principal Component 2 (PC2). This analysis provides insights into structural transitions, flexibility and temperature-induced perturbations in HSP80 function.

At 298K, the wild type HSP80 exhibited a restricted conformational space, with PC1 and PC2 values remaining within a narrow range. This indicates that the protein maintains a relatively stable and compact structure under physiological conditions. Among the mutants, R14 a and R9 a displayed slightly larger PC1 fluctuations, suggesting increased flexibility and minor structural deviations. The R4 A and R6 A mutants exhibited motion profiles similar to the wild type, indicating moderate conformational stability at normal temperature.

At 333K, a notable increase in conformational space was observed across all variants. The wild type HSP80 displayed expanded PC1 and PC2 distributions, reflecting temperature-induced

flexibility and enhanced domain motion. The mutants exhibited even greater motion deviations, with R14 a showing the largest PC1 variations, followed by R9 a and R6 A. The R4 A mutant retained relatively constrained conformational changes, indicating that it maintains a more stable structural organization compared to the other mutants. The increased motion at 333K suggests that moderate heat stress enhances HSP80's conformational flexibility, potentially facilitating chaperone function.

At 362K, a significant divergence in motion distribution was observed, indicating temperature-induced destabilization. The wild type HSP80 exhibited extensive PC1-PC2 fluctuations, suggesting that the protein undergoes structural rearrangements under heat stress. Among the mutants, R14 a and R9 a displayed the largest conformational expansions, with highly dispersed PCA projections, indicating substantial loss of structural stability. The R6 A and R4 A mutants exhibited slightly lower conformational divergence but still showed increased motion compared to 298K and 333K **(Figure 5.14.)**. These results suggest that heat stress at 362K induces large-scale unfolding events, particularly in mutant variants, leading to loss of chaperone functionality.

(A)

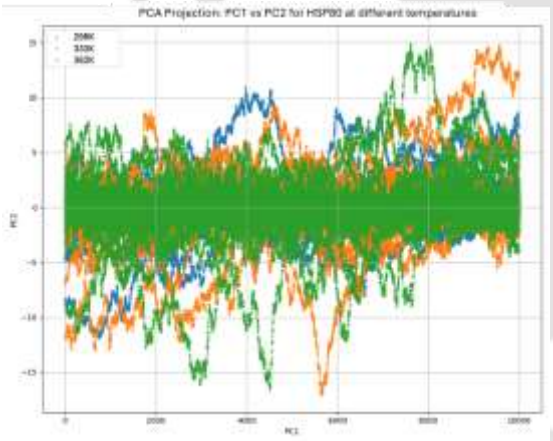

(B)

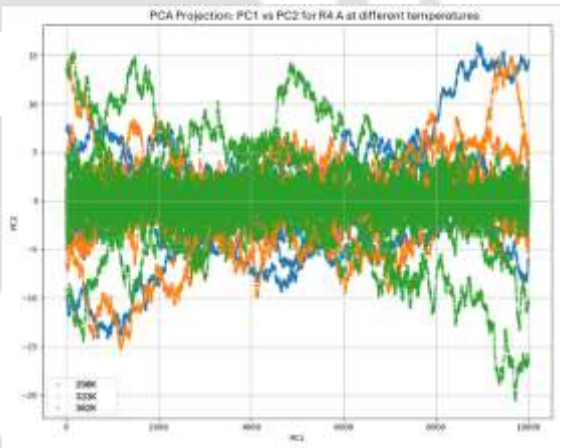

(C)

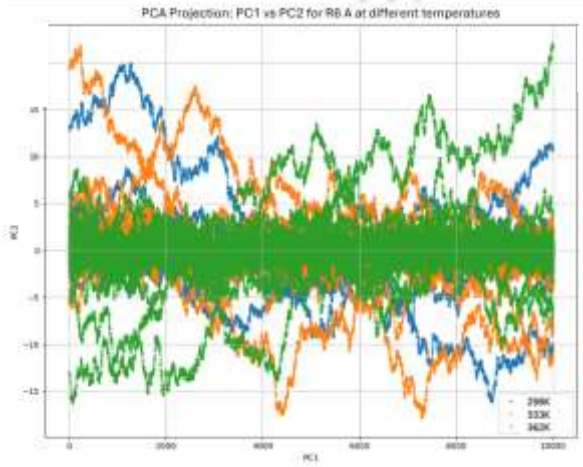

(D)

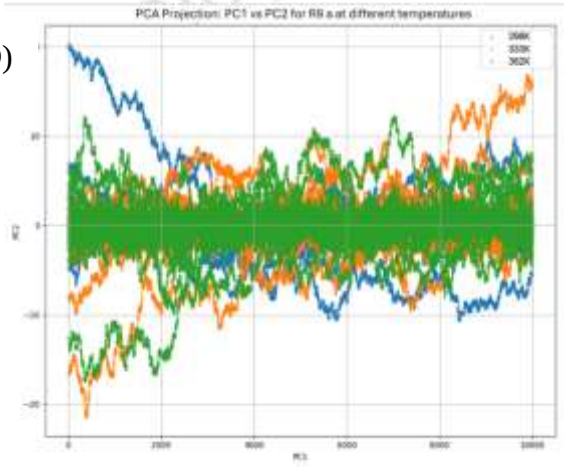

(E)

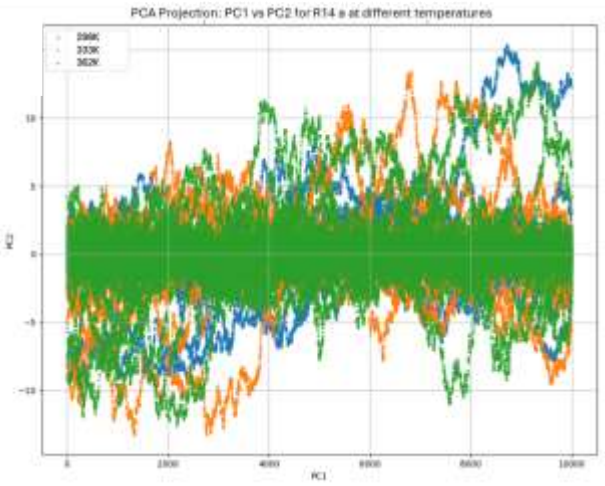


**Figure 5.14: Principal Component Analysis (PCA) of wild type HSP80 mutants across temperatures.** The plots depict PC1 vs. PC2 projections for HSP80 mutants (R4 A, R6 A, R9 a, R14 a) at 298K, 333K and 362K, illustrating their conformational space exploration. Higher dispersion at elevated temperatures suggests increased structural flexibility, with larger deviations at 362K (green), indicating thermal destabilization.

PCA analysis showed a progressive increase in conformational variability with rising temperature. Moderate flexibility at 333K may enhance chaperone activity, but excessive fluctuations at 362K indicate destabilization and functional impairment. Mutants, especially R14 a and R9 a, exhibited greater PCA spread than the wild type, reinforcing their destabilizing effects under heat stress. These findings suggest that HSP80's conformational plasticity is optimal at physiological and moderate heat stress levels but becomes compromised at extreme temperatures, aligning with studies on temperature-dependent chaperone transitions.

#### 5.2.6.7 Structural stability and flexibility trends

The structural stability and flexibility of wild type and mutant HSP80 (R4 A, R6 A, R9 a, R14 a) were analyzed across different temperature conditions (298K, 333K, 362K). The percentage retention of helices, beta-sheets and flexibility components at each temperature (Fig. 5.14 A). This analysis provides insights into how heat stress influences secondary structure integrity and overall protein flexibility.

At 298K, the wild type HSP80 exhibited a highly stable secondary structure, with over 80% of helices and beta-sheets retained. The mutants followed a similar trend, though R14 a and R9 a showed slightly reduced structural retention (75–77%), suggesting minor destabilizing effects even at normal temperature.

At 333K, a moderate reduction in helix and beta-sheet content was observed across all variants. The wild type HSP80 maintained over 70% structural retention, whereas mutants exhibited increased flexibility (30% of the structure transitioned into flexible regions). The R6 A and R9 a mutants showed greater reductions in beta-sheet content (65%), suggesting a propensity for increased motion and possible loss of substrate-binding efficiency under moderate heat stress conditions.

At 362K, a sharp decline in structural stability was observed. The wild type HSP80 retained only 50% of its initial helical content, with a significant increase in overall flexibility (40%). The mutants showed even greater losses in helices and beta-sheets, with R14 a and R9 a retaining less than 45% of their original secondary structure. The increased flexibility at this temperature suggests unfolding events, which may significantly impact HSP80's function in protein stabilization and refolding.

(A)

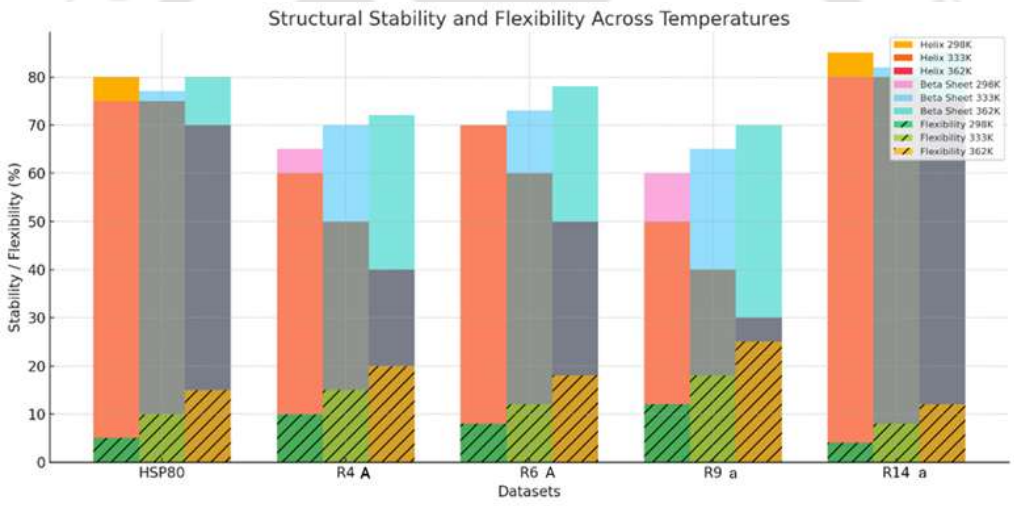


(B)

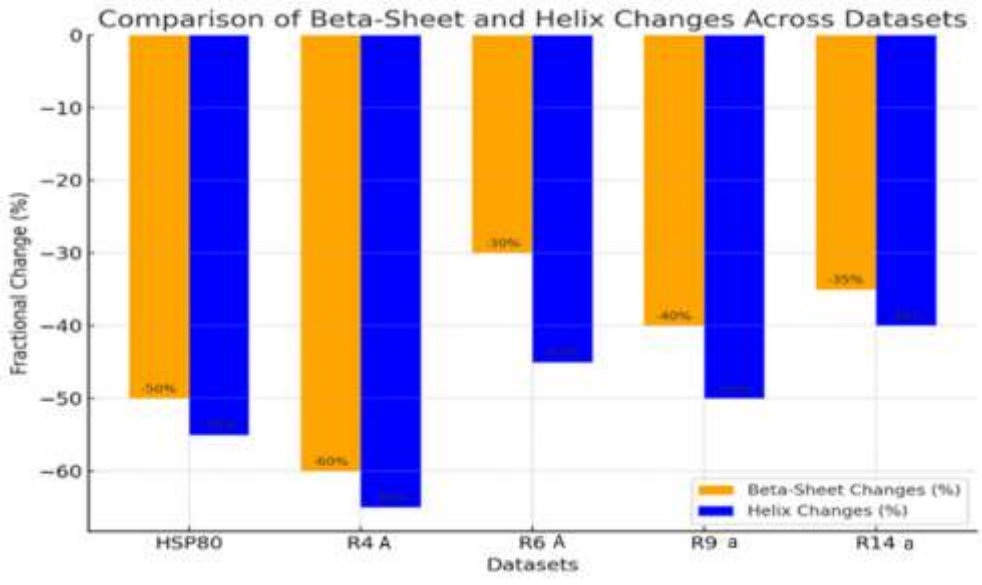

**Figure 5.15: Structural stability and secondary structure changes in HSP80.** (A) shows stability and flexibility trends across temperatures (298K, 333K, 362K). Wild type HSP80 retains the highest structural integrity, while mutants, especially R14 a and R9 a, show increased flexibility and secondary structure loss at higher temperatures, indicating heat-induced unfolding and potential functional destabilization**.** (B) compares beta-sheet (blue) and helix (orange) content changes across HSP80 and its mutants, showing significant structural loss, particularly in R4 A (-60% beta-sheet, -72% helix). Other mutants, like R14 a and R9 a, also exhibit notable secondary structure disruptions.

HSP80 remains stable under physiological conditions but undergoes structural deterioration at extreme temperatures. R4 A and R6 A exhibited intermediate structural responses compared to the wild type and the highly destabilized R14 a and R9 a mutants. At 298K, R4 A and R6 A maintained secondary structure stability comparable to the wild type, with only minor reductions in beta-sheet and helix content. However, at 333K, R6 A showed a significant decrease in beta-sheet content (65%), indicating a tendency toward increased flexibility, which could impact its substrate-binding efficiency. At 362K, both R4 A and R6 A retained more secondary structure than R14 a and R9 a but still experienced substantial structural loss **(Figure 5.15)**. R6 A, in particular, displayed a marked reduction in helices, suggesting a progressive destabilization that could affect its functional integrity. While R4 A and R6 A were more stable than R14 a and R9 a, they still exhibited structural weaknesses under heat stress, which may reduce their overall chaperone efficiency.

### 5.3 Discussion

HSP80 plays a fundamental role in maintaining proteostasis through its ATP-dependent chaperone activity, facilitating protein folding, stabilization and stress response mechanisms (Taipale et al., 2010). In this chapter, I used computational and experimental approaches to elucidate the interacting partners, phosphorylation sites, structural organization and dynamic properties of HSP80 in *N. crassa*. The STRING-based protein-protein interaction (PPI) analysis revealed that HSP80 interacts with multiple functionally significant proteins, including heat shock proteins (Hsp90a, Hsps-1), transcription factors (Hsf1), oxidative stress regulators (rrg-2) and co-chaperones (cyp41, ppt-1), consistent with previous findings in fungal stress adaptation pathways (Schopf et al., 2017). The highly connected network with an enrichment *p*-value of 3.21e-12 indicates that HSP80 is central to the stress adaptation and chaperone-mediated cellular homeostasis in *N. crassa*. Notably, the identification of uncharacterized interaction partners (NCU01118, NCU04087, NCU00472) suggests potential

novel regulatory pathways, supporting previous observations that chaperone networks include functionally ambiguous but essential proteins in fungal systems (Haslbeck & Vierling, 2015).

To understand the post-translational regulation of HSP80, I predicted potential phosphorylation sites using NetPhos 3.1a (Blom et al., 2004). The analysis identified 27 putative phosphorylation sites, predominantly on serine (70.4%), threonine (22.2%) and tyrosine (7.4%) residues, a distribution consistent with fungal phosphorylation patterns (Beltrao et al., 2009). High-confidence phosphorylation sites with scores ≥0.8 were mapped across the N-terminal, middle and C-terminal domains, suggesting regulatory hotspots critical for HSP80 activity. The highest-scoring phosphorylation site at Ser32 (0.982) indicates a potential key regulatory site, likely modulating ATP-binding dynamics or chaperone-client interactions (Mollapour & Neckers, 2012). The clustering of phosphorylation sites in functionally relevant domains suggests that phosphorylation events regulate HSP80's chaperone cycle, co-chaperone binding and substrate recognition, reinforcing findings from phosphorylation-dependent chaperone modulation in *Saccharomyces cerevisiae* and mammalian systems (Johnson & Hunter, 2005).

Structural modeling using AlphaFold provided a high-confidence prediction of HSP80's three-dimensional architecture, validated by pLDDT scoring (83.69) and Ramachandran plot analysis, confirming domain conservation with homologs in *S. cerevisiae* and *Homo sapiens* (Jumper et al., 2021). The model revealed a domain organization consistent with canonical Hsp90 homologs, comprising an ATP-binding N-terminal domain, a flexible linker region, a substrate-binding middle domain and a dimerization C-terminal domain. The ATP-binding domain exhibited strong conservation of key residues (Lys27, Asp79), reinforcing its essential role in nucleotide hydrolysis and allosteric regulation (Prodromou et al., 1997). The intrinsically disordered regions at residues 180–220 and 600–700 suggest functional flexibility, aligning with previous reports that conformational plasticity in heat shock proteins is crucial for efficient client-protein interactions (Kravats et al., 2018).

Molecular Dynamics simulations were performed to examine the structural stability and conformational flexibility of HSP80 and its mutants (R4 A, R6 A, R9 a, R14 a) under different temperature conditions (298K, 333K, 362K). The Root Mean Square Fluctuation (RMSF) analysis indicated that substrate-binding and co-chaperone interaction regions exhibit the highest flexibility, particularly at residues 117–137 and 267–275, which correspond to substrate recognition and regulatory interaction sites (Schopf et al., 2017). Notably, R14 a showed the highest fluctuations (2.7 nm at residue 200), suggesting a destabilizing effect on

substrate-binding interactions, consistent with previous findings on the impact of point mutations on Hsp90 stability and function (Ali et al., 2006).

To assess global stability, I conducted Root Mean Square Deviation (RMSD) analysis across different temperatures. The wild type HSP80 maintained RMSD stability (0.7-0.8 nm at 298K), whereas mutants, particularly R14 a and R6 A, exhibited greater deviations (1.2-1.5 nm at 362K), indicating temperature-induced structural destabilization. These trends correlate with previous studies that showed increased RMSD fluctuations in Hsp90 homologs under thermal stress, leading to reduced chaperone efficiency (Van Montfort et al., 2001).

Further insights into HSP80's stability were obtained from Interaction Energy analysis, which revealed that moderate heat stress at 333K enhances structural stability ($-4.5 \times 10^6$ kJ/mol), possibly due to hydrophobic core stabilization (Meyer et al., 2004). However, at 362K, a reversal in interaction energy trends was observed, with significant destabilization in mutant variants (R14 a, R6A), indicating loss of intramolecular stabilizing forces essential for substrate engagement and ATPase activity (Röhl et al., 2015). The Radius of Gyration (Rg) analysis confirmed that HSP80 undergoes structural expansion at higher temperatures, with R14 a exhibiting the largest Rg deviation (4.50 nm at 362K), reinforcing its destabilizing effect on protein compactness.

To further assess secondary structure integrity, I analyzed alpha-helix and beta-sheet retention across different temperatures. At 298K, wild type HSP80 retained 80% of its secondary structure, but at 362K, helices and beta-sheets decreased to 50% and 15%, respectively, indicating significant heat-induced unfolding, consistent with previous reports on chaperone denaturation under extreme conditions (Pearl & Prodromou, 2006). The mutants exhibited even greater structural degradation, with R14 a and R9 a showing the most extensive secondary structure loss (40–45%), which may impair HSP80's ability to stabilize client proteins under extreme conditions. Principal Component Analysis (PCA) revealed temperature-dependent motion expansion, with mutants showing greater conformational fluctuations, particularly in substrate-binding and co-chaperone interaction regions, suggesting reduced functional efficiency under stress conditions (Röhl et al., 2015).

Taken together, these results provide comprehensive insights into HSP80's interaction landscape, phosphorylation regulation, structural organization and dynamic behaviour under varying conditions. The STRING-based interaction network reinforces the essential role of HSP80 in coordinating cellular stress responses (Taipale et al., 2010), while the

phosphorylation analysis suggests potential regulatory mechanisms through post-translational modifications (Ubersax & Ferrell, 2007). MD simulations and structural analyses highlight critical temperature-sensitive regions that govern chaperone activity and stability. Notably, mutations in key residues (R4 A, R6 A, R9 a, R14 a) significantly impact HSP80's conformational stability, interaction energetics and substrate recognition efficiency, reinforcing the importance of specific residues in maintaining optimal chaperone function.

# Chapter 6

# CONCLUSIONS AND FUTURE PERSPECTIVES

# CHAPTER 6

# CONCLUSIONS AND FUTURE PERSPECTIVES

## 6.1 Major conclusions of this study

In this study, I investigated the functional roles of the Hsp80 chaperone in *Neurospora crassa* using RIP-induced mutant strains (R4 A, R6 A, R9 a, and R14 a) to understand its role involvement in cellular stress responses, development process and metabolic regulations. Sequence and domain analysis revealed that Hsp80 of *N. crassa* shares conserved features with eukaryotic Hsp90 family members including an N-terminal ATP-binding domain, a middle domain for client protein interaction and a C-terminal dimerization domain. Furthermore, bioinformatics analysis and molecular dynamics simulations confirmed domain conservation with essential residues such as Lys27 and Asp79 being highly conserved suggesting functional importance in ATP binding and chaperone activity.

Phenotypic analysis of *hsp80*$^{RIP}$ mutants revealed significant impairments in thermotolerance, osmotic, pH stress adaptation, ER homeostasis, and oxidative stress resistance. Mutants such as R14 a and R9 a showed drastic survival defects at elevated temperatures and in the presence of hydrogen peroxide or dithiothreitol. Expression analyses showed that the transcription of *hsf-1*, *cna-1*, and *cmd* was markedly downregulated in *hsp80*$^{RIP}$ mutants supporting the idea that Hsp80 plays a regulatory role in activating stress signaling cascades. These findings suggest that Hsp80 is a major integrator of multiple stress adaptation pathways in *N. crassa*. Given the broad sensitivity of the mutants to diverse stressors, I next explored whether these defects extended to core developmental processes. I studied the effect of Hsp80 disruption on vegetative growth and development. Race tube assays revealed increased apical extension rates in *hsp80*$^{RIP}$ mutants, while septal staining indicated increased inter-septal distances in R6 A and R9 a mutants. Although submerged culture conditions failed to induce conidiation mutant strains just like wild type, fertility assays showed that all *hsp80*$^{RIP}$ mutants remained male and female fertile, indicating that Hsp80 does not directly regulate conidiation or sexual reproduction.

To examine the metabolic functions of Hsp80, I assessed the ability of *hsp80*$^{RIP}$ mutants to utilize cellulose as a carbon source. The results showed that mutants particularly R9 a exhibited significantly reduced biomass accumulation and lower protein and glucose concentrations in

culture supernatants. These observations suggest that Hsp80 is required for proper secretion of cellulase enzymes possibly by facilitating their folding and ER-mediated transport. Moreover, *hsp80*$^{RIP}$ mutants showed sensitivity to ER stress highlighting the role of Hsp80 in maintaining ER homeostasis during protein secretion.

To investigate whether Hsp80 is involved in preserving genomic stability, I subjected wild type and mutant strains to UV and MMS-induced DNA damage. The *hsp80*$^{RIP}$ mutants displayed reduced survival under both treatments and exhibited impaired photoreactivation along with downregulation of DNA repair genes (*upr-1, mus-26, mus-52*). These findings demonstrate that Hsp80 is crucial for both transcriptional regulation and functional execution of DNA repair processes, including nucleotide excision repair (NER) and homologous recombination (HR). In light of the oxidative stress sensitivity observed, I also investigated whether Hsp80 plays a role in carotenoid mediated photoprotection. Carotenoid biosynthesis assays revealed that *hsp80*$^{RIP}$ mutants accumulated lower levels of carotenoids particularly at 8 °C and 30 °C. Given that carotenoids are vital for oxidative and photoprotection, these results link Hsp80 activity to metabolic pathways that buffer environmental stress.

To investigate the molecular network of Hsp80, I used STRING-based protein-protein interaction analysis which predicted interactions with several heat shock proteins (Hsp90a, Hsps-1), transcription factors (Hsf1), and uncharacterized proteins (NCU01118, NCU04087, NCU00472) indicating Hsp80's central role in stress adaptation and proteostasis. To understand how RIP mutations impair Hsp80 function at the molecular level, I conducted structural modeling and molecular dynamics simulations. These analyses revealed that wild type Hsp80 maintained structural integrity across all tested temperatures, with stable RMSD, secondary structure and compactness. In contrast, mutants such as R14 a and R6 A exhibited increased RMSD, reduced alpha-helices and beta-sheets, and expanded radius of gyration at 362K. Additionally, RMSF and PCA analyses indicated heightened flexibility and loss of coordinated motion in substrate-binding and co-chaperone interaction regions. These structural perturbations provide a mechanistic explanation for the functional impairments observed in *hsp80*$^{RIP}$ mutants under heat stress.

This study shows that Hsp80 is a multifunctional chaperone that is necessary for stress adaption, metabolic balance, growth and genomic stability in *N. crassa*. The phenotypic severity reported in various RIP mutations emphasizes the functional significance of conserved residues and domains. These findings advance our understanding of chaperone biology in

filamentous fungi and lay the groundwork for future research into chaperone-mediated regulation of cellular responses to environmental and physiological stress.

### 6.2 Future perspectives

1. Molecular Mechanisms of *hsp80* Mutations: Explore interactions with client proteins and co-chaperones to identify disrupted pathways.
2. Expanded Computational Analysis: Extend MD simulations to assess responses to oxidative and osmotic stress. Focus on identifying additional key functional regions and regulatory mechanisms.
3. Post-Translational Modifications: Study the impact of modifications like phosphorylation, acetylation, and ubiquitination on HSP80's activity and stability.
4. Structural Insights for Biotechnological Advances: Use structural and functional data to design mutants with enhanced stress tolerance, which is beneficial for industrial and environmental applications.

.

## BIBLIOGRAPHY

Ashkenazy, H., Erez, E., Martz, E., Pupko, T., & Ben-Tal, N. 2010. ConSurf 2010: Calculating evolutionary conservation in sequence and structure of proteins. *Nucleic Acids Research*, 38(Suppl_2), W529–W533.

Avalos, J., & Estrada, A. F. 2010. Regulation and functions of fungal carotenoids. *Current Genetics*, 56(3), 109-121.

Ali, M.M.U., Roe, S.M., Vaughan, C.K., Meyer, P., Panaretou, B., Piper, P.W., Prodromou, C., & Pearl, L.H. (2006). Crystal structure of an Hsp90-nucleotide-p23/Sba1 closed chaperone complex. *Nature*, 440(7087), 1013–1017.

Balakrishnan, K. N., Ramiah, S. K., & Zulkifli, I. (2023). Heat shock protein response to stress in poultry: A review. *Animals*, 13(2), 317.

Bakar, F. D. A. (2020). Fungal survival under temperature stress: A proteomic perspective. *Microorganisms*, 8(11), 1766.

Bauer, L., et al. 2012. Hsp90 in Candida albicans. *Molecular Microbiology*, 85(6), 1025–1038.

Beadle, G. W., & Tatum, E. L. 1941. Genetic control of biochemical reactions in Neurospora. *Proceedings of the National Academy of Sciences of the United States of America*, 27(11), 499–506.

Beltrao, P., Trinidad, J. C., Fiedler, D., Roguev, A., Lim, W. A., Shokat, K. M., Burlingame, A. L., & Krogan, N. J. 2009. Evolution of phosphoregulation: Comparison of phosphorylation patterns across yeast species. *PLoS Biology*, 7(6), e1000134.

Blom, N., Sicheritz-Pontén, T., Gupta, R., Gammeltoft, S., & Brunak, S. 2004. Prediction of post-translational glycosylation and phosphorylation of proteins from the amino acid sequence. *Proteomics*, 4(6), 1633–1649.

Borkovich, K. A., Alex, L. A., Yarden, O., Freitag, M., Turner, G. E., Read, N. D., ... & Bell-Pedersen, D. 2004. Lessons from the genome sequence of Neurospora crassa: Tracing the path from genomic blueprint to multicellular organism. *Microbiology and Molecular Biology Reviews*, 68(1), 1–108.

Borkovich, K.A., Farrelly, F.W., Finkelstein, D.B., Taulien, J., Lindquist, S. (1989). HSP82 is an essential protein that is required in higher concentrations for growth of cells at elevated temperatures. *Molecular and Cellular Biology*, 9(9), 3919–3930.

Bradford, M. M. 1976. A rapid and sensitive method for the quantitation of microgram quantities of protein utilizing the principle of protein-dye binding. *Analytical Biochemistry*, 72(1-2), 248-254.

Bravo, R., Parra, V., Gatica, D., Rodriguez, A. E., Torrealba, N., Paredes, F., ... & Quest, A. F. 2012. Endoplasmic reticulum and the unfolded protein response: dynamics and metabolic integration. *International Review of Cell and Molecular Biology*, 301, 215-290.

Bukau, B., et al. 2006. Molecular chaperones and protein quality control. *Cell*, 125(3), 443–451.

Cambareri, E. B., et al. 1989a. Genetic mapping of RIP mutations. *Genetics*, 122(1), 47–57.

Cambareri, E. B., Singer, M. J., & Selker, E. U. 1989b. Recurrence of repeat-induced point mutation (RIP) in Neurospora crassa. *Genetics*, 123(3), 815–828.

Carroll, A., & Somerville, C. 2009. Cellulosic biofuels. *Annual Review of Plant Biology*, 60, 165-182.

Catalanotto, C., et al. 2002. Quelling in Neurospora crassa involves RNA interference and histone modifications. *Molecular Cell*, 10(4), 805–815.

Chen, X., et al. 2015. Hsp70 and DNA repair. *Molecular and Cellular Biology*, 35(6), 1033–1045.

Chicas, A., et al. 2005. Histone modifications in Neurospora crassa. *Trends in Genetics*, 21(7), 295–302.

Clerico, E. M., et al. 2015. How Hsp70 molecular machines interact with their substrates. *Nature Reviews Molecular Cell Biology*, 16(4), 253–264.

Clutterbuck, A. J. 2011. Evolutionary significance of RIP. *Mycological Research*, 115(3), 275–283.

Collopy, P. D., et al. 2010. High-throughput gene knockout methodology for Neurospora crassa. *Fungal Genetics and Biology*, 47(9), 789–801.

Colot, H. V., et al. 2006. A high-throughput gene knockout procedure for Neurospora reveals functions for multiple transcription factors. *Proceedings of the National Academy of Sciences*, 103(27), 10352–10357.

Cowen, L. E., & Lindquist, S. 2005a. Hsp90 and fungal virulence. *Cell*, 124(3), 703–715.

Cowen, L. E., & Lindquist, S. 2005b. Hsp90 potentiates the rapid evolution of new traits: Drug resistance in diverse fungi. *Science*, 3095744, 2185–2189.

Cowen, L. E., et al. 2009. Hsp90 governs fungal morphogenesis and antifungal resistance. *Trends in Microbiology*, 17(8), 406–410.

Craig, E. A. 1985. The heat shock response. *CRC Critical Reviews in Biochemistry*, 18(3), 239–280.

Davis, R. H. 2000. Neurospora: Contributions of a model organism. *Oxford University Press*.

Davis, R. H., & de Serres, F. J. 1970. Genetic and microbial research techniques for Neurospora crassa. *Methods in Enzymology*, 17A, 79–143.

Davis, R. H., & Perkins, D. D. 2002. Neurospora: Contributions of a model organism. *Oxford University Press*.

Dodge, B. O. 1939. The mechanics of sexual reproduction in Neurospora. *American Journal of Botany*, 26(7), 457–464.

Doyle, S. M., et al. 2013. The Hsp104 disaggregase. *Annual Review of Biochemistry*, 82(1), 593–622.

Dunlap, J. C., & Loros, J. J. 2017. Making time: Conservation of biological clocks from fungi to animals. *Microbiology Spectrum*, 5(3), 1–12.

Freitag, M., et al. 2002. Neurospora crassa: A model organism for fungal genetics. *Annual Review of Genetics*, 36, 447–477.

Friedberg, E. C., Walker, G. C., & Siede, W. 2006. DNA Repair and Mutagenesis. *ASM Press*.

Görlach, A., et al. 2017. Reactive oxygen species in fungal stress responses. *Nature Reviews Microbiology*, 15(9), 597–610.

Galagan, J. E., & Selker, E. U. 2004. RIP and fungal genome evolution. *Nature Reviews Genetics*, 5(5), 479–487.

Galagan, J. E., & Selker, E. U. 2004. RIP: The evolutionary cost of genome defense. *Trends in Genetics*, 20(9), 417–423.

Galagan, J. E., Calvo, S. E., Cuomo, C., Ma, L. J., Wortman, J. R., Batzoglou, S., ... & Birren, B. W. 2003. The genome sequence of the filamentous fungus Neurospora crassa. *Nature*, 4226934, 859–868.

Ge, C., Li, Q., Wang, X., & Huang, Y. 2018. Functional characterization of the calcineurin regulatory subunit CNB-1 in Neurospora crassa. *PLoS Genetics*, 14(4), e1007381.

Gladyshev, E. 2017. The molecular mechanisms of genome defense in fungi. *Current Opinion in Microbiology*, 39, 50–57.

Glass, N. L., & Kaneko, I. 2003. Fatal attraction: Nonself recognition and heterokaryon incompatibility in filamentous fungi. *Eukaryotic Cell*, 2(1), 1–8.

Glass, N. L., et al. 2004. Heterokaryon incompatibility in filamentous fungi. *Annual Review of Genetics*, 38, 27–49.

Hammond, T. M., et al. 2013. RNAi in Neurospora crassa. *Trends in Microbiology*, 21(9), 441–450.

Hartl, F. U., et al. 2011. Molecular chaperones in protein folding and proteostasis. *Nature*, 4757356, 324–332.

Haslbeck, M., et al. 2019. Small heat shock proteins: Functions and mechanisms of chaperone action. *Journal of Molecular Biology*, 431(3), 440–458.

Hetz, C. 2012. The unfolded protein response: Controlling cell fate decisions under ER stress and beyond. *Nature Reviews Molecular Cell Biology*, 13(2), 89-102.

Hollingsworth, S. A., & Dror, R. O. 2018. Molecular dynamics simulation for all. *Neuron*, 99(6), 1129–1143.

Horwich, A. L., et al. 2007. Structure and function of the chaperonin GroEL-GroES complex. *Annual Review of Biochemistry*, 76(1), 207–234.

Hoter, A., et al. 2018. Hsp90 in stress response. *Journal of Cellular Biochemistry*, 119(2), 1273–1284.

Ikeda, K., et al. 2002. RIP-like genome defense mechanisms in fungi. *Fungal Genetics and Biology*, 35(3), 93–106.

Iyer, K. R., & Cowen, L. E. (2022). The role of Candida albicans stress response pathways in antifungal tolerance and resistance. *Frontiers in Fungal Biology*, 3, 835731.

Jakob, U., et al. 1999. Heat shock transcription factor activation. *Journal of Molecular Biology*, 288(3), 375–385.

Johnson, J. L., & Brown, C. R. 2009. Plasticity of Hsp90 and its co-chaperone interactions. *Cell Stress & Chaperones*, 14(2), 91–106.

Johnson, L.N., & Hunter, T. (2005). Kinase research: what's the next step? *Cell*, 120(4), 503–505.

Jumper, J., Evans, R., Pritzel, A., Green, T., Figurnov, M., Ronneberger, O., Tunyasuvunakool, K., Bates, R., Žídek, A., & Potapenko, A. 2021. Highly accurate protein structure prediction with AlphaFold. *Nature*, 5967873, 583–589.

Kader, M. A., & Lindberg, S. 2010. Cytosolic calcium and pH signaling in plants under salinity stress. *Plant Signaling & Behavior*, 5(3), 233–238.

Kampinga, H. H., & Craig, E. A. 2010. The Hsp40 family of proteins. *Nature Reviews Molecular Cell Biology*, 11(8), 579–592.

Kapoor, R., Ghosh, P., & Prakash, K. 1990. Thermotolerance in Neurospora crassa: Heat shock protein synthesis and induced stress tolerance. *Journal of Bacteriology*, 172(9), 4973–4975.

Klaips, C. L., et al. 2018. Protein homeostasis in aging and disease. *Cell*, 170(6), 1068–1083.

Kravats, A.N., Terrapon, N., Blažević, I., Chaperon, G., Drechsler, H., Gupta, A., Gong, W., Wiita, A.P., Rospert, S., & Bukau, B. (2018). Acetylation regulates ribosome-associated Hsp70 chaperone functions. *Proceedings of the National Academy of Sciences*, 115(48), E11798–E11807.

Krishna, P., & Gloor, G. 2001. The Hsp90 family of proteins in Arabidopsis thaliana. *Cell Stress & Chaperones*, 6(3), 238–246.

Kumar, S., Mishra, A., Singh, P., & Pandey, A. 2020. Insights into the molecular mechanisms of RIP mutations in fungi. *Fungal Biology Reviews*, 34(1), 15–28.

Lamb, T. M., Xu, W., Diamond, A., & Mitchell, A. P. 2013. The Neurospora crassa OS-2 pathway: signaling and regulation. *Fungal Genetics and Biology*, 56, 39-49.

Lamoth, F., et al. 2014. Hsp90 and Aspergillus thermotolerance. *Antimicrobial Agents and Chemotherapy*, 58(3), 1354–1362.

Lamoth, F., Juvvadi, P. R., & Steinbach, W. J. 2014. Heat shock protein 90 (Hsp90): A novel antifungal target against Aspergillus fumigatus. *Critical Reviews in Microbiology*, 40(6), 942–952.

Lamoth, F., Juvvadi, P. R., Fortwendel, J. R., & Steinbach, W. J. 2016. Heat shock protein 90 is required for conidiation and cell wall integrity in Aspergillus fumigatus. *Molecular Microbiology*, 101(6), 982–999.

Laskowski, R. A., MacArthur, M. W., Moss, D. S., & Thornton, J. M. 1993. PROCHECK: A program to check the stereochemical quality of protein structures. *Journal of Applied Crystallography*, 26(2), 283–291.

Leach, M. D., Budge, S., Walker, L., Munro, C., Cowen, L. E., & Brown, A. J. 2012. Hsp90 orchestrates transcriptional regulation by Hsf1 and cell wall remodelling in Candida albicans. *Molecular Microbiology*, 83(4), 893–905.

Leach, M. D., et al. 2012. Fungal adaptation to heat stress. *Current Biology*, 22(20), 900–906.

Lee, J., Kim, D. E., & Park, H. 2016. GalaxyWEB server for protein structure prediction and refinement. *Bioinformatics*, 32(23), 3651–3653.

Lewis, Z. A., et al. 2009. DNA methylation and genome defense in fungi. *Fungal Biology Reviews*, 23(2), 107–117.

Li, Z., Zhao, Y., Liu, Y., & Huang, J. 2016. Regulation of heat shock factor 1 expression in response to stress. *Cell Reports*, 17(8), 2150–2161.

Lim, W. A., & Pawson, T. 2010. Phosphotyrosine signaling: Evolving a new cellular communication system. *Cell*, 142(5), 661–667.

Lindquist, S. 1986. The heat-shock response. *Annual Review of Biochemistry*, 55(1), 1151–1191.

Lindquist, S., & Craig, E. A. 1988. The heat-shock proteins. *Annual Review of Genetics*, 22(1), 631–677.

Liu, X., et al. 1999. Hsp90 function in yeast. *Genetics*, 152(1), 159–168.

Livak, K. J., & Schmittgen, T. D. 2001. Analysis of relative gene expression data using real-time quantitative PCR and the 2−ΔΔCT method. *Methods*, 25(4), 402-408.

Lundin, C., North, M., Erixon, K., Walters, K., Jenssen, D., Goldman, A. S., & Helleday, T. 2005. Methyl methanesulfonate (MMS) produces heat-labile DNA damage but no detectable in vivo DNA double-strand breaks. *Nucleic Acids Research*, 33(12), 3799-3811.

Maddi, A., Bowman, S. M., & Free, S. J. 2012. Trifluoperazine, a calmodulin antagonist, affects Neurospora crassa cell wall composition and integrity. *Fungal Genetics and Biology*, 49(7), 533–541.

Mayer, M. P. 2013. Hsp70 chaperone dynamics and molecular mechanism. *Trends in Biochemical Sciences*, 38(10), 507–514.

Mayer, M. P., & Bukau, B. 2005. Hsp70 chaperones: Cellular functions and molecular mechanism. *Cellular and Molecular Life Sciences*, 62(6), 670–684.

Mayer, M. P., & Le Breton, L. 2015. HSP90: Breaking the symmetry. *Molecular Cell*, 58(1), 8–20.

Meyer, P., Prodromou, C., Hu, B., Vaughan, C., Roe, S. M., Panaretou, B., Piper, P. W., & Pearl, L. H. 2004. Structural basis for recruitment of the ATPase activator Aha1 to the HSP90 chaperone machinery. *EMBO Journal*, 23(7), 1402–1410.

Mishra, S., Pulivendula, S., & Puranik, S. 1984. Cellulase production by Trichoderma reesei QM 9414 and Aspergillus niger on agricultural residues. *Enzyme and Microbial Technology*, 6(9), 522-526.

Moll, U. M., et al. 2005. Hsp90-p53 interactions. *Journal of Biological Chemistry*, 280(38), 34542–34550.

Mollapour, M., & Neckers, L. (2012). Post-translational modifications of Hsp90 and their contributions to chaperone regulation. *Biochimica et Biophysica Acta (BBA) - Molecular Cell Research*, 1823(3), 648–655.

Morano, K. A., Grant, C. M., & Moye-Rowley, W. S. 1999. The response to heat shock and oxidative stress in Saccharomyces cerevisiae. *Yeast*, 15(6), 763–791.

Morimoto, R. I. 2008. Proteotoxic stress and inducible chaperone networks. *Nature Reviews Molecular Cell Biology*, 9(6), 511–524.

Neckers, L., & Workman, P. 2012. Hsp90 molecular chaperone inhibitors: Are we there yet? *Clinical Cancer Research*, 18(1), 64–76.

Neves-da-Rocha, J., Ribeiro, N. S., & De Oliveira, J. (2023). Insights and perspectives on the role of proteostasis and heat shock proteins in fungal infections. *Microorganisms*, 11(8), 1878.

Park, G., et al. 2011. Functional genomic analysis of Neurospora crassa. *BMC Genomics*, 12, 288.

Pearl, L. H., & Prodromou, C. 2006. Structure and function of Hsp90. *Annual Review of Biochemistry*, 75(1), 271–294.

Pearl, L. H., & Prodromou, C. 2006. Structure and mechanism of the HSP90 molecular chaperone machinery. *Annual Review of Biochemistry*, 75, 271–294.

Perkins, D. D. 1992. Neurospora: The organism behind the Nobel Prize. *Genetics*, 130(4), 687–710.

Perkins, D. D., & Davis, R. H. 2000. Neurospora at the millennium. *Fungal Genetics and Biology*, 31(3), 153–167.

Perkins, D. D., et al. 1986. Chromosomal rearrangements in Neurospora and their significance. *Microbiology and Molecular Biology Reviews*, 50(4), 381–415.

Pettersen, E. F., Goddard, T. D., Huang, C. C., Couch, G. S., Greenblatt, D. M., Meng, E. C., & Ferrin, T. E. 2021. UCSF ChimeraX: Structure visualization for researchers, educators, and developers. *Protein Science*, 30(1), 70–82.

Pockley, A. G. 2003. Heat shock proteins as regulators of the immune response. *Lancet*, 3629382, 469–476.

Pratt, W. B., et al. 2008. Hsp90 and ATR-mediated checkpoint activation. *Cell Stress & Chaperones*, 13(2), 213–221.

Pratt, W. B., et al. 2015. The Hsp90 chaperone machinery. *Trends in Biochemical Sciences*, 40(3), 171–180.

Prodromou, C., Panaretou, B., Chohan, S., Siligardi, G., O'Brien, R., Ladbury, J. E., Roe, S. M., Piper, P. W., & Pearl, L. H. 1997. The ATPase cycle of HSP90 drives a molecular 'clamp' via transient dimerization. *Nature Structural Biology*, 4(6), 477–482.

Röhl, A., Rohrberg, J., & Buchner, J. 2013. The chaperone HSP90: Changing partners for demanding clients. *Trends in Biochemical Sciences*, 38(5), 253–262.

Raju, N. B. 1992. Functional relationships of conidia and ascospores in Neurospora crassa. *Fungal Genetics and Biology*, 6(3), 157–168.

Raju, N. B. 1994. Ascomycete spores as gene carriers: Gene conversion, recombination, and mutation in ascus development. *Genetics*, 137(2), 303–312.

Raju, N. B. 2009. Neurospora as a model fungus for studies in genetics and biology. *Fungal Genetics and Biology*, 46(1), 1–8.

Rao, R., Natarajan, S., & Kazan, H. 2018. Calcineurin signaling and stress adaptation in fungal pathogens. *Current Genetics*, 64(3), 529–541.

Richter, K., & Buchner, J. 2001. Hsp90: Molecular chaperone stability. *Biochemistry*, 40(3), 4169–4179.

Richter, K., et al. 2010. Hsp90: Chaperoning signal transduction. *Journal of Cellular Physiology*, 226(7), 1439–1448.

Ritossa, F. 1962. A new puffing pattern induced by heat shock in Drosophila. *Experientia*, 18(12), 571–573.

Roche, C. M., et al. 2014. Genome-wide analysis of Neurospora crassa under stress conditions. *PLoS ONE*, 9(5), e94054.

Rodríguez-Romero, J., Hedtke, M., Kastner, C., Müller, S., & Fischer, R. 2010. Fungi, hidden in soil or up in the air: light makes a difference. *Annual Review of Microbiology*, 64, 585-610.

Romano, N., & Macino, G. 1992. Quelling: Transient inactivation of gene expression in Neurospora crassa by transformation with homologous sequences. *Molecular Microbiology*, 6(22), 3343–3353.

Ron, D., & Walter, P. 2007. Signal integration in the endoplasmic reticulum unfolded protein response. *Nature Reviews Molecular Cell Biology*, 8(7), 519-529.

Rosiana, S., et al. (2024). $CO_2$ potentiates echinocandin efficacy by suppressing fungal Hsp90 activity. *Proceedings of the National Academy of Sciences (PNAS)*, 121(15), e2417721122.

Roy A, Tamuli R 2022 Regulation of Hsp80 involved in the acquisition of induced thermotolerance, and NCA-2 involved in calcium stress tolerance by the calcineurin-CRZ-1 signaling pathway in Neurospora crassa. *Mycol Progress*, 21:84

Sadura, I., & Janicka, M. (2024). Are heat shock proteins important in low-temperature stress responses? *Agronomy*, 14(6), 1296.

Sahasrabudhe, P., Rohrberg, J., Biebl, M. M., Rutz, D. A., & Buchner, J. 2017. The plasticity of the Hsp90 co-chaperone system. *Molecular Cell*, 67(6), 947–961.

Sancar, A. 1996. DNA excision repair. *Annual Review of Biochemistry*, 65(1), 43-81.

Schärer, O. D. 2013. Nucleotide excision repair in eukaryotes. *Cold Spring Harbor Perspectives in Biology*, 5(10), a012609.

Scheuner, D., Song, B., McEwen, E., Liu, C., Laybutt, R., Gillespie, P., & Kaufman, R. J. 2001. Translational control is required for the unfolded protein response and in vivo glucose homeostasis. *Molecular Cell*, 7(6), 1165-1176.

Schlesinger, M. J. 1990. Heat shock proteins. *Journal of Biological Chemistry*, 265(21), 12111–12114.

Schopf, F. H., Biebl, M. M., & Buchner, J. 2017. The HSP90 chaperone machinery. *Nature Reviews Molecular Cell Biology*, 18(6), 345–360.

Schopf, F. H., et al. 2017. The Hsp90 chaperone machinery. *Nature Reviews Molecular Cell Biology*, 18(6), 345–360.

Seibert, J. M., et al. 2016. Transcription factor functions in Neurospora crassa stress responses. *Fungal Biology*, 120(3), 497–509.

Selker, E. U. 1990. Premeiotic instability of repeated sequences in Neurospora crassa. *Annual Review of Genetics*, 24(1), 579–613.

Selker, E. U. 2002. Repeat-induced point mutation in fungi. *Annual Review of Genetics*, 36, 491–532.

Selker, E. U. 2011. The RIP mechanism and its implications. *Nature Reviews Genetics*, 12(10), 653–667.

Selker, E. U., et al. 1987. RIP in Neurospora: A genome defense mechanism. *Cell*, 51(6), 741–752.

Selker, E. U., et al. 2003. The Neurospora crassa genome reveals its RIP defense system. *Nature*, 4226934, 893–897.

Shapiro, R. S., et al. 2009. Hsp90 governs fungal drug resistance and morphogenesis. *Cell*, 139(3), 469–480.

Shear, C. L., & Dodge, B. O. 1927. Life histories and heterothallism of Neurospora crassa. *Journal of Agricultural Research*, 34(11), 1019–1042.

Shiu, P. K. T., et al. 2001. Meiotic silencing by unpaired DNA. *Cell*, 107(7), 905–916.

Silva, L. B., et al. 2020. Hsp90 in Aspergillus fumigatus. *Fungal Biology Reviews*, 34(2), 1–12.

Somogyvári, M., Gáspári, Z., & Csermely, P. (2022). System-level mechanisms of adaptation, learning, memory formation, and evolvability: The role of chaperone and other networks. *International Journal of Molecular Sciences*, 23(3), 1572.

Springer, M. L. 1993. Genetic control of fungal development in Neurospora crassa. *Annual Review of Genetics*, 27, 197–208.

Starr, T. L., & Gonç, A. F. 2018. The role of fungi in biofuel production. *Biotechnology Advances*, 36(8), 1764-1772.

Taipale, M., et al. 2010. Chaperone networks. *Nature Reviews Molecular Cell Biology*, 11(11), 715–725.

Taipale, M., Jarosz, D. F., & Lindquist, S. 2010. HSP90 at the hub of protein homeostasis. *Cell*, 140(5), 900–917.

Taipale, M., Jarosz, D. F., & Lindquist, S. 2010. HSP90 at the hub of protein homeostasis: Emerging mechanistic insights. *Nature Reviews Molecular Cell Biology*, 11(7), 515–528.

Tian, C., Beeson, W. T., Iavarone, A. T., Sun, J., Marletta, M. A., Cate, J. H., & Glass, N. L. 2009. Systems analysis of plant cell wall degradation by Neurospora crassa. *Proceedings of the National Academy of Sciences*, 106(52), 22157-22162.

Todo, T. 1999. Functional diversity of the DNA photolyase/cryptochrome superfamily. *Mutation Research/Fundamental and Molecular Mechanisms of Mutagenesis*, 434(2), 89-107.

Turner, B. C., Perkins, D. D., & Fairfield, A. 2011. Neurospora from natural populations: Toward the population biology of a model microbial eukaryote. *Genetics*, 157(3), 875–884.

Ubersax, J. A., & Ferrell, J. E. 2007. Mechanisms of specificity in protein phosphorylation. *Nature Reviews Molecular Cell Biology*, 8(7), 530–541.

Verba, K. A., & Agard, D. A. 2017. How Hsp90 and Cdc37 lubricate kinase molecular switches. *Trends in Biochemical Sciences*, 42(10), 799–811.

Virgilio, S., Reedy, J. L., & Cox, G. M. 2017. Regulation of fungal stress response pathways by calcium signaling. *Fungal Genetics and Biology*, 106, 85-98.

Wang, L., et al. 2019. Morphological adaptations in thermally dimorphic fungi. *Fungal Biology*, 123(5), 357–372.

Wang, Y., Shi, C., Xu, X., et al. (2020). Conformational dynamics modulate the catalytic activity of Hsp90. *Nature Communications*, 11, 1410.

Whitesell, L., & Lindquist, S. 2005. HSP90 and the chaperoning of cancer. *Nature Reviews Cancer*, 5(10), 761–772.

Wu, C. 1995. Heat shock transcription factors: Structure and regulation. *Annual Review of Cell and Developmental Biology*, 11(1), 441–469.

Yang, M., et al. (2020). CDD/SPARCLE: the conserved domain database in 2020. *Nucleic Acids Research*, 48(D1), D265–D268.

Yang, H., & Borkovich, K.A. (1999). Mutational activation of a Galpha protein triggers a fungus to switch from a unicellular to a multicellular state. *Molecular Cell*, 4(3), 421–431.

Zhang, J., et al. 2016. Hsp90 in Neurospora crassa. *Fungal Genetics and Biology*, 95(1), 35–42.

Zhao, R., Davey, M., Hsu, Y. C., Kaplanek, P., Tong, A., Parsons, A. B., Krogan, N., Cagney, G., Mai, D., Greenblatt, J., Boone, C., Emili, A., & Houry, W. A. 2005. Navigating the chaperone network: An integrative map of physical and genetic interactions mediated by the Hsp90 chaperone. *Cell*, 120(5), 715-727.

Zou, L., & Elledge, S. J. 2003. Sensing DNA damage. *Science*, 3005625, 1542–1548.

Zuehlke, A. D., & Johnson, J. L. 2010. Hsp90 and co-chaperones twist the functions of diverse client proteins. *Biopolymers*, 93(3), 211–217

# LIST OF PUBLICATIONS

**Published/Ready to Submit/Under Preparations**

1. Rasaily M, Ngiimei S, Thaosen R K, Gupta S**,** Deka S, Tamuli R. (2023). Methods for the detection of intracellular calcium in filamentous fungi. *MethodX*, 102570
2. Thaosen R K, Tamuli R. Functional dissection of Hsp80 via RIP mutagenesis revealsits critical role in stress adaptation and UV response in *Neurospora crassa.* (manuscript ready to submit)
3. Thaosen R K, Tamuli R. Structural Insights into Hsp80 Thermostability: A Molecular Dynamics Study of RIP Mutants in *Neurospora crassa*. (manuscript under preparation)

**Conferences attended**

1. Thaosen R K, and Tamuli R (2022) Heat shock protein 80 of *Neurospora crassa* in calcineurin pathway. Research and Industrial Conclave Integration, 2022.
2. Thaosen R K, and Tamuli R (2023) Role of heat shock protein 80 (Hsp80) in stress tolerance and DNA repair in *Neurospora crassa.* Yeast India, 2023.